Conference Proceedings

National Conference

on

Thermo-mechanical Processing of Steels

&

5th Gleeble User Workshop India (GUWI-2015)

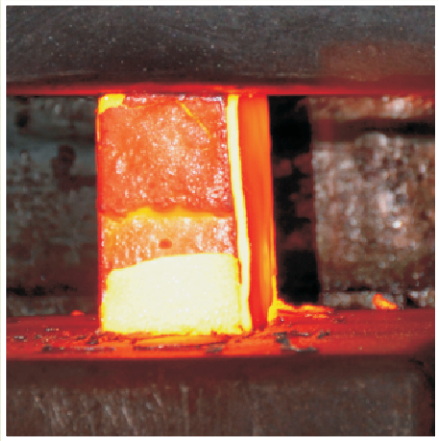

August 6-7, 2015

Organized by

IIM
Metallurgy
Materials Engineering

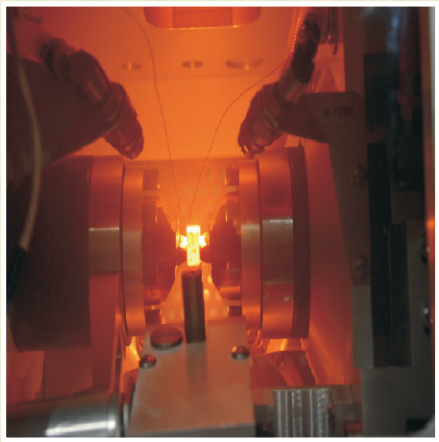

CSIR-National Metallurgical Laboratory
Jamshedpur
&
IIM Jamshedpur Chapter

(In association with GUFI)

National Conference on Thermo-mechanical processing of Steels &
5th Gleeble User Workshop India (GUWI-2015),
August 6-7, 2015, pp 1-8.

CONTENTS

National Conference on Thermo-mechanical processing of Steels &
5th Gleeble User Workshop India (GUWI-2015),
August 6-7, 2015, pp 1-8.

Parametric Optimization of Hot Compression Process of Medium Carbon Steel by Using Taguchi Method

Md. Israr Equbal[1], R.K. Ohdar[1], P. Talukdar[1] and Vinod Kumar[2]

[1]Department of Forge Technology, National Institute of Foundry and Forge Technology, Ranchi -834003, India

[2]R&D Centre for Iron and Steel, Steel Authority of India Limited, Ranchi -834002, India

Email : israr_equbal@yahoo.co.in, rkohdar@yahoo.com, pinaki.t@rediffmail.com, vkumar@sail-rdcis.com

ABSTRACT

In this study hot compression test has been performed on Gleeble-Thermo mechanical Simulator (TMS) on a commercial medium carbon forging steel (AISI 1035). The influence of process parameters viz. deformation temperature, strain rate and cooling rate after hot deformation on the residual stress has been investigated. Analysis of variance (ANOVA) is employed to determine significant parameters. Final microstructures and hardness of the deformed samples have been also evaluated. The results indicated that the cooling rate has a remarkable effect on the microstructure and other properties at room temperature.

Keywords *: hot compression test, thermo-mechanical simulator, taguchi method, ANOVA*

INTRODUCTION

Medium carbon steels are being widely used for many general purpose parts including connecting rods, automotive crankshaft, rams, spindles, etc.[1]. Optimization of hot compression process depends upon many variable but the vital parameters which can have major influence are strain rate, temperature, cooling rate with respect to material properties. Temperature plays vital role in achieving better flow stress in order to decrease the load with increasing die life. Apart from temperature strain rate also plays major role in selection of hot compression process if high strain rate can achieve better mechanical properties by producing finer grain size components which in return in prove the durability and fatigue life of component then strain should also be considered, in order to achieve a valid relationship between strain rate and deformation temperature. The cooling rate after finishing deformation stage has a significant effect on the mechanical properties. Higher cooling rates lead to a decrease of ferrite grain size and formation of high strength, hardness, dislocation density and fine phases whereas slow cooling rates lead to transformation into soft, coarse, and less

dislocated phases like polygonal ferrite [2]. Since hot compression process is complex one and the parameters exhibit interdependency among themselves, selection of the optimal parametric combination for a particular application becomes difficult. Designs of experiment (DOE) based approach is considered as preferred tool for the purpose. Taguchi method, being an efficient and cost effective method for analyzing large number of process parameters, is extensively used in industries. In the present work hot compression of Medium Carbon AISI 1035 steel has been carried out using thermo-mechanical simulator (GLEEBLE-3500) to analyse the effect of forging temperature, strain rate and cooling rates on residual stress. Residual stress can be defined as the stress which remains in a material in the absence of any external forces or thermal gradients. In other words residual stresses in a structural material or component are those stresses which exist in the object without the application of any service or other external loads. The basic cause of residual stress is non uniform strains due to some previously performed operations. Residual stresses can be sufficient to cause a metal part to suddenly split into two or more pieces after it has been resting on a table or floor without external load being applied. Residual stresses can result in visible distortion of a component.

EXPERIMENTAL PROCEDURE

The objective of present study involves the study of effect of hot compression process parameters on residual stress which affects the product quality. To achieve this Taguchi experimental method is utilized to design the parameter combinations so as to identify the relative influence of each parameter on the studied response. Furthermore, a statistical analysis of variance (ANOVA) is performed to find significant factors. Finally, a confirmation experiment is conducted to verify the optimal process parameters obtained from the process parameter design. The Taguchi approach enables a comprehensive understanding of the individual and combined effects of various design parameters to be obtained from a minimum number of experimental trials[3]. The aim of the Taguchi design method is to establish the parameter settings which render the product quality robust to unavoidable variations in external noise. It had been extensively used in the engineering design and the analysis of optimal manufacture. The most important stage in this method lies in the selection of control factors. The purpose of this research is to determine the effects caused by varying the process parameters temperature, strain rate and cooling rate on residual stress. These parameters each at three levels are considered for the present study as shown in Table 1. The

total degree of freedom (DOF) for three factors each at three levels is 6. Therefore L9 orthogonal array is selected for experimental design and is shown in Table 2.

The material used in this study is the commercial grade of medium carbon steel AISI 1035. The chemical composition of as-received material is given in Table 3. All simulations were done using cylindrical compression testing specimen geometry, 10 mm (0.394 in) diameter by 15 mm (0.591 in) long given in Fig. 1. Both opposite surfaces of the specimen were parallel to ensure uniform deformation during testing.

Table 1: Factors and their levels

Factors	Level		
	1	2	3
Temperature (T)	900^0C	1000^0C	1100^0C
Strain rate (S_R)	0.2 s^{-1}	2 s^{-1}	20 s^{-1}
Cooling Rate (C_R)	0.5^{o}C/s	1 ^{o}C/s	Water quenching

Table 2 L9 Orthogonal array

Exp. No.	T (^{0}C)	S_R (s^{-1})	C_R (^{0}C)
1	1	1	1
2	1	2	2
3	1	3	3
4	2	1	2
5	2	2	3
6	2	3	1
7	3	1	3
8	3	2	1
9	3	3	2

Table 3 Chemical Composition of Experimental AISI 1035 steel (wt.%)

AISI 1035	C	Mn	Si	S	P
	0.3-0.4	0.5-0.8	0.15-0.35	0.02-0.03	0.035

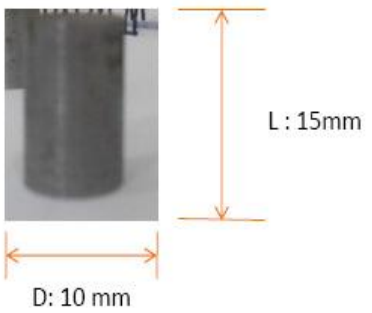

Fig.1. Sample prepared; D= 10 & H= 15 mm

The first step in preparation of sample for testing is welding of thermocouple. All specimens had a 0.254 mm (0.010 in) diameter type K control thermocouple spot welded on the surface at the centre of the specimen. Thermocouple wire was PFA (a fluorocarbon polymer) coated to prevent shorting between the wires away from the specimen. After which specimens are fixed between the anvils exactly at the centre without any deviation such that deformation axis is straight and doesn't result in formation irregular shape as shown in Fig. 2.

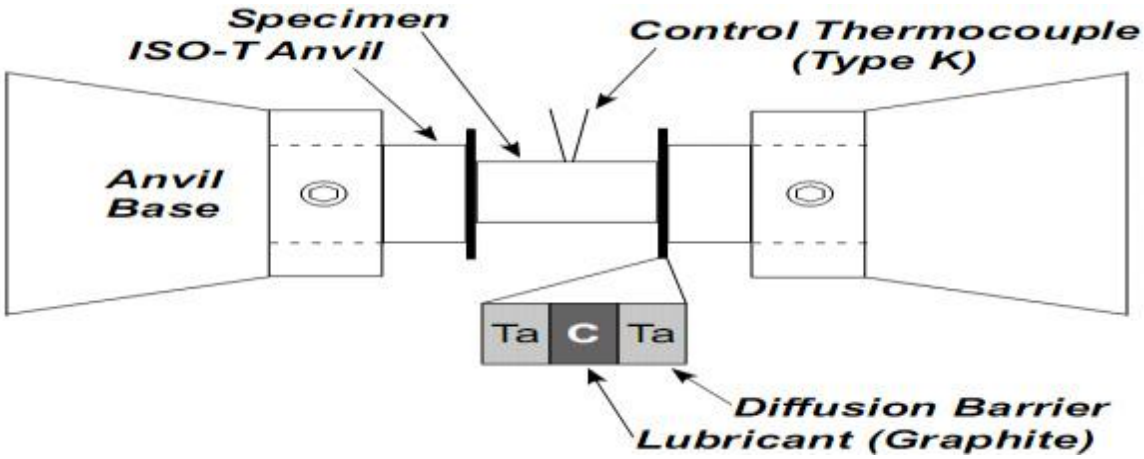

Fig.2: Schematic arrangement of the assembled ISO-TTM compression fixture

The fixtures contain anvil at the centre which are of tungsten carbide (WC), these anvil are degradable and usually does not last for high repetition of cycles. The specimens are hold together by the anvils with graphite foil in between with nickel-based anti-seize compound grease applied in order to prevent the diffusion of carbon from graphite foil on to specimen at high temperatures. Graphite foils are used for temperatures below 1100^0C where in case of temperature greater then these tantalum foils are used which act as lubricant between anvils and specimen. The experiments were performed with standard experimental procedures on a thermo-mechanical simulator (Gleeble-3500) to give a different strain rate. The specimens were deformed to 66 % and the flow stress data were recorded. All the tests were carried out under isothermal conditions. Gleeble systems incorporate a closed-loop thermal system and a closed-loop hydraulic servo system under synchronous digital computer control, providing the performance that is needed to perform accurate testing and physical simulations. Heating rates of $10{,}000^0$C per second, stroke rates exceeding 1,000 mm per second and 22,000 lbs. of tension and compression force are available on a standard Gleeble 3500. Gleeble systems are unique in that they are the only systems capable of maintaining uniform temperature cross sections - isothermal planes - at the midspan of the specimen, even while heating or cooling

rapidly. Because of these isothermal planes, material researchers can be confident that results will accurately reflect the material being tested, regardless of specimen size.

RESIDUAL STRESS ANALYSIS

Residual stress analysis was carried on thermo mechanical simulation samples and as well as raw material in order to check the presence of residual stress before and after simulation process. It was carried out residual stress analyser by X-ray Diffraction Method of range - Psi Oscillations - 0 to ±8° Psi tilt ± 56° geometry as shown in Fig. 3. The measurement of residual stress by X-ray diffraction (XRD) relies on the fundamental interactions between the wave front of the X-ray beam, and the crystal lattice. Bragg's Law does the basis of XRD measurements. For the following medium carbon steel Chromium (**Cr K-**α) X-ray anode tube was used with specified Brag angle 156 ° and (h k l) -(2 1 1) plane. The locations considered for stress measurement is centre of the specimen in direction the deformation which is longitudinal direction.

Fig. 3: Performing Residual Stress Analysis of AISI 1035 steel raw material

RESULTS AND ANALYSIS

After conducting all the simulations, the residual stress has been noted for further analysis and optimization. Based on the experimental layout depicted in Table 3, the response residual stress has been measured. Residual stress is measured in Mega pascal (MPa) as well as hardness (HRC) of the deformed samples is depicted in Table 4.

Table 4 Simulation results of Residual Stress (MPa)

Exp. No.	F. T.	S. R.	C.R.	Residual stress (MPa)	S/N ratios	Hardness (HRC)
1	1	1	1	52.53	-34.4081	158
2	1	2	2	67.73	-36.6156	155
3	1	3	3	70.08	-36.9119	159
4	2	1	2	88.55	-38.9438	175
5	2	2	3	103.52	-40.3005	158
6	2	3	1	81.51	-38.2242	176

7	3	1	3	147.59	-43.3811	149
8	3	2	1	75.26	-37.5313	147
9	3	3	2	129.98	-42.2775	151

In Taguchi method, the basic method converts the objective parameters to signal-to-noise (S/N) ratio treated as the quality characteristics evaluation index. The least variation and the optimal design are obtained by means of the S/N ratio. The higher the S/N ratio, the more stable the achievable quality. Usually, there are three categories of quality characteristic in the analysis of the S/N ratio, i.e., the-lower-the-better, the higher-the-better, and the-nominal-the-better characteristics. Die stress in this study is the quality characteristic with the objective ‘‘the lower-the-better”. So the S/N ratio is defined by,

$$\eta_j = -log_{10}(\tfrac{1}{n}) \sum_{i=1}^{n} \tfrac{1}{y^2_{ij}} \qquad (1)$$

Where, η_j is S/N ratio for the i^{th} alternative, n is number of replications; y_{ij} is observed response value of i^{th} alternative j^{th} replication.

Fig. 4 shows the S/N ratio plot for residual stress. The optimum parameters combination for residual stress is T= 900^0C, S.R= $2s^{-1}$ and C.R. = 0.5^0C corresponding to the largest values of S/N ratio for all control parameters.

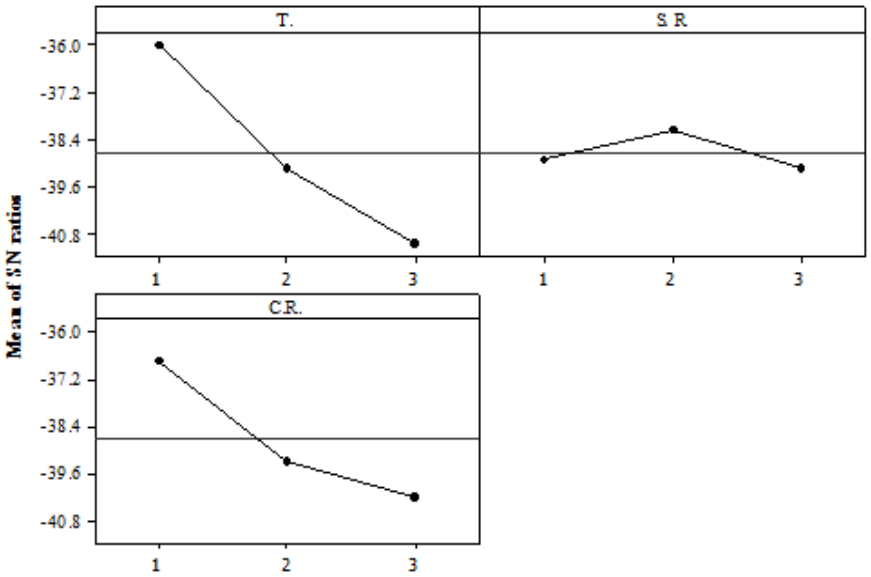

Fig. 4: S/N ratio response graph for residual stress

Relative influence of each factor is determined by analysis of variance method (ANOVA) and results are presented in Table 5. F- value is the statistic used to test the hypothesis that all the factor level means are equal. It is calculated as the mean square for the factor divided by the mean squares for error. F is used to determine the % contribution. ANOVA depicts that

the process parameter namely Temperature and cooling rate are the most significant parameters affecting the Forging load under 95% confidence level. Microstructural analysis indicates that the microstructures of of slow cooled specimens are mainly composed of finer ferrite and pearlite as well as small quantity of widmanstaten ferrite. Water quenching leads to a formation of relatively fine ferrite and pearlite as shown in Fig. 5.

Table 5 ANOVA Table for residual stress

Factor	DOF	SS	Variance	F-value	% Contribution
Temperature	2	39.589	19.795	9.41	62.57
Strain rate	2	1.610*		-	-
Cooling rate	2	19.473	9.737	4.63	30.78
Error	2	4.205	2.103		
Total	8	63.267			

*pooled, DOF- Degree of freedom, SS- Sum of square

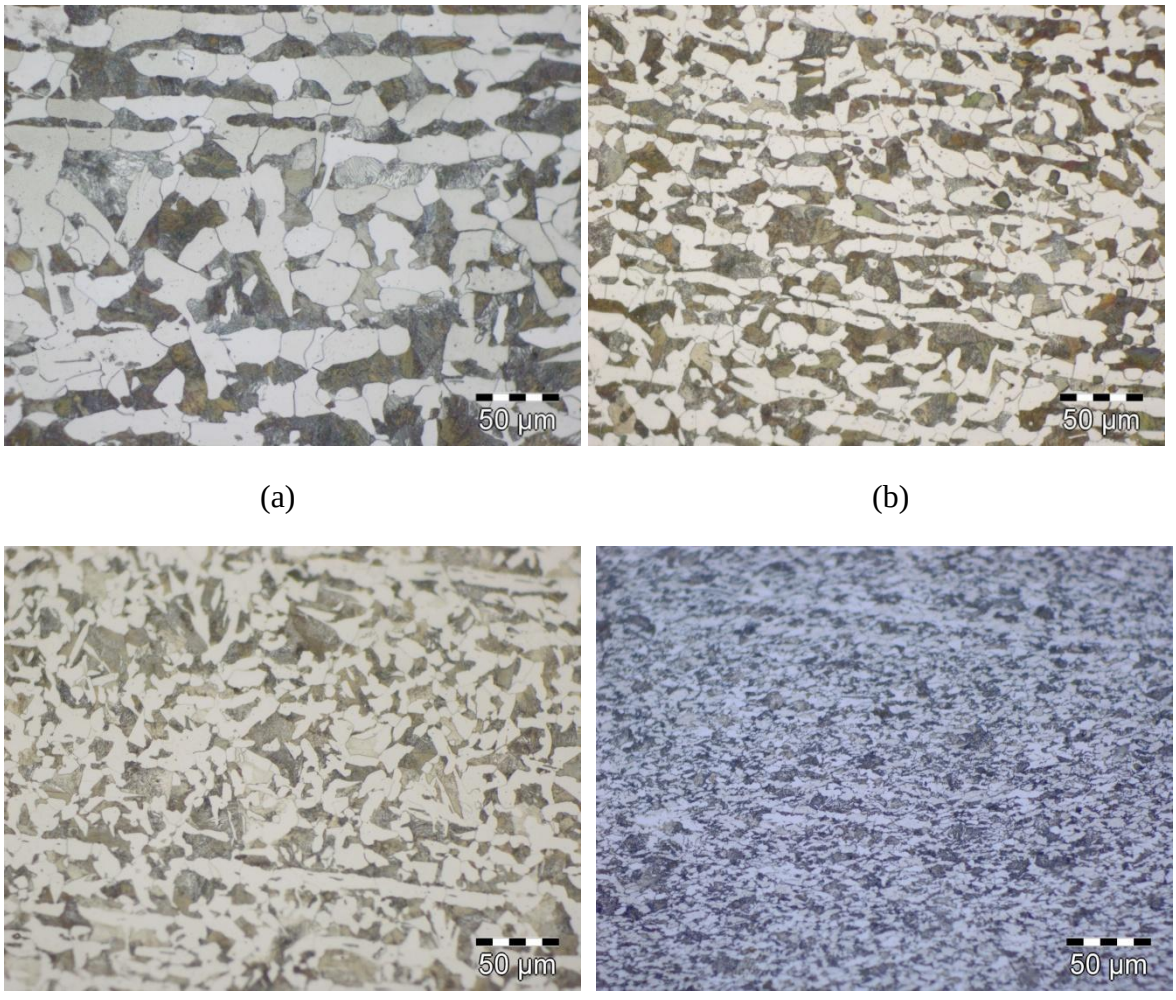

(a) (b)

(c) (d)

Fig. 5: Microstructures of AISI 1035 steel under conditions of (a) As-Received (b) 900^{0}C,

$0.2S^{-1}$, 0.5^oC (c) 900^0C, $0.2S^{-1}$, 1^oC and (d) 900^0C, $0.2S^{-1}$, water quenched

CONFIRMATION TEST

The optimum parameter level for die stress on the basis of main effect plots illustrated in Fig. 3 are T= 900^0C, S_R= $2s^{-1}$ and C_R = 0.5^0C/s. The confirmation test at the optimal parameter setting is conducted to evaluate the value of residual stress. The value of residual stress obtained from the confirmation experiment is 33.83 MPa, which is minimum from all the values as obtained by Taguchi's experiment.

CONCLUSION

The research involved analyzing the effects of parameters viz. temperature, strain rate and cooling rate for the response residual stress during hot compression process. Thermo-mechanical simulator (GLEEBLE-3500) along with Taguchi method has been used to simulate the hot compression process and then performing a series of optimization iterations in order to obtain the optimum level of process parameters. Analysis of variance (ANOVA) is employed to determine significant parameters. Temperature and cooling rate observed as the most significant parameters affecting the response. Optimization of the process parameters leading to a lower residual stress and it is also verified through a confirmation experiment for the validation of the results.

REFERENCES

[1]. Mirzadeh, H. et al. (2011) Hot deformation behavior of a medium carbon microalloyed steel, Materials Science and Engineering A, 528, pp. 3876–3882.

[2]. Gunduz, S., Capar, A. (2005) Influence of forging and cooling rate on microstructure and properties of medium carbon microalloy forging steel, J Mater Sci, 41, pp. 561–564, November 2005.

[3]. P.G. Stuart: Taguchi methods: a Hand on Approach, Addison Wesley, New York (1993).

National Conference on Thermo-mechanical processing of Steels &
5th Gleeble User Workshop India (GUWI-2015),
August 6-7, 2015, pp 9-21.

Determination of Adiabatic Temperature Rise during High Strain Rate Deformation of Ti-6al-4v Alloy

A. J. Dawari[1] and B.P. Kashyap[2]

[1]Kalyani Centre for Technology & Innovation, Bharat Forge Ltd, Pune- 411036, India

[2]Department of Metallurgical Engineering & Materials Science, IIT Bombay, Mumbai- 400076, India

Email : ashishdawari@bharatforge.com, bpk@iitb.ac.in

ABSTRACT

During the plastic deformation of Ti-6Al-4V alloy, adiabatic heating leads to increase in temperature of the work piece which contributes to flow softening. This temperature rise can be studied during the hot compression tests. Moreover, this rise in the temperature can be estimated theoretically or it can be predicted using FEM software's. Constant strain rate hot compression tests were conducted on Gleeble 3500 Thermo-Mechanical Simulator with cylindrical specimens of Ti-6Al-4V material in the temperature range of 700 °C - 1000 °C and strain rate range of 1 s^{-1} - 100 s^{-1} up to a true strain of 0.7. Experimental results show that the flow stress of Ti-6Al-4V alloy decreases with the increase in temperature and decrease in strain rate. During test, adiabatic temperature rise was measured using thermo-couple. The temperature rise was also estimated theoretically by using the amount of work done from the uncorrected stress-strain curve. The estimated and experimental temperature rise has been compared for various test temperatures and strain rates. This temperature rise is significant at lower temperatures and higher strain rates. In present work, maximum temperature rise is observed to be 103 °C at strain rate of 50 s^{-1} and test temperature of 700 °C. The flow stress-strain curves were corrected for temperature rise. Simulation was also performed in DEFORM 3D FEA software for prediction of temperature rise for various strain rates and temperatures which shows good agreement with experimental values.

Keywords : *adiabatic heating, Gleeble 3500, Ti-6Al-4V, flow stress, DEFORM*

INTRODUCTION

Titanium ASTM Grade V (Ti-6Al-4V) is an α + β alloy which is heat treatable to achieve moderate increase in strength. This alloy is widely used in aircraft turbine engine components, aircraft structural components, aerospace fasteners, high-performance automotive parts, marine industries, medical devices and sports equipment due to its properties like high

strength-to-weight ratio, good corrosion resistance, high thermal stability and better mechanical properties at high working temperature [1,2]. Titanium alloys are more challenging to forge than most steels and aluminum alloys due to the required process control [1, 3]. Control of the forging temperature is essential to achieve good formability and to produce the microstructure required to achieve specified mechanical properties in service. Temperature controls should not only be limited to the furnace set point but must also account for adiabatic heating, die chill and heat loss to the environment [1, 3].

During high strain rate deformation, plastic work is transformed into heat. Due to low thermal conductivity of Ti-6Al-4V alloy, there is no significant heat exchange with environment, thus increasing its temperature. This increase in temperature is called 'adiabatic heating'. Flow softening behavior observed during plastic deformation may be attributed to adiabatic heating and microstructure evolution [1-4]. Adiabatic heating, not only raises the temperature of the test piece but, also increases the proportion of the soft β phase [1]. If test piece temperature goes beyond β transus temperature, this may cause excessive grain growth in the single phase field. Moreover, cooling from this β phase results into a coarse and acicular structure which needs to be refined by subsequent processing. When the hot deformation is carried out near or above β transus temperature, the flow stress becomes almost constant, suggesting that dynamic recovery and dynamic recrystallization (DRX) occurs [2]. At high temperatures and strain rates, thermal softening erases the stabilizing effect of work hardening and can cause material instability. Increase in the proportion of soft beta phase during deformation has effect on the material flow.

Several studies have been carried out to model the deformation during forging at different temperatures and strain rates. Some of the energy of plastic deformation is dissipated as heat and the remaining is stored in the material as strain energy due to dislocations, dislocation interactions and residual strains caused by incompatible slip in grains of different orientations [2,3]. In mechanics, interest in the dissipation of energy is due to the heating it produces during rapid deformations such as shear banding and dynamic crack growth. The objective of the present work is to investigate precise temperature rise due to adiabatic heating by experimental work, theoretical analysis and simulation. The said simulation results are validated with the help of experimental results.

EXPERIMENTAL PROCEDURE

Ti-6Al-4V alloy was procured from TIMET, UK, in the form of 60 mm diameter rolled bars in mill annealed condition. The composition in wt % is given in Table 1. For compression test, cylindrical specimens of 10 mm diameter and 15 mm height were prepared along the rolling direction of the as-received bar according to the ASTM E209 standard. A small hole of 0.8 mm diameter and 5 mm depth was drilled at mid height of the specimens for embedding a thermocouple used for the measurement of actual temperature of the specimens as shown in Fig. 1a. The temperature of the specimens was monitored using a chromel–alumel thermocouple. A Gleeble 3500C thermo mechanical simulator was employed to perform hot compression tests under constant strain rates, ranging from 1 s^{-1} to 100 s^{-1} with an interval of an order of magnitude and in the temperature range of 700 °C to 1000 °C with an interval of 50 °C. The specimens were heated to the deformation temperature at a rate of 5 °C / sec, held for 120 sec and then compressed for a true strain of 0.693 under constant strain rates (Fig. 1b). The adiabatic temperature rise during deformation was recorded. After testing, the samples were water quenched. Kroll's reagent was used for etching and microstructural analysis was carried out with an optical microscope of Carl Zeiss make. The results obtained from the experimental work was further analysed which is explained in the next section.

Table 1: Chemical Composition

Element	Sn	Mo	Zr	Cu	Fe	Mn	V	Si	Al	C	N
Wt (%)	<0.04	<0.04	<0.04	<0.04	0.15	<0.04	4.07	<0.04	6.53	0	0.004

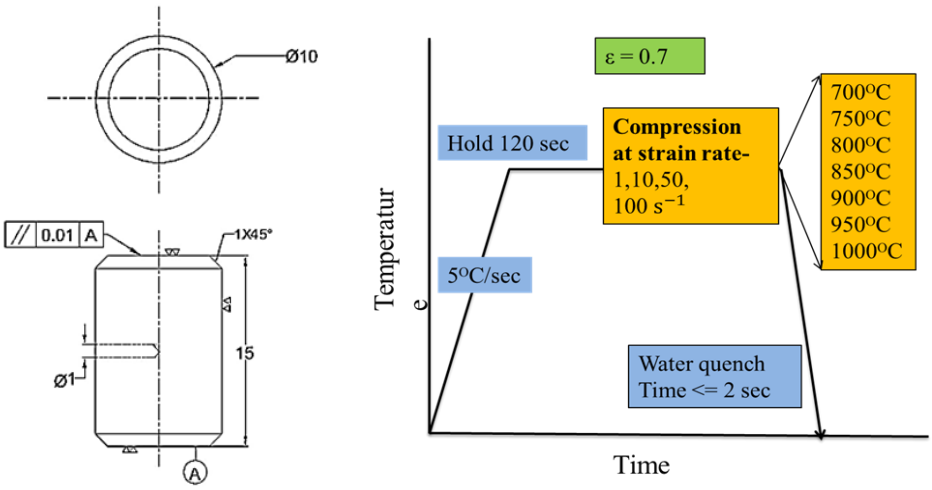

Fig.1: a) Test sample b) Experimental procedure

RESULTS AND DISCUSSION

Microstructural observations

The microstructure of as received material shows equiaxed α phase with average grain size of 15.33 µm and β phase at grain boundaries with 40 % volume fraction (Fig.2). β transus temperature of selected alloy is 995-1000°C.

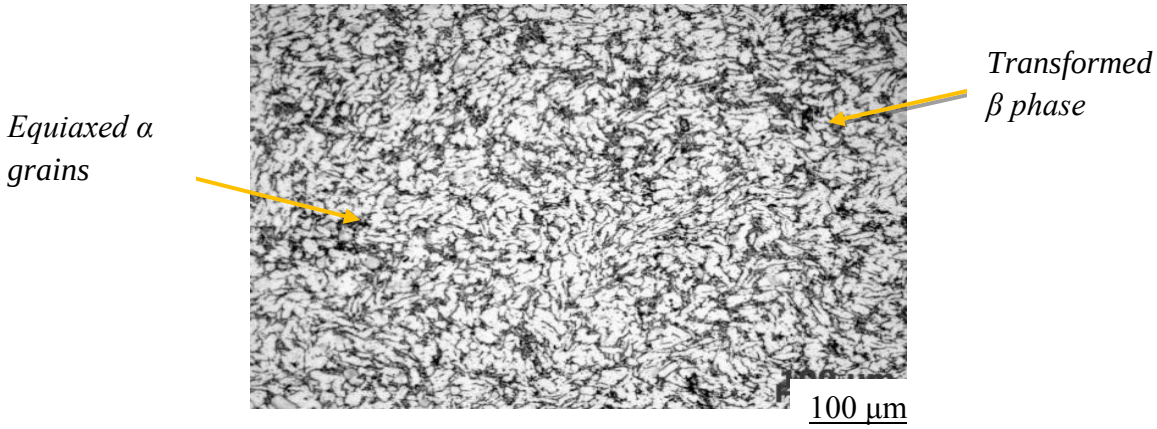

Fig.2: Optical micrograph of as received material (100X).

Stress–strain behaviour

By using standard procedures, the true stress–true strain curves were obtained from load-stroke data after compression testing [4]. True stress- strain curves obtained are shown in Fig.3 to Fig.6. The flow curves can be broadly classified into three categories:

1. In the temperature range of 700 °C to 900 °C, for strain rates lower than 50 s^{-1}, continuous flow softening after a peak stress was observed (Fig. 3-4). For temperatures 950°C and 1000°C, flat stress–strain curves were observed (Fig.3-4) which indicates the steady state flow behaviour.
2. At strain rates of 50 s^{-1} and 100 s^{-1}, for all temperatures of testing, broad oscillations were observed and it approaches to steady state at higher strains (Fig. 5-6). There are different mechanisms which may cause these oscillations like dynamic recrystallization, dynamic aging, flow localization or unstable flow [5].

The flow softening is caused due to adiabatic heating. Due to adiabatic heating, the resulting flow stress will be lower than the actual flow stress for the desired test temperature. Thus, determination of temperature rise becomes important.

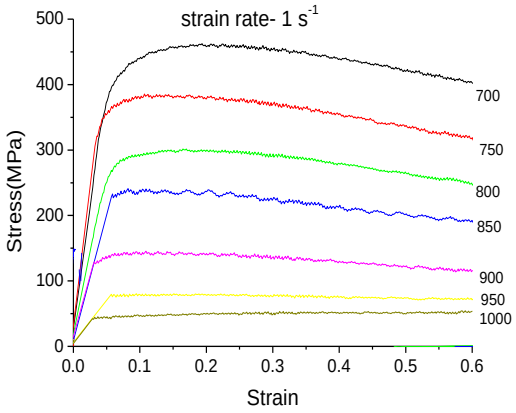

Fig.3: True stress-true strain curve at various temperatures and at 1 s^{-1}.

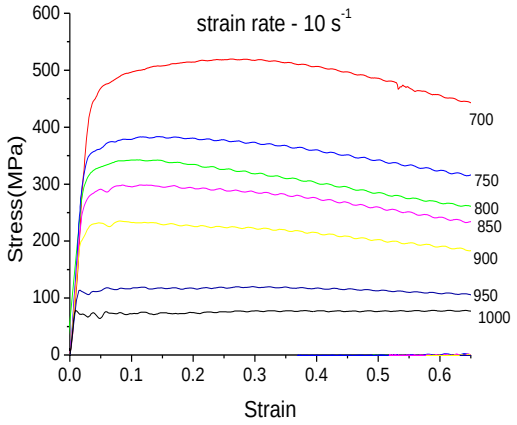

Fig.4: True stress-true strain curves at various temperatures and at 10 s^{-1}.

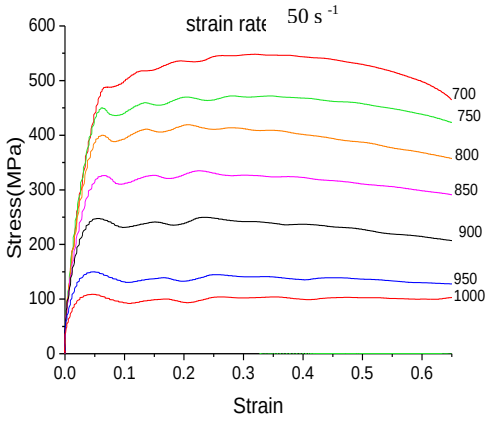

Fig.5: True stress-true strain curve at various temperatures and at 50 s^{-1}.

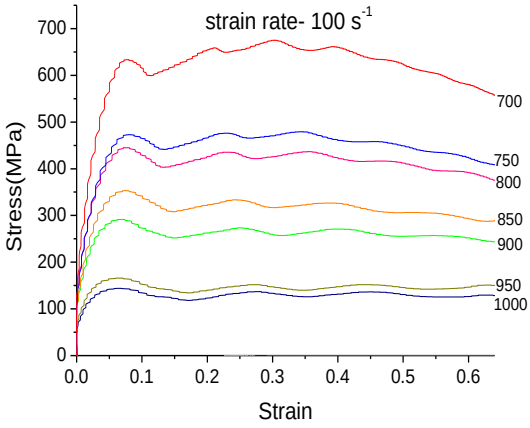

Fig.6: True stress-true strain curves at various temperatures and at 100 s^{-1}.

Temperature rise (ΔT) due to adiabatic heating in compression

Experimental determination

During compression, the actual temperature was measured through thermocouple. Temperature at the core of the sample is plotted against time for each temperature and strain rate combination. The same for 700 °C and 1 s^{-1} is shown in Fig. 7. Peak in graph shows temperature rise due to adiabatic heating during deformation. Considerable temperature rise (60 °C) was observed. Temperature rise (ΔT) has been determined for all temperature and strain rate range. The same is presented in Fig. 8. Significant adiabatic heating is observed at lower temperatures and higher strain rates.

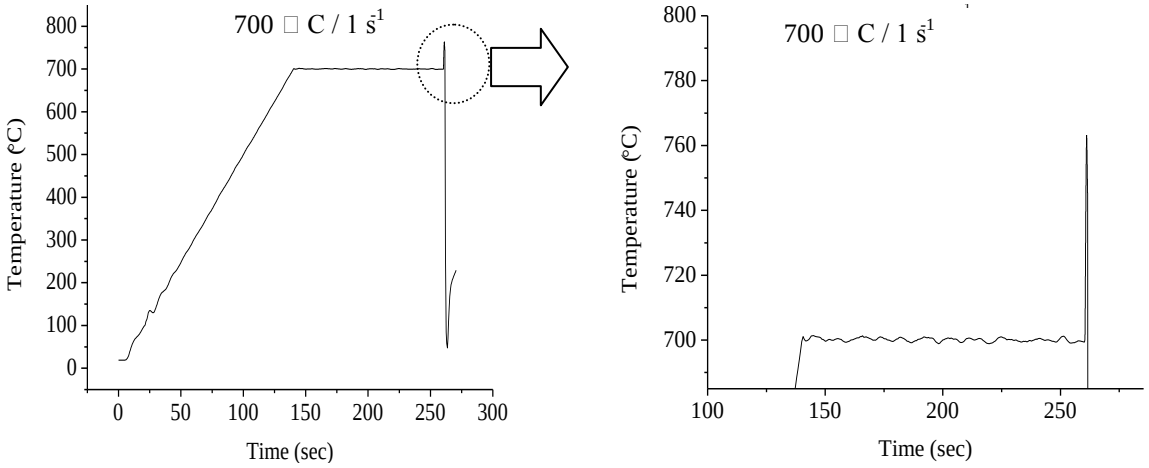

Fig.7: Core temperature of sample (°C) deformed at 700 °C and at 1 s^{-1}.

For a given strain rate, ΔT decreases with increase in test temperature. At constant temperature, ΔT increases with increase in strain rate. Contrary to the trend, at strain rate of 100 s^{-1} and temperature below 850 °C, the temperature rise was observed to be less than that at strain rate of 50s^{-1}. This may be due to error in thermocouple readings. Maximum temperature rise because of adiabatic heating was observed to be 103°C for strain rate of 50s^{-1} and test temperature of 700 °C.

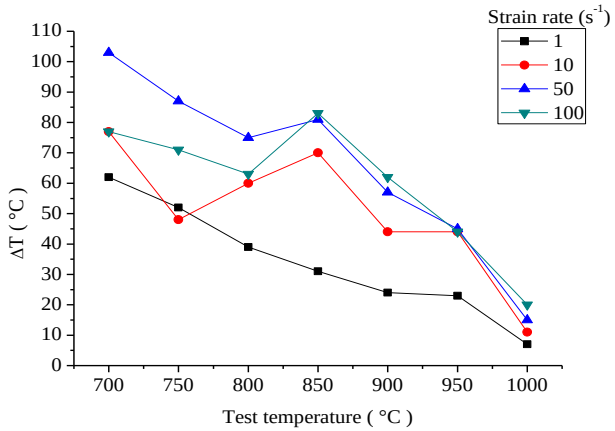

Fig. 8: ΔT at various test temperatures and strain rates.

Theoretical calculations

Adiabatic heat rise can be calculated by using the eq. (1),

$$\Delta T = \eta \frac{\beta}{\rho C_p} \int_{\varepsilon 1}^{\varepsilon 2} \sigma(\varepsilon) d\varepsilon \qquad (1)$$

Here, ρ - density in kg/ $m^{3,}$ Cp - Heat capacity J/kg K, η - adiabatic correction factor, β- Fraction of heat dissipation caused by the plastic deformation, $\int_{\varepsilon 1}^{\varepsilon 2} \sigma(\varepsilon) d\varepsilon$ – amount of work (calculated from area under the uncorrected stress-strain curve).

The adiabatic correction factor η indicates the fraction of adiabatic heat rise retained in the sample after heat loss. This can be calculated by using eq. (2). This correction factor is used to get the accurate temperature rise at different strain rate conditions [11].

$$\eta = \frac{\Delta T_{actual}}{\Delta T_{adiabatic}} \qquad (2)$$

Here, ΔT_{actual} - difference in set and actual temperature considering actual condition where heat loss to environment and dies. $\Delta T_{adiabatic}$ - difference in set temperature and actual measured considering no heat loss to environment and dies. There are many arguments on the conversion of plastic work to heat during high strain rate deformation. Taylor and Quinney measured the fraction of heat conversion and found that it is of the order of 0.9 with copper specimens [7]. Most researchers still use 0.9, e.g., S.Bruschi, et al. and Q.Bai et al. have taken hot compression tests on Ti-6Al-4V material and for calculating temperature rise, β was taken as 0.95 and 0.9, respectively [8,9]. In present study β is considered as constant and taken as 0.9. Different methods like Simpson's rule, trapezoidal rule and ORIGIN software can be used to calculate area under curve. In present work these values were generated from ORIGIN 8.0 software. The specific heat values were taken from literature and the same is given in Table 2 [2, 3,10, 11]. η was assumed to be 0.9, 0.97, 0.99 and 0.99 for strain rates of 1 s^{-1}, 10 s^{-1}, 50 s^{-1} and 100 s^{-1} respectively based on literatures [1, 2,4, 11].

Table 2: Specific heat for different temperatures [2-4, 11]

Temperature (^{0}C)	700	750	800	850	900	950	1000
Specific Heat C (J/Kg K)	822	865	910	921	930	940	950

The temperature rise as a function of strain rate by experimental and theoretical methods are compared and the same for 1, 10, 50 and 100 s^{-1} at 900 °C is shown in Fig. 9. At lower strain rate they show good agreement but at higher strain rate theoretical temperature rise is less than experimental one. One of the reasons for this variation may be due to the assumptions made in constants. ΔT determined at various temperatures and strain rates, using eq. (2), is presented in Fig.10. In present work an attempt has been made to compare actual and theoretical temperature rise and to minimise experimental thermocouple error through

theoretical analysis. In comparison with experimental ΔT (Fig. 8), similar trend was observed in the graphs. Experimental error at high strain rates has been taken care of, by theoretical analysis.

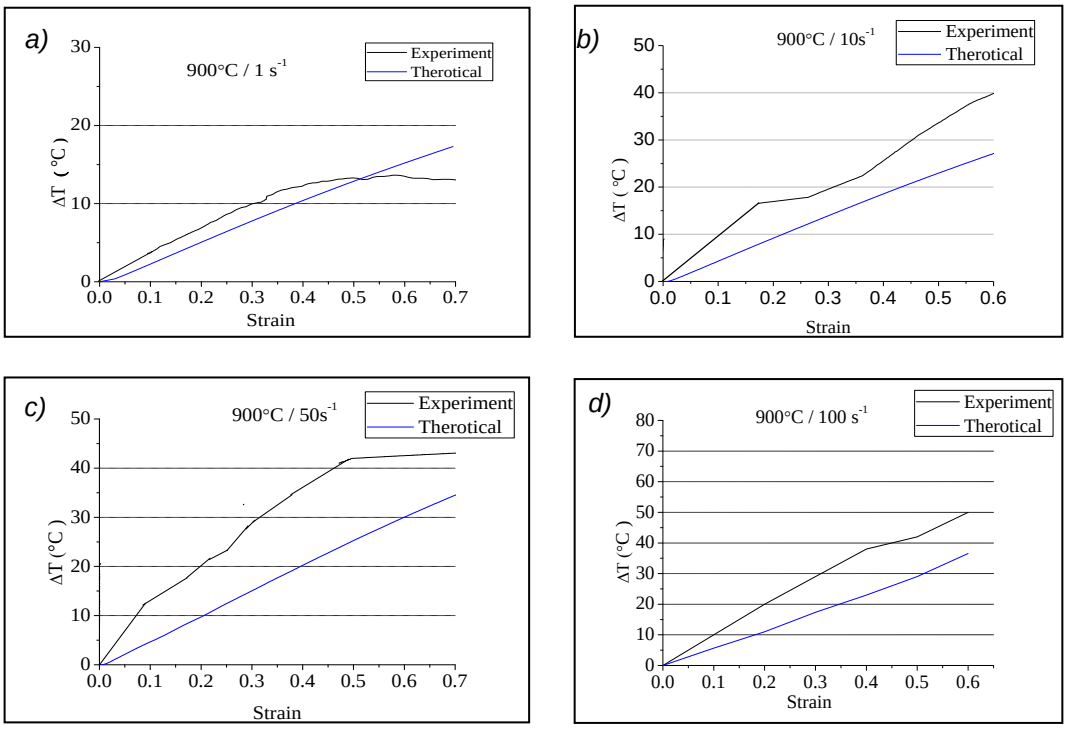

Fig.9. Rise in temperature with strain at 900℃ and strain rate a) 1 s^{-1} b) 10s^{-1} c) 50s^{-1} d) 100s^{-1}

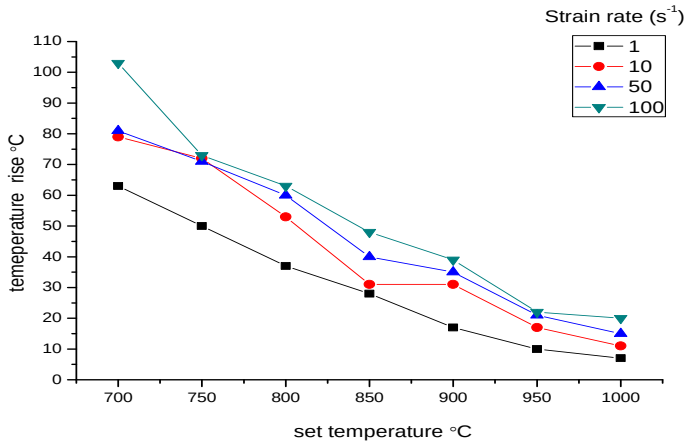

Fig.10: Temperature rise at different test temperatures and strain rates -Theoretical results.

Flow stress data correction for adiabatic heating

Stress- strain graph is corrected for adiabatic heating based on the plot of stress vs (1/T) [11, 12]. An almost linear relation can be observed between the two parameters. Fig. 11 shows the same plot for strain rate of 1 s^{-1}. The change in flow stress value is determined by eq. (3).

$$\delta\sigma = \left[\frac{\partial\sigma}{\partial(1/T)}\right]_{\partial\varepsilon,\ \dot{\varepsilon}} \left[\frac{1}{\delta T + T_{iso}} - \frac{1}{T_{iso}}\right] \ldots\ldots\ldots\ldots\ldots\ldots\ldots\ldots\ldots\ldots\ldots\ldots\ldots\ldots\ldots\ldots\ldots\ldots\ldots\ldots. (3)$$

Here, $\left[\frac{\partial\sigma}{\partial(1/T)}\right]_{\partial\varepsilon,\ \dot{\varepsilon}}$ - slope of plot stress vs (1/T), δT - Temperature rise due to adiabatic heating (°K), T_{iso} - Test Temperature (°K).

Flow stress corrected for adiabatic heat rise is shown in Table 3 for various strains. The stress- strain graph is corrected for both actual and theoretical temperature rise for various temperatures and strain rates. Fig 12 (a-d) shows corrected stress - strain graph for 700 °C.

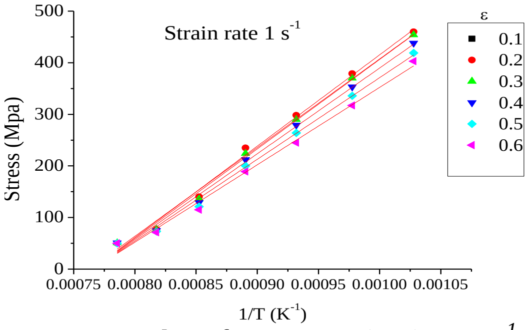

Fig.11: Plot of stress v/s (1/T) at 1 s^{-1}.

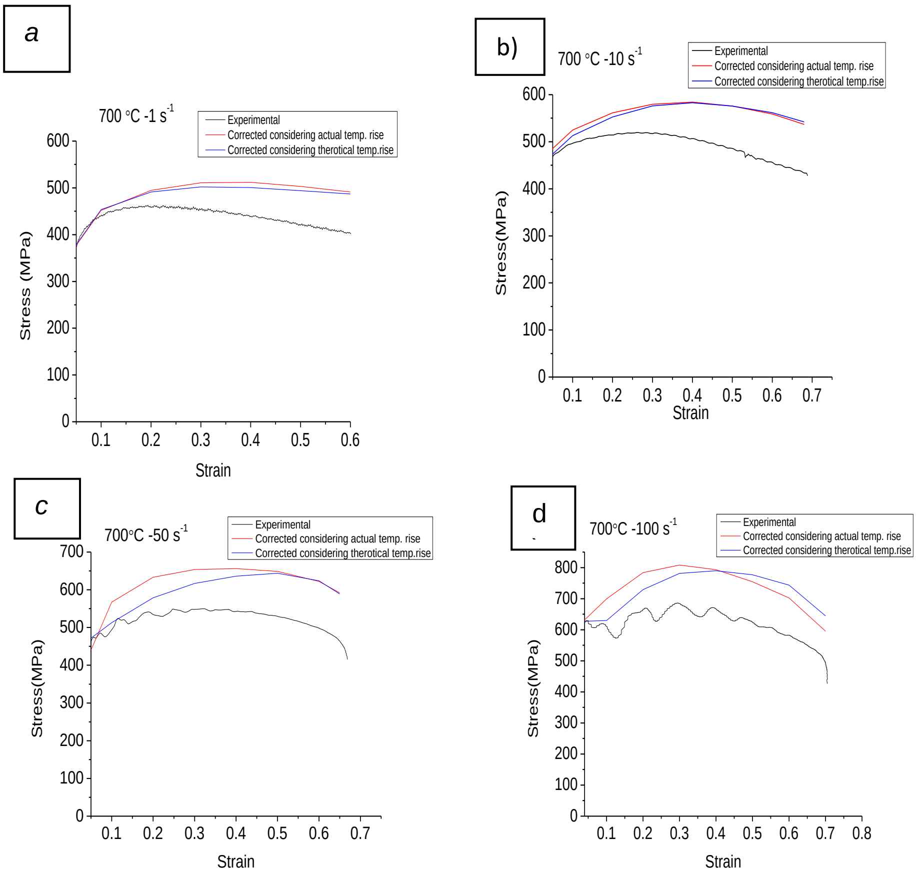

Fig. 12: True stress- true strain curves corrected for adiabatic heating at 700°C
a) 1 s^{-1} b) 10 s^{-1} c) 50 s^{-1} d) 100 s^{-1}

Table 3: Flow stress corrected for adiabatic heat rise

Flow stress values (MPa) at different temperature and strain rates for various strains (Corrected for adiabatic heat rise)									
Sr. no.	Strain	Strain rate, s^{-1}	Temperature (^{0}C)						
			700	750	800	850	900	950	1000
1	0.1	1	452	384	298	240	147	86	61
2		10	525	482	371	330	249	128	104
3		50	567	494	401	344	249	131	126
4		100	699	545	502	417	339	179	147
5	0.2	1	495	381	318	245	149	103	68
6		10	561	501	377	335	248	138	115
7		50	633	556	457	389	273	143	130
8		100	784	569	517	427	330	167	140
9	0.3	1	511	369	321	240	148	105	71
10		10	580	502	371	333	244	146	121
11		50	654	554	451	397	286	160	137
12		100	808	563	492	398	311	192	168
13	0.4	1	512	356	314	232	145	99	70
14		10	584	495	362	334	243	154	122
15		50	656	564	453	389	291	163	133
16		100	793	539	484	425	339	196	165
17	0.5	1	503	449	299	220	137	96	70
18		10	576	475	347	327	240	153	123
19		50	649	565	451	375	283	169	135
20		100	755	535	465	402	313	180	151
21	0.6	1	491	409	276	210	130	94	69
22		10	559	466	338	317	193	112	82
23		50	622	551	434	360	267	167	130
24		100	702	507	420	381	314	182	151

FEM Simulation of compression test

The hot compression test was simulated with commercial FEA software (DEFORM 3D^{TM}) using a Lagrangian implicit code for Ti-6Al-4V alloy. For simulation, the workpiece parameters considered are given in Table 4. The convection heat transfer coefficient to environment, emmisivity and Poisson's ratio were taken as 0.02 N/ (sec mm°C), 0.7 and 0.31, respectively. Flow stresses at various temperatures and strain rates are considered for simulation. For each test temperature and strain rate, simulation has been done to co-relate with actual temperature rise. Temperature profile section view is shown in Fig. 13 for 900°C and at the strain rate 10 s^{-1}.The actual and experimental results are compared and presented in Table 5. The simulation results are in good agreement with experimental values of temperature rise within ± 10 °C error.

Table 4: Work piece parameters

Specification	**Values**
Geometry of workpiece	Dia = 10 mm, Height=15 mm
Meshing type	Tetrahedral mesh
Workpiece mesh size	Elements=27801, Nodes=6240

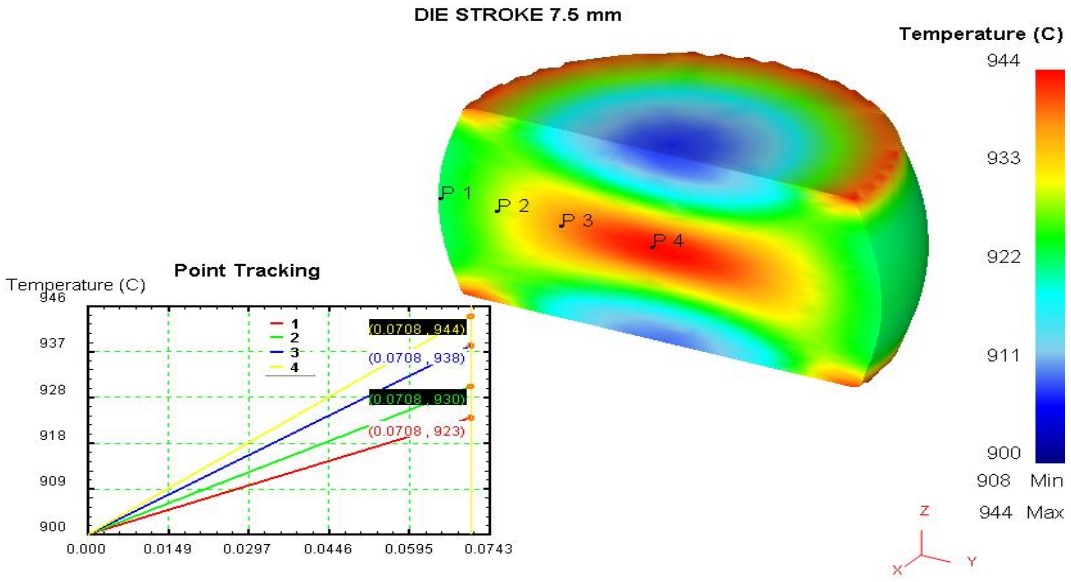

Fig.13: Compression at 900° C and strain rate 10 s^{-1}

Table 5: Comparison of simulated actual results for temperature rise

Temp. (°C)	Strain rate (s^{-1})	Experimental (°C)	Simulation (°C)	% absolute error
700	1	62	67	-8
	10	77	78	-1
	50	77	82	-6
	100	103	102	1
800	1	39	42	-8
	10	60	59	2
	50	75	70	7
	100	63	67	-6
900	1	21	23	-10
	10	44	44	0
	50	46	45	2
	100	56	57	-2

CONCLUSIONS

1. At lower temperatures and higher strain rates adiabatic heating is significant. Maximum rise in temperature being observed as 103 °C for strain rate of 50 s^{-1} and test temperature of 700°C.
2. Flow softening behaviour due to adiabatic temperature rise was observed in stress-strain curves. Stress- Strain curves were corrected for adiabatic heating.
3. Temperature rise was estimated from DEFORM 3D simulation software. A good agreement was found between temperature rise estimated by FEM simulation and experimental values.

ACKNOWLEDGEMENTS

I am thankful to Material characterization laboratory at Kalyani Centre for Technology and Innovation (KCTI), Pune for their help in carrying out my experiments and microstructure analysis work. I deeply appreciate Dr. Kumar V. (RDCIS) for his extended help during compression test, conducted at Steel Authority of India Ltd., Ranchi. Finally, I would like to thank to professors, laboratory assistants, librarians, and my friends at Indian Institute of Technology Bombay, who directly or indirectly helped me completing this work. Finally, the authors would like to express special thanks and gratitude to review committee and top management of Bharat Forge Ltd for granting the permission to publish/present the research work.

REFERENCES

[1]. T. Altan, F.W. Boulger, J.R. Becker, N. Akgerman, H.J. Henning; "Forging equipment, materials, and practices", Columbus, Ohio: Metals and Ceramics Information Center (1973) pp. 141-143, 203-209.

[2]. A. S. Khan, Y. S. Suh, R. Kazmi (2004): International Journal of Plasticity, 20, 2233-2248.

[3]. Q. Zhao, G. Wu, W. Sha (2000): Computational Materials Science, 50, 516-526.

[4]. D. Rittel (1999): Mechanics of Materials, 31 (2), 131-139.

[5]. T. Seshacharyulu, S.C. Medeiros, W.G. Frazier, Y.V.R.K. Prasad (2002) : Materials Science and Engineering A325, 112-125.

[6]. P. Sirilar, P. Srichandra (2000): Journal of Materials Processing Technology, 70, 70-78.

[7]. G.I Taylor, H. Quinney (1934): Proceedings of the Royal Society Series, A 143, 307-326.

[8]. S. Bruschi, S. Poggio, F. Quadrinib, M.E. Tatab (2004): Materials Letters, 58, 3622-3629.

[9]. Q. Bai, J. Lin, T.A. Dean, D.S. Balint, T. Gao, Z. Zhang (2013): Materials Science and Engineering, A 559, 352-358.

[10]. R.L. Goetz, S.L. Semiatin (2001): JMEPEG 10, 710–717.

[11]. Y.V.R.K.Prasad, S. Sasidhara, "Hot Working Guide - A Compendium of Processing Maps", ASM International,Ohio, 1997.

[12]. I. Balasundar, T.Raghu, B.P.Kashyap (2013): Progress in Natural Science: Materials International 23(6), 598–607.

National Conference on Thermo-mechanical processing of Steels &
5th Gleeble User Workshop India (GUWI-2015),
August 6-7, 2015, pp 22-28.

Microstructural Evolution in Hot Compressed IMI 834 Titanium Alloy

Basanth Kumar K[1], Kuldeep K Saxena[2], Suhash R. Dey[1], Vivek Pancholi[2], Amit Bhattacharjee[3]

[1]Department of Materials Science and Metallurgical Engineering, Indian Institute of Technology Hyderabad, Yeddumailaram-502205, Telangana, INDIA
[2]Department of Metallurgical and Materials Engineering, Indian Institute of Technology Roorkee, Roorkee-247667, Uttarakhand, INDIA
[3]Titanium Alloy Group, Defence Metallurgical Research Laboratory (DMRL), Kanchanbagh-500058, Telangana, INDIA

Email: basanthkumar.kodli@gmail.com: saxena0081@gmail.com: suhash@iith.ac.in: vivekfmt@iitr.ac.in: amitb@dmrl.drdo.in

ABSTRACT

IMI 834 is a near alpha titanium alloy, widely used for gas turbine engine applications such as disc and blades for high pressure compressors. One drawback of this alloy is that it is susceptible to cold dwell fatigue, which is due to the presence of micro-textured zones. Thus, appropriate processing parameters (i.e. temperature, strain and strain rate) are required to reduce the size of the micro-textured region. In order to find out the optimized processing parameters, hot compression tests were performed up to 50% engineering strain at temperatures range of 900^0C-1050^0C and strain rate range of 10^{-3} to $10^1 s^{-1}$using Thermo-mechanical simulator (Gleeble 3800®). Flow behavior characteristics were studied from the data obtained during hot compression and processing map was developed at true strain of 0.6 using Dynamic Materials Modelling (DMM) approach. Microstructural examination of deformed IMI 834 titanium alloy were carried out at a particular strain rate of 10^{-3} $s^{-1}$and temperatures of 900^0C, 950^0C, 975^0C, 1000^0C and 1050^0C. Microstructural examination consists of orientation image mapping along compression direction using electron backscatter diffraction. Hot compression mostly resulted into new DRX alpha grains at 900^0C, mixture of deformed large alpha grains containing sub grain boundaries and transformed beta phase consisting of secondary alpha laths at 950^0C and 975^0C and alpha laths transformed from deformed beta grains at 1000^0C and 1050^0C.

Keywords:*hot compression, dynamic materials modelling, microstructure, micro-texture, dwell fatigue*

INTRODUCTION

Titanium alloys have good corrosion resistance and are light weight material. IMI 834, a near alpha titanium alloy, is an alloy for high temperature application and is used in gas turbine engine parts such as high pressure compressor disc and blades [1-2]. Hence, IMI 834 alloy

requires good creep and dwell fatigue properties. The maximum temperature for application of IMI 834 alloy is around 600^0C and it provides optimized creep properties at elevated temperature with good fatigue life due to its bimodal microstructure, i.e. containing equiaxed primary alpha (α_p), grains with transformed beta(β)grains [3]. Proper thermomechanical processing can lead to the required bimodal microstructure. Gopala Krishna et al.[4] examined the workability conditions of IMI 685 titanium alloy at a temperature range 775^0C-1025^0C and strain rate range of 0.001-10 s^{-1}. They reported good workability of IMI 685 (near α titanium alloy)at 975^0C (in α+β region) and strain rate less than 0.02 s^{-1}.Prasad et al. [5]developed the processing maps of various titanium alloys(commercially pure Ti, Ti-6Al-4V and IMI 685) and correlated it with their microstructures. They reported that the lower strain rates responsible for spheroidization of α laths at lower temperatures and dynamic recrystallization (DRX) of β grains at higher temperatures. They also found wide range of unstable flow regions at higher strain rates in these titanium alloys, mainly exhibiting adiabatic shear bands formation. Similar processing was reported by Wanjara et al. [6]at a true strain of 1.2 with detailed optical microstructural correlation on IMI 834 titanium alloy. They also reported α_S lath deformation in α+β region and DRX of β grains at single β region. Miaquani et al.[7]studied the isothermal compression of Ti-5.6Al-4.8Sn-2Zr alloy performed on a Thermecmaster-Z simulator at deformation temperature range of 960^0C-1060^0Cwith strain rate range of 0.001- 10 $s^{-1}$and analyzed it through stress-strain plots, kinetics and processing map. He et al.[8]performed tensile tests (up to 0.2 strain) on Ti-6Al-2Zr-1Mo-1V (a near α titanium alloy) in temperature range of 750^0C-850^0C and strain rate range 0.001-0.1 $s^{-1}$and explained deformation mechanism of α phase through EBSD (Electron Back Scattered Diffraction) study. They noticed thermally activated dislocation glide at 750^oC towards dislocation creep, whereas self-diffusion at 800^oC and 850^oC as deformation mechanism in the α phase. Recently, Balasundar et al.[9] reported isothermal compression of IMI 834 titanium alloy having a bimodal microstructure in temperature range of 850^0C-1060^0C and strain rate range of $3x10^{-4}$-$10^{-3}s^{-1}$, and developed processing map at a true strain of 0.5 using dynamic materials model (DMM),producing selective micrographs at various temperatures and strain rates regions in the processing map. They could estimate the activation energy of deformation and correlated well with the recrystallization of α phase.

The main objectives of the present study is to perform the hot compression test on IMI 834 titanium alloy in the temperature range of 900^0C-1050^0C and strain rate range of 10^{-3}-$10s^{-1}$using thermomechanical simulator (Gleeble 3800). Processing map is developed at true

strain of 0.6, and characterization of the microstructure evolution through inverse pole figure color maps at constant strain rate of 10^{-3} s^{-1}, for all deformation temperatures obtained using EBSD technique.

EXPERIMENTAL WORK

As received IMI 834 alloy was in the form of pan cake having dimensions: 245 mm diameter and 12 mm height. The chemical composition of IMI 834 titanium alloy is given in Table 1. The optical microstructure of the as received material contains primary alpha (α_p) grains and transformed β grains matrix. Hot compression tests are carried out on cylindrical samples of 12mm height and 10 mm diameter scooped out from the pancake. To avoid friction between the anvils and the specimen during deformation, concentric grooves of 0.4 mm depth were made. A 45^0chamferwas provided at the edges of the samples to avoid folding at the initial stages of deformation. Hot compression tests were conducted at five temperatures (900^0C, 950^0C, 975^0C, 1000^0C and 1050^0C) with five strain rates (10^{-3}, 10^{-2}, 10^{-1}, 1 and $10s^{-1}$) up to 50% deformation. To measure the deformation temperature, thermocouple was welded in the middle of the specimen. The heating rate is 5^0C/s and holding time for homogenization is 300 s. Samples were water quenched just after deformation to arrest the high temperature microstructure.

Further microstructural characterization on the surface parallel to the compression direction was carried out on deformed specimens. Orientation Imaging Microscopy (OIMs) were obtained using FEG-SEM equipped with EBSD detector and were analyzed using TSL® (Tex Sem Laboratory) software. The specimens for EBSD were prepared by using electro chemical polishing with a solution containing 600 ml methanol, 300 ml butanol and 100ml per chloric acid at 20 V and -5^0C. EBSD scan of the central section of the compressed specimen was carried out at 70^0 specimen tilt using voltage of 20 KV EHT with 15 mm working distance along with0.4 μm beam step size. Three side by side continuous scans were stitched together for the orientation information from a larger area.

Table.1: Chemical composition of IMI 834 Titanium alloy with weight percentage.

Ti	Al	Sn	Zr	Nb	Si	V	C	Mn
Balance	6.30	3.84	3.71	0.54	0.32	0.11	0.08	0.04

RESULTS AND DISCUSSION

Figure.1 shows the processing map of IMI 834 titanium alloy at a true strain of 0.6, developed using stress- strain data obtained from hot compression. Processing map shown in Figure.1suggeststhe safe working conditions of IMI 834 titanium alloy (in terms of strain rate, temperature and amount of deformation).The stable domains having positive values of efficiency of power dissipation varying from 0.12 - 0.56 are the regions in which the alloy can be processes well. In Figure.1, each contour color region represents a particular value of efficiency and it depends mainly on strain rate sensitivity (m) of material. Strain rate sensitivity (m) of the material generally depends on the deformation temperature (T), strain rate ($\dot{\varepsilon}$) and amount of strain (ε). Negative values of efficiency in power dissipation map represented by the shaded region, and is associated with adiabatic shear band formation, strain localization, dynamic strain aging, which normally occurs at higher strain rates of $1s^{-1}$ and $10s^{-1}$and at lower deformation temperature of 900^0Cand can be clearly identified in Figure.1.

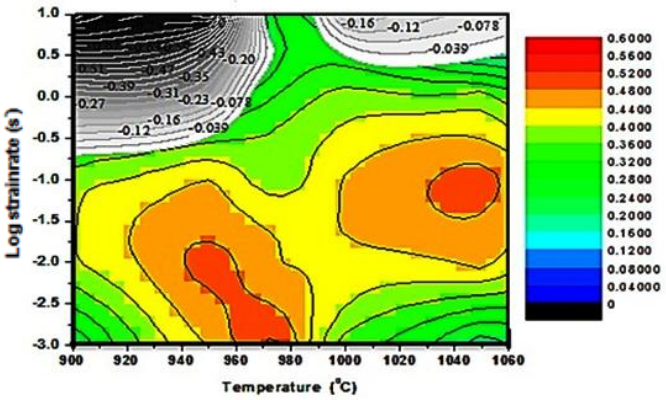

Fig.1: Processing map of IMI 834 titanium alloy at true strain of 0.6.

The efficiency of power dissipation values for hot deformation at $0.001s^{-1}$ strain rate at different temperatures such as 900^0C, 950^0C, 975^0C, 1000^0C and 1050^0C are 0.32, 0.48, 0.56, 0.36, and 0.20 respectively. Power dissipation value gives an indication of the percentage the given load which is utilized for microstructural changes. Here, the highest efficiency of 0.56 is obtained at 975^0Cat a strain rate of $0.001s^{-1}$.

Figure.2 shows the Inverse Pole Figure (IPF) color map of (a) as-received, and 50% deformed specimen at $0.001s^{-1}$strain rate at different deformation temperatures of (b) 900^0C (c) 950^0C (d) 975^0C (e) 1000^0C (f) 1050^0C.

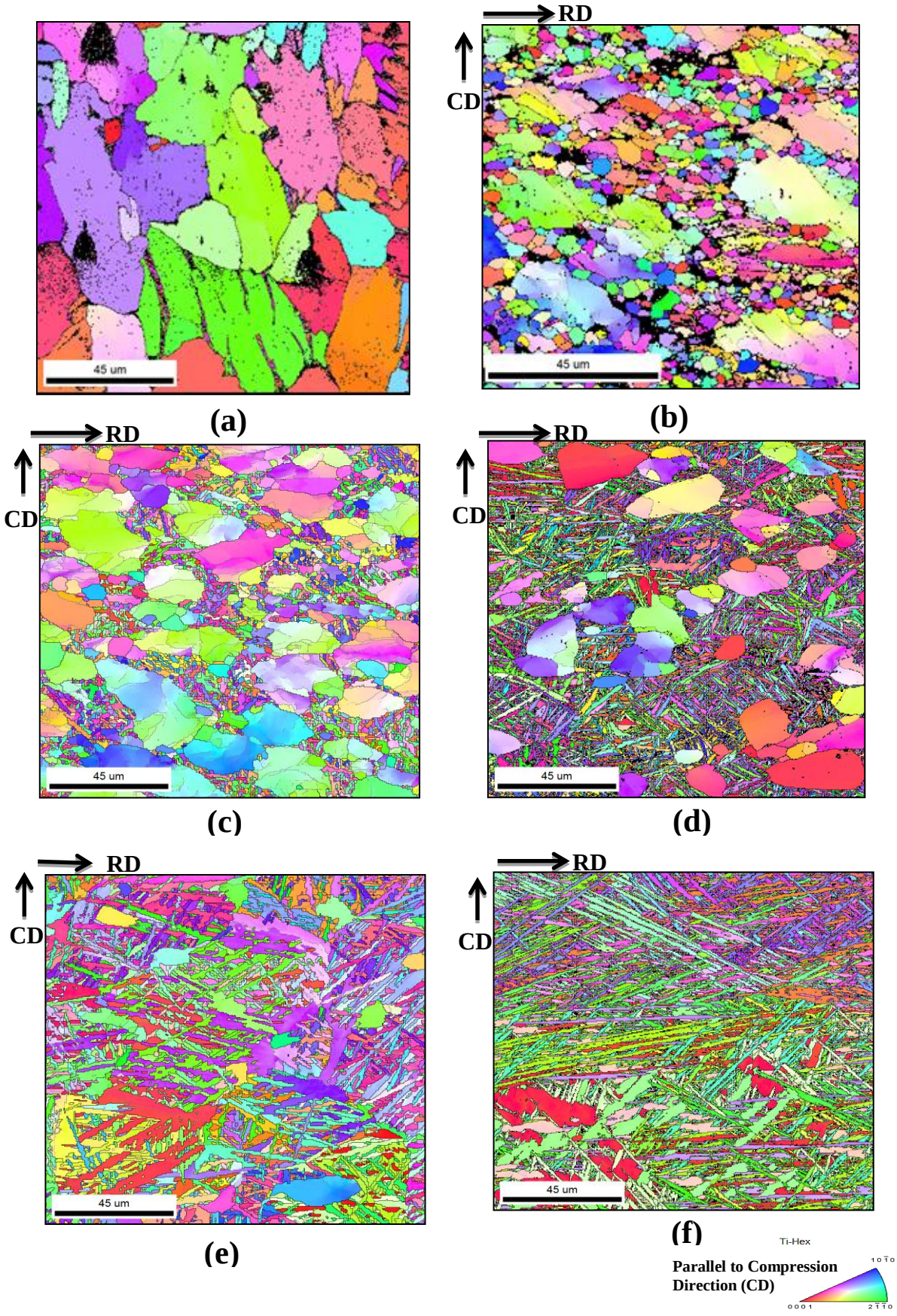

Fig.2: Inverse Pole Figure (IPF) color map of as received and 50% hot compressed IMI 834 titanium alloy at 0.001/s strain rate: (a) As Received (b) 900^{0}C (c) 950^{0}C (d) 975^{0}C(e)1000^{0}C (f) 1050^{0}C.CD and RD represent Compression Direction and Rolling Direction.

The as-received material has large equiaxed α_p grains and thick α_s lamellae (in transformed β). Hot compression of IMI 834 at 900^0C at a strain rate of $0.001s^{-1}$, shown in figure 2(b), resulted in deforming the big α grains and the thick α lamellae into sub grains and developed new strain-free small α grains through DRX. IMI 834 alloy at 900^0C mostly contains α phase [6] and hence, deformation of α grains into sub grains and then dynamically recrystallized small grains are expected[8]. Increasing the temperature up to 950^0C and 975^0C results in nearly 10% and 20% of β phase [6] and hence, hot compression at these temperatures results in two phase deformation condition.Figure.2(c) and 2(d) shows the deformed microstructures of IMI 834 alloy at 950^0C and 975^0C respectively at a strain rate of $0.001s^{-1}$. There is a mix of structures found in 950^0C microstructure (Figure 2(c)): which consists of deformed big α grains having sub grain boundaries and also small DRX α grains and α lamellae. On the other hand, microstructure of the material deformed at 975^0C (Figure 2(d)) showed only deformed big α grains having sub grain boundaries and thin α lamellae. Further higher temperatures take IMI 834 alloy close to the single β phase region and hence mostly results into β phase deformation only. Figure 2(e) shows 1000^0C(near single β phase region) deformed microstructure which consists of very small fraction of deformed equiaxed α_p grains and mostly remaining β phase transformed α_s laths. Further deformation at 1050^0C temperature (single β phase region) at a strain rate of 0.001/s, as shown in Figure 2(f), clearly shows the absence of equiaxed α_p grains and presence of α laths from a transformed beta condition. Mostly deformation occurs in the β grains (BCC) which upon further cooling got converted into secondary alpha laths (α_s) laths following Burger Orientation Relationship (BOR).

CONCLUSIONS

Processing map is developed for 50% deformation using hot compression tests on IMI 834 titanium alloy(consisting of equiaxed α_p and transformed β microstructure) at five temperatures (900^0C, 950^0C, 975^0C, 1000^0C and 1050^0C) and five strain rates (0.001/s, 0.01/s, 0.1/s,1/s and 10/s). Microstructural observations are presented for 0.001/s strain rate and temperatures of 900^0C, 950^0C, 975^0C, 1000^0C and 1050^0C. The following conclusions may be drawn:

- Maximum power dissipation efficiency value (0.56) is obtained at 975^0Cat a strain rate of 0.001/s.
- Hot compression at 900^0Cis mostly resulted into breaking down of big equiaxed α grains into sub grains and several small DRX α grains are formed.

- Hot compression at 950^0C and 975^0C (in α+β region) generated deformed α grains having sub grain boundaries, small DRX α grains and α lamellae.
- Near single β phase region (at 1000^0C and 1050^0C) hot compression mostly resulted in deformation of β phase and a transformed β structure

REFERENCES

[1]. T Noda, M Okabe, S Isobe, S Nishikiori, H. Hattori (1995);Proceedings of the VIII World Conference on Titanium, Birmingham, U.K (1995) pp.2258–2264.

[2]. R.R. Boyer (1996); Materials Science and Engineering A, 213, 103–114.

[3]. D.F. Neal (1988). In: Proceedings of the 6th World Conference on Titanium, France (1988) pp. 253-258.

[4]. V Gopala Krishna, Y.V.R.K. Prasad, N.C. Birla, G.Sambasiva Rao (1997); Journal of Materials Processing Technology 71, 377-383.

[5]. Y.V.R.K. Prasad, T. Seshacharyulu (1998); Materials Science and Engineering A, 243, 82–88.

[6]. P Wanjara, M Jahazi, H Monajati, S Yue (2006); Materials Science and Engineering A, 416, 300–311.

[7]. L Miaoquan, P Hongsi, L Yingying, L Jiao (2007); Journal of Materials Processing Technology 183, 71–76.

[8]. D He, J.C. Zhu , Z.H. Lai, Y Liu , X.W. Yang (2013); Materials and Design 46, 38–48.

[9]. I Balasundar, T Raghu, B.P. Kashyap (2013); Materials Science Forum Vol. 710, 533-538.

National Conference on Thermo-mechanical processing of Steels &
5th Gleeble User Workshop India (GUWI-2015),
August 6-7, 2015, pp 29-40.

Overview of Experimental Activities Using Gleeble 3800 system at IPR

Alpesh Patel*, Shailesh Kanpara, K.P.Singh, Sudhir Tripathi, Mayur Mehta, Kalpesh Galodiya, S.S.Khirwadkar

Institute for Plasma Research, Bhat, Gandhinagar 382 428, India

*Email : akpatel@ipr.res.in

ABSTRACT

Gleeble 3800 system at Institute for Plasma Research (IPR) has been used for various materials research activities which include development of pure tungsten & tungsten alloys by powder metallurgy, miniature specimen testing, dissimilar materials joining, thermal fatigue tests, high temperature tensile tests, HAZ simulations, Compression tests, etc. Single step sintering of tungsten powder having APS 6-10µm was performed using graphite mould at 1600°C-1800°C and 40MPa pressure. The density of the sintered tungsten could achieve 94% of theoretical density of tungsten. Miniature specimen testing technique has been established in which XM-19 steel specimen having dimension 1mm (thickness) x 14mm (length) has undergone the tensile test at 200°C under vacuum environment, controlled heating of the small size sample specimen was a problem and challenging task so the parallel heating technique was used to heat the specimen. Series of experiments were performed on diffusion bonding for dissimilar materials joining such as SS 316L to CuCrZr, Tungsten to CuCrZr and Tungsten to SS 316L using different interlayer at temperatures range from 800°C-1000°C, with varying pressure of 5MPa to 15MPa and holding time of 15min-30min and then optimized the diffusion bonding parameters. Thermal fatigue tests on Tungsten coated SS 316LN sample was performed at 500°C for 1000nos. cycles to qualify samples for its operational requirements. Similarly, thermal fatigue test was performed on EB welded CuCrZr samples at temperature range of 200°C-50°C for 5000nos. of cycles. Tensile testing of tungsten flat specimen having dimension 2.50mm (thickness) and 100mm (length) was performed from 400°C-1100°C. The methodology adopted for conducting the different experiments, and results of the experiments will be presented and discussed in the paper.

***Keywords** : Tungsten Sintering, Miniature specimen testing, Dissimilar materials joining, Thermal fatigue Test, Tensile testing*

INTRODUCTION

First wall and divertor components of ITER like plasma fusion reactor involves various technological challenges like development of high temperature materials - pure tungsten and tungsten alloys, Characterization of materials at elevated temperatures, dissimilar material

joining of CuCrZr to Tungsten, CuCrZr to SS 316LN, Tungsten to SS 316LN, SS 316LN to XM 19, operational qualification of the various tungsten coated SS 316LN components, welded joints, diffusion bonded joints and brazed joints [1-10]. Gleeble 3800 system at IPR has been used extensively for all above experimental research studies. Sintering experiments, dissimilar material joining experiments like diffusion bonding and brazing, thermal fatigue tests, tungsten tensile tests and miniature specimen tests are discussed in this paper.

PURE TUNGSTEN SINTERING EXPERIMENTS

Tungsten's characteristics of high melting point of 3420°C, high density of 19.3g/cm^3, low thermal expansion coefficient and superior mechanical properties at high temperature makes it one of the best suitable material for plasma facing components of fusion reactor. To develop the tungsten & tungsten alloy material, pure tungsten sintering experiments are performed using Gleeble 3800 system. For the optimization of pure tungsten sintering parameters, we have considered sintering temperature range from 1600°C to 2200°C & pressing force range from 30 MPa to 100 MPa in order to achieve higher sintered density and other desired properties of Tungsten. We have approached to fabricate the sintered pallet of size 15 mm dia x 3-7mm thick. For these, graphite fixtures are developed as shown in Fig. 1. Tungsten powder of APS 6-10µm is used for the sintering. K type thermocouple is attached to graphite fixture to control the temperature up to 1000°C and above it pyrometer is used to control the temperature of the sintering setup. Experiments are programmed for 1800°C temperature but Gleeble could not heat the sintering fixture set up above the temperature of 1600°C. Sintered pallet at 1600°C is removed from the graphite fixtures and further processed at desired parameters in second stage. In second stage sintered pallet is heated to 1800°C temperature and pressure of 40MPa is applied. Experiments are performed in vacuum environment.

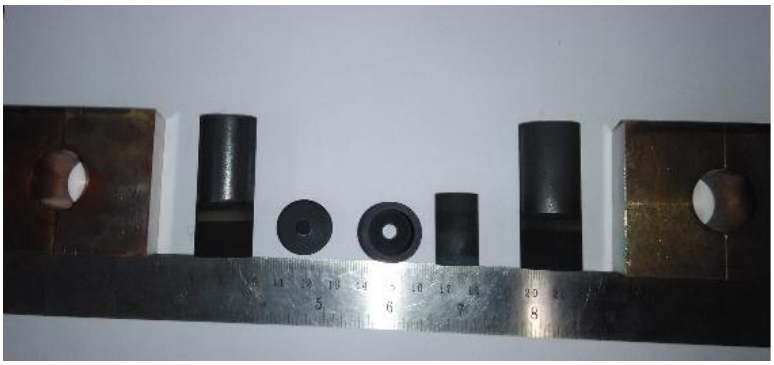

Fig. 1: Graphite Fixtures for sintering experiments

Figure 2 represents the tungsten sintered pallet, synthesized using Gleeble 3800 system. Sintered density of tungsten pallet was measured using Archimedes method which is achieved ~ 93.50% of theoretical density Figure 3 shows microstructural analysis of the tungsten sintered pallet obtained through optical microscopy. Average grain size of as sintered pallet is found to be 6 to 8µm.

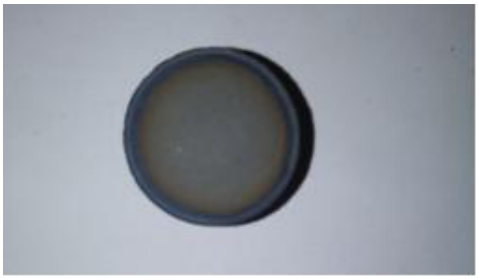

Fig. 2: Gleeble processed Tungsten sintered pallet

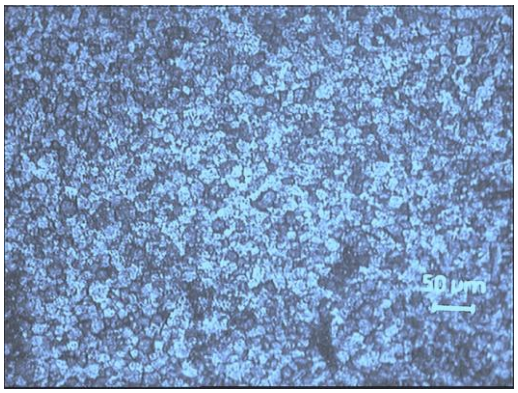

Fig. 3: Microstructure of as sintered Tungsten pallet

DISSIMILAR MATERIAL JOING EXPERIMENTS

Diffusion bonding experiments and brazing experiments are performed using Gleeble 3800 system. The three key variables for diffusion bonding are (i) Temperature (ii) Pressure and (iii) Holding time which decides the best diffusion bonding condition of two dissimilar materials. The temperature was chosen generally 0.7 to 0.9 of absolute m.p of the lowest parent material. Pressure was applied gradually to the materials with bare minimum (below yield stress) to have diffusion bond with least macroscopic plastic deformation in the materials. Sufficient hold time was provided for the interaction of the material (interdiffusion) at the interface. The dissimilar materials joining experiments are performed with an aim to optimize the joining techniques of CuCrZr to SS 316L, Tungsten to SS316L and CuCrZr to Tungsten etc.

Diffusion bonding of SS316L to CuCrZr

Diffusion bonding of the SS316L to CuCrZr materials has been performed with Nickel interlayer and without Nickel interlayer material under deep vacuum with various experimental conditions by varying parameters such as temperatures: 800°C to 1000°C, pressure: 5MPa to 20 MPa and holding time: 15 min to 30min. The pressure was applying gradually from room temperature to the set temperature. Figure 4 shows the photograph of the diffusion bonded samples processed at 1000C, 5MPa, 15Mins hold.

Fig. 4: Diffusion bonded specimen SS/Ni/CRZ processed at 1000C, 5MPa, 15 min

The amount of Nickel diffusion towards Cu side as well as SS side was initiated from 900C onward temperature. From the optical image Fig. 5, uniform Ni diffusion at CRZ and SS side was observed in the specimen processed at 1000C, 5MPa and 15min.

Fig. 5: Optical image of diffusion bonded specimen SS/Ni/CRZ

Diffusion bonding of WCu to CuCrZr

Diffusion bonding of W/Cu/CuCrZr specimen was conducted under vacuum environment in Gleeble system. Bi-material W/Cu (10mm x10mmx7mm) with CRZ (10mmx10mmx10mm) has undergone diffusion bonding experiment with the parameter of 900°C, 5MPa for 5mins. Joining of the material is observed after the experiment. The pressure is applied gradually to 5 MPa on heating from 3 MPa @RT and gradually decreasing from 5MPa to 3MPa @RT. 3MPa is applied to hold the specimen @ Room temperature. Figure 6 show the diffusion bonded sample and diffusion bonding cycle.

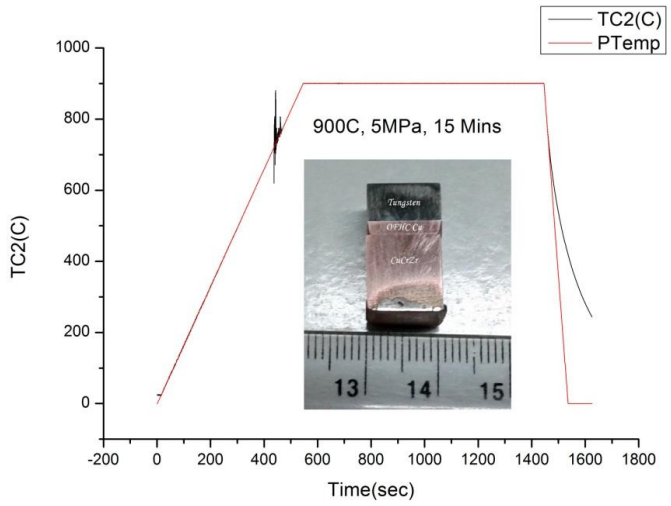

Fig.6: Diffusion bonding cycle and diffusion bonded specimen

Diffusion bonding of Tungsten to SS 316L

Pure tungsten material with SS316L material were undergone diffusion bonded using Titanium interlayer under vacuum environment with different experimental conditions by varying parameters such as temperature: 800°C to 1100°C, pressure: 5MPa to 20 MPa and holding time: 15 min to 20 min. Figure 7 shows the specimen processed at 1000°C, 5MPa and 15 mins hold.

Fig. 7: Diffusion bonded specimen W/Ti/SS processed at 1000C, 5MPa and 15 min

Several joining of the dissimilar materials such as W to SS using Ti inter layers and Ni interlayer have been carried out successfully by diffusion bonding approach. The joint integrity was undergone ultrasonic tested.

Brazing Experiments

Short cycle brazing experiment for SS316L joining with CuCrZr material has been carried out @ 970°C for 5 mins hold using Gleeble system using NiCuMn-37 filler material under deep vacuum of 10^{-5} mbar environment. Figure 8 shows the brazing cycle. Total time taken to braze the specimen was 1200sec i.e. 20 minutes.

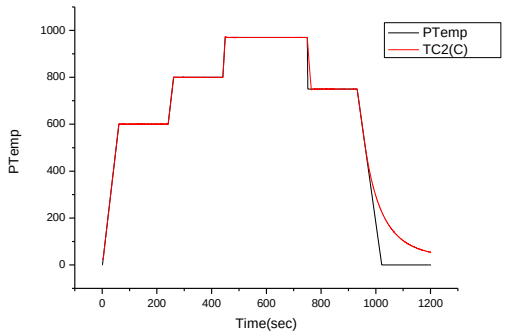

Fig. 8: Vacuum Brazing cycle for SS316L to CuCrZr @ 970C

THERMAL FATIGUE TESTS

Thermal fatigue experiments are performed on tungsten coated SS 316LN specimen and EB welded CuCrZr specimen to qualify them for their functional requirements.

Thermal fatigue tests of Tungsten Coated SS 316LN specimen

Total 1000nos. of thermal fatigue cycles are performed on Tungsten (W) coating on SS 316LN substrate sample which is developed using Atmospheric Plasma Spray (APS) technique at ARCI, Hyderabad. Figure 9 shows the Tungsten coated SS 316LN specimen loaded into the Gleeble test chamber. Figure 10 shows the SEM image at the interface between tungsten coating and SS substrate. Average thickness of Tungsten coating measured more than 200micron.

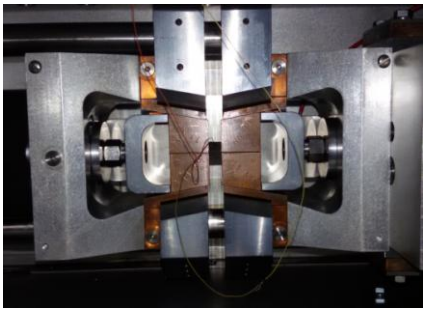

Fig. 9: Tungsten Coated SS sample loaded in to Gleeble test chamber

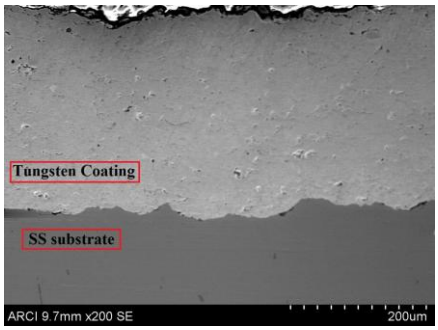

Fig. 10: SEM image at the interface between Tungsten Coating and SS Substrate

Thermal Cycles are performed for maximum temperature of 500°C and minimum programmed temperature of 50°C. Holding time at 500°C is 5Sec. Sample is heated at the rate of 50°C/sec and programmed cooling rate was 30°C/sec. Full contact square copper grips are used to hold the specimen during the experiments. Experiments are performed in high vacuum conditions. After 1000nos. of thermal fatigue cycle no delamination of coating is observed. Figure 11 shows the recoded thermal fatigue cycles on the sample.

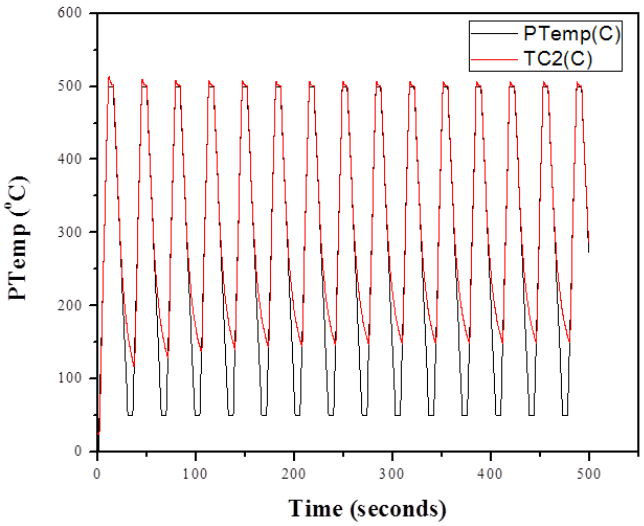

Fig. 11: Thermal Cycles performed on to the specimen

Thermal Fatigue tests of EB welded CuCrZr specimen

Thermal Fatigue tests are performed on EB welded CuCrZr specimen using Gleeble 3800 systems. Figure 12 shows the EB welded CuCrZr Specimen. Specimen is having dimensions of 10mmX20mmX20mm.

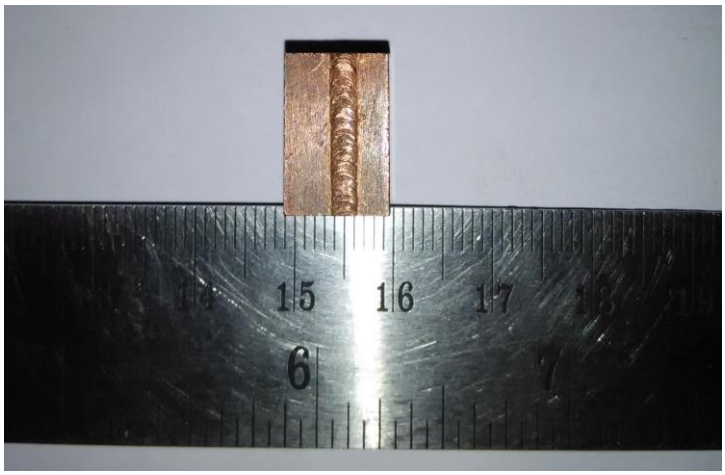

Fig. 12: EB welded CuCrZr Specimen

Total 5000 nos. of thermal cycles are performed onto the specimen. In each cycle specimen is heated to 200°C temperature in 3sec and kept hold for 1sec at 200°C then it was water quenched for 3sec to room temperature. High flow water quench system is used to quench the specimen from 200°C to room temperature. Thermal cycles performed on the specimen are recorded as shown in Fig. 13.

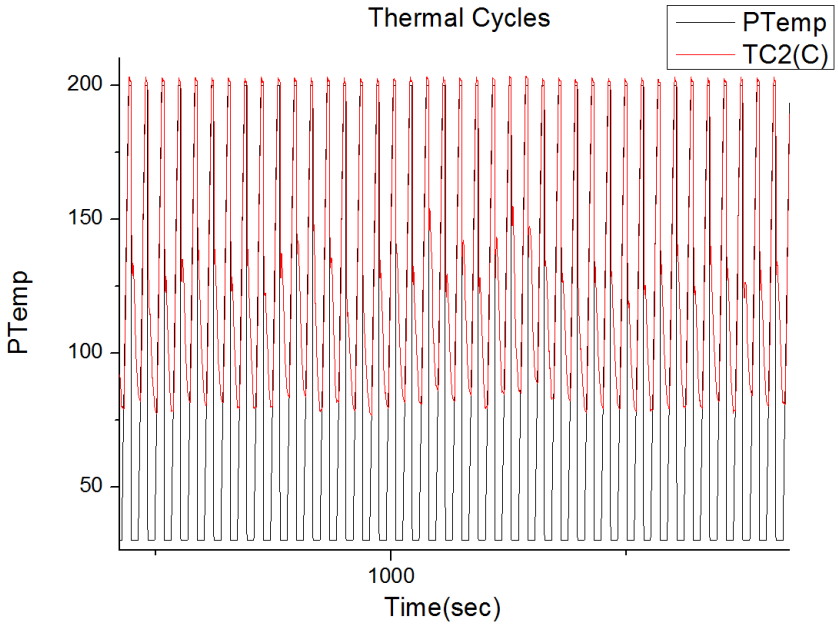

Fig. 13: Thermal cycles performed on the specimen

PURE TUNGSTEN TENSILE TESTS

Pure Tungsten tensile tests are conducted using Gleeble 3800 system. These tests are performed using flat shape tungsten specimens. The test specimens are prepared from commercially available tungsten sheet (purity~99.9%) (make Plansee Inc), with thickness of 2.5mm. Tungsten sub size specimen for tensile testing has been prepared by employing EDM wire cut method. Tungsten being a highly brittle material at room temperature, loading of sample in Gleeble test chamber needs to be done very precisely. K type thermocouple is been used to control the temperature during the experiments.

Tests are performed at strain rate of 0.01 and in temperature range of 400°C-1200°C. Tests are performed successfully above the 600°C temperature but the test at 400°C remains failed as specimen broke down from the pin contact region. Figure 14 shows the tensile tested tungsten specimens at different temperatures.

Fig. 14: Tensile tested specimens

MINIATURE SPECIMEN TESTING

Miniature specimen testing is attempted using Gleeble 3800 system. Miniature specimens and fixtures are fabricated from the XM-19(UNS S20910) material using EDM wire cut technique. Miniature specimen is having thickness of 1mm and length of 14mm. Specimen is tested at 200°C temperature and 0.01 of strain rate. Controlled Heating of miniature size specimen is the challenging part of these experiments. Parallel heating technique is used for controlled heating of the specimen.

Figure 15 shows the tensile tested miniature specimen. Figure 16 shows the programmed temperature and controlled heating of the specimen. Measured UTS of the XM-19 specimen is 592MPa at 200°C as shown in fig. 17.

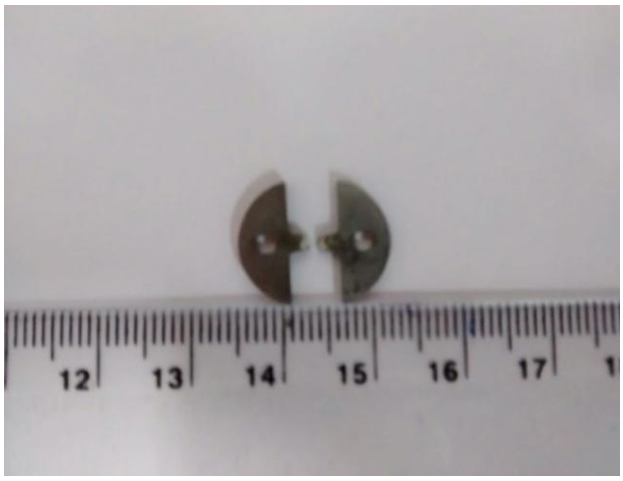

Fig. 15: Tensile tested miniature size specimen

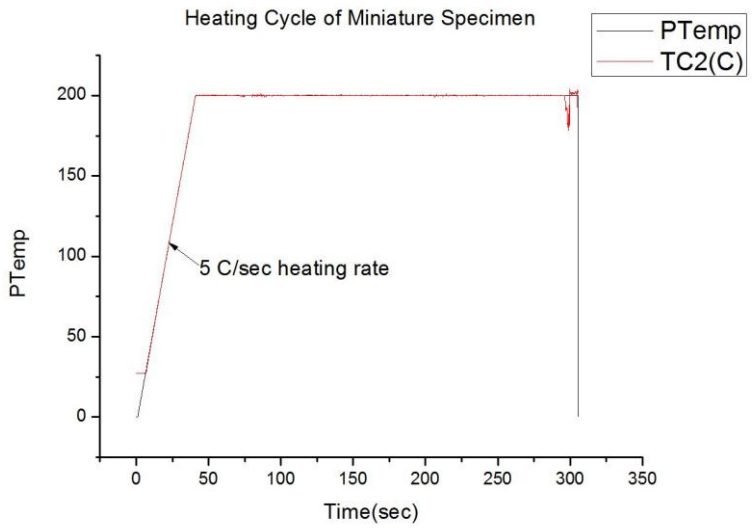

Fig. 16: Heating Cycle of Miniature Specimen

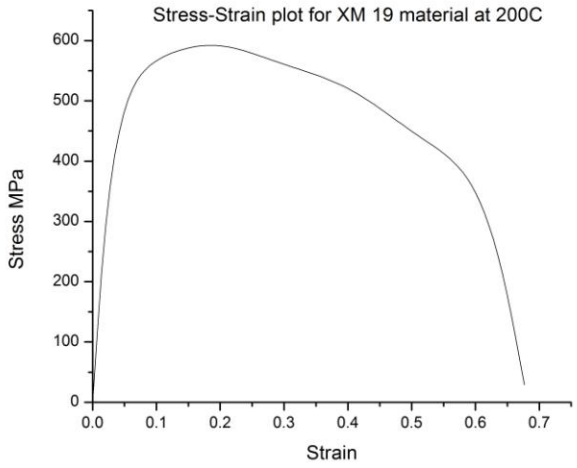

Fig. 17: Stress Strain Plot for XM 19 material at 200°C

CONCLUSION

Pure tungsten sintering experiments are performed using Gleeble 3800 systems. Maximum 93.50% of theoretical density is achieved of sintered pallet. Future work will be focused on optimization of the sintering fixture and sintering parameters to achieve higher densification of tungsten material with desired properties. Dissimilar material joining experiments were performed successfully by diffusion bonding and vacuum brazing methods. Diffusion bonding parameters like pressure, temperature and holding time are the crucial parameter to

define the sound joint between two dissimilar materials. Optimization of the process parameter for diffusion bonding and vacuum brazing is an ongoing works.

Thermal fatigue cycle experiments are successfully performed as per the operation requirements of different specimens. Tungsten tensile tests are performed at various temperature of 400C-1200°C. It is found that for temperature above 600°C, tensile tests are performed successfully. Tensile test at 400°C remains failed as specimen broken down from the pin region in grip contacts. Miniature specimen testing using Gleeble 3800 system is attempted. Miniature specimen is successfully tested at 200°C temperature.

ACKNOWLEDGEMENT

The authors are sincerely thankful to Mr. Jainish Topiwala and Mr. Hitesh Patel for their contribution in conducting thermal fatigue tests of EB welded CuCrZr material specimen. The authors are thankful to Dr. Charulata Dubey for her contribution in conducting tungsten tensile tests. The authors are also thankful to ARCI, Hyderabad for providing the Tungsten coated samples to carry out thermal fatigue experiments.

REFERENCES

[1]. G. Partheepan, D.K. Sehgal, et al. "Finite Element Application to Estimate In-service Material Properties using Miniature Specimen" International Journal of Aerospace and Mechanical Engineering 2:2 2008

[2]. Sunil Goyal, V. Karthik, et al. "Finite element analysis of shear punches testing and experimental validation" Materials and Design 31 (2010) 2546–2552

[3]. V. Karthik, P. Visweswaran, et al. "Tensile–shear correlations obtained from shear punch test techniqueusing a modified experimental approach" Journal of Nuclear Materials 393 (2009) 425–432

[4]. Avijit Mondal, Anish Upadhyaya "Effect of heating mode on sintering of tungsten" Int. Journal of Refractory Metals and Hard Materials 28 (2010) 597–600

[5]. Small Specimen Test Techniques - 5th Volume – Journal of ASTM international special technical publication STP1502

[6]. Powder Metallurgy: Science, Technology, and Materials – Anish Upadhyaya, G.S. Upadhyaya

[7]. Charu Lata Dube, Alpesh Patel, et al. "High Temperature Tensile Properties of Tungsten" 1st International conference on structural integrity – ICONS 2014

[8]. K.P Singh, Alpesh Patel, et al. "Study the Effect of Thermal Cyclic On SS316L to CuCrZr Brazed Joint" 29th National Symposium on Plasma Science & Technology (PLASMA 2014)

[9]. Shailesh Kanpara, G. Sivakumar, et al. "Development of Tungsten Coating using Atmospheric Plasma Spraying for First Wall Applications in Fusion TOKAMAK" 6th Asian Thermal Spray Conference (ATSC-2014)

[10]. K.P Singh, S.S Khirwadkar, et al. "Studies for The Optimization Of Brazed PFC Using Coupon Based Samples" 27th National Symposium on Plasma Science & Technology (PLASMA 2012)

National Conference on Thermo-mechanical processing of Steels &
5th Gleeble User Workshop India (GUWI-2015),
August 6-7, 2015, pp.41-56.

Role of Precipitate in Strain Induced Martensitic Transformation during Cold Deformation of SS 321

Sayandeep Kundu[a], R Maladkar[a] , A. K. Singh[a] and M. M. Hussain[a]

[a]Atomic Fuels Division, Bhaba Atomic Research Centre
Email : sayank@barc.gov.in; maladkar@barc.gov.in; arunks@barc.gov.in; hussain@barc.gov.in

ABSTRACT

Austenitic stainless steels are extensively used in many areas of application because of their superior corrosion resistance and satisfactory mechanical properties. Amongst various grades of stainless steel, titanium stabilized SS 321 is chiefly used for high temperature structural application due to its extraordinary stability against sensitization at higher temperature. Titanium tends to form carbides/carbonitrides, thereby reducing the carbon content in the austenitic matrix. This helps preventing sensitization problem. The stability of austenitic phase at room temperature is key factor to govern the propensity of strain induced martensitic transformation during cold deformation of austenitic stainless steels. Titanium is a strong ferrite stabilizer. The effect of dissolved titanium content in austenite/ the percentage precipitation of titanium on the stability of austenite were studied. Solutionized and as-received specimens were considered for experiments. Solutionizing was done at 1100^0C for 30 mins and then water quenched. One of the solutionized specimens was heated at a slow rate of approx. 5^0 C/minute from room temperature to 1100^0C, while the other one was rapidly heated upto the solutionizing temperature. As received structure showed austenitic matrix along with coarse titanium carbide precipitates. Tensile tests on samples were carried out and the volume percentage of the strain induced martensite in each specimen was estimated with a calibrated ferritscopic measurement. Optical microscopy, SEM and EDAX were also performed to find out grainsize, morphology and composition of titanium rich precipitates and regions of austenitic matrix. The results showed a higher propensity of strain induced martensitic transformation in case of solutionized samples. The effect of strain rate on the transformation was also realized through carrying out tensile tests at different strain rates on as received specimens. A faster test was seen to hinder martensitic transformation, quite expectedly, possibly because of adiabatic heating.

Keywords: *Austenitic stainless steel, Titanium, Strain Induced Martensite*

INTRODUCTION

Austenitic stainless steels are used in wide range of applications for their superior corrosion resistance and acceptable formability. AISI 321 grade has titanium carbide precipitates on austenitic matrix, which provides high temperature resistance to sensitization problems. For manufacturing structural parts with complex geometry, it is imperative to predict the

deformation behaviour of the concerned material. The austenitic phase of stainless steels is known to be in a metastable state at room temperature and therefore is prone to transform into martensitic phase subject to cold deformation. This martensitic transformation is popularly known as strain induced martensitic tranfsormation. The propensity of martensitic transformation depends on several factors namely composition, strain rate during deformation and temperature. Researchers[1] have found a close correlation between the stacking fault energy and the propensity of martensitic transformation during cold deformation. Olson and Cohen[2] have shown the mechanism of strain induced martensitic transformation at the intersections of shear bands on austenitic matrix during cold deformation. The tendency of shear band formation depends directly on the stacking fault energy, which again depends largely on composition and temperature. In many cases the strain induced martensite is hcp, in many cases with continued straining hcp transforms to bcc, whereas in other cases it is only the bcc martensite that has been observed during deformation[3]. The autocatalytic nature of martensitic transformation during deformation has a direct effect on the deformation behaviour. A uniaxial tensile test on metastable austenitic stainless steels shows an increasing work hardening rate due to the transformation, which increases the uniform elongation as per the Considere criterion.

It is a well known fact that titanium is a strong ferrite stabilizer. This can be demonstrated using Schaffler's Phase Map [Fig.7] using nickel chromium equivalents. Moreover dissolved titanium content in austenite has been reported to reduce stacking fault energy of austenite. AISI 321 in the as-received condition has titanium carbide precipitates on austenitic matrix. The dissolved titanium content in austenitic phase is essentially little or zero in this condition. A solutionizing heat treatment at a higher temperature should increase the dissolved titanium content in austenitic matrix. The following study attempts to find out the effect of dissolved titanium content or the percentage precipitation of titanium on the deformation behaviour of SS 321 through martensitic transformation.

THERMODYNAMICS OF STRAIN INDUCED MARTENSITIC TRANSFORMATION

A mechanical driving force (Fig. 1) combined with the chemical driving force is essential to induce martensitic transformation fecilitating yielding below a temperature M_S^{σ} (Fig.2).[4] Beyond this temperature, plastic deformation facilitates the formation of martensite. Olson et al[5] demarcated the two types of martensite as stress induced and strain induced martensite

respectively. The upper limiting temperature for strain induced martensitic transformation is referred to as M_d. While the mechanical driving force for stress induced martensite is a function of normal and shear components along with orientations, the same for strain induced martensite transformation remains unclear. Olson et al argued that the deformation aids in stain induced nucleation by formation of energetically favorable nucleation sites for martensite nucleation. The effect of applied stress on the other hand enhances its growth.

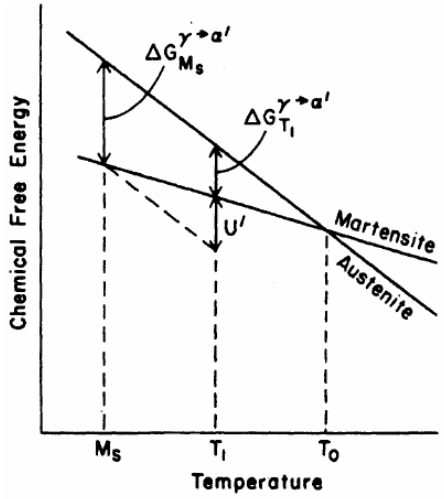

Fig. 1: Thermodynamic driving force for martensitic transformation (Wayman and Bhadeshia, 1996)

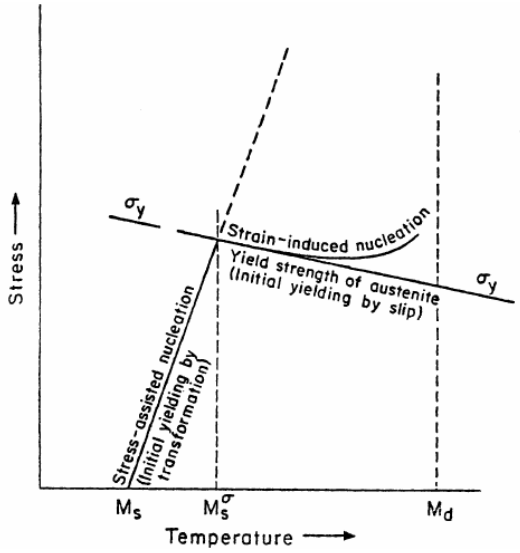

Fig. 2: Illustration of stress-assisted and strain induced nucleation of martensite (Olson and Cohen, 1972)

In austenitic stainless steels, intersections of shear bands on austenitic matrix have been observed to serve as the nucleation sites for martensitic transformation. This has been explained thoroughly in the work of Olson et al on the basis of an earlier work by Bogers et al. [6] Researchers [7] [8] have found the presence of both bcc and fcc martensites at the intersections of shear bands consisting stacking faults, mechanical twins or highly faulted hcp martensites.

INFLUENCE OF STACKING FAULT ENERGY

Stacking fault plays a major role in governing the nature of deformation. For inducing shear bands to intersect either for $\gamma \rightarrow \varepsilon \rightarrow \alpha'$ transformation or for $\gamma \rightarrow$ mechanical twins $\rightarrow \alpha'$ transformation, the stacking fault needs to be lower. A higher stacking fault energy will gradually change the mode of deformation from ε martensite transformation to complete mechanical twinning and then to slip. Hence a greater propensity of α' martensitic transformation is expected for austenite with lower stacking fault energy if it is considered that ε martensite in the shear band acts as the precursors to α' transformation. The influence of stacking fault energy can be well understood with the schematic suggested by Remy and Pineau [9] for Fe-Mn-Cr-C alloys. (Fig. 3).

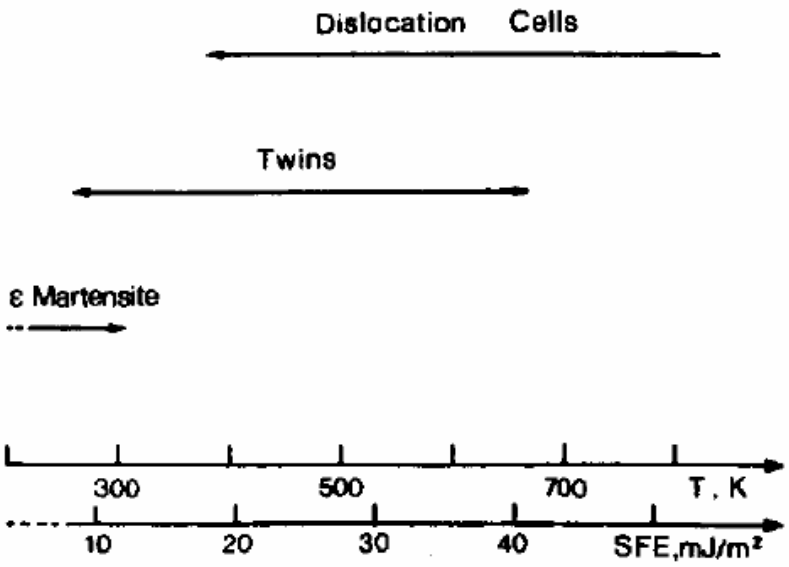

Fig. 3: Effect of temperature and stacking fault energy on deformation structure for Fe-Mn-Cr-C system (Remy and Pineau, 1977)

EXPERIMENTAL PROCEDURE

AISI 321 strips and tensile specimens of thickness 0.4 mm (Fig. 4) were taken for experiments. An XRF measurement was done to estimate the composition of the strips in the experiment (Table 1). Samples considered for the subsequent experiments were of three categories: a) as-received b) solutionized at 1100^0C for 30 mins and water quenched and c) heated from room temperature to 1100^0C at 5^0C/min and solutionized for 30 mins and water quenched. Optical microscopy and Scanning Electron Microscopy with EDAX were done on the specimens for characterization as well as percentage dissolution/precipitation of titanium in the as received and heat treated conditions. Tensile tests at strain rates ranging from 10^{-4}/sec to .047 /sec were done on as-received specimens. As far as the solutionized samples are considered, for category (b), tensile tests were carried out at strain rates ranging from 10^{-4}/sec to 10^{-2}/sec and for category (c), only at strain rate 10^{-3}/sec. All the tensile samples were drawn till necking, and the necked specimens were investigated through a well calibrated Ferritscope for estimation of strain induced martensitic content at different regions in the gauge part of each specimen. The Ferritscope was calibrated against reference samples containing ferrite of 0.53%, 2.48%, 14.1%, 14.4%, 30.9% and 85%. (Fig. 5).

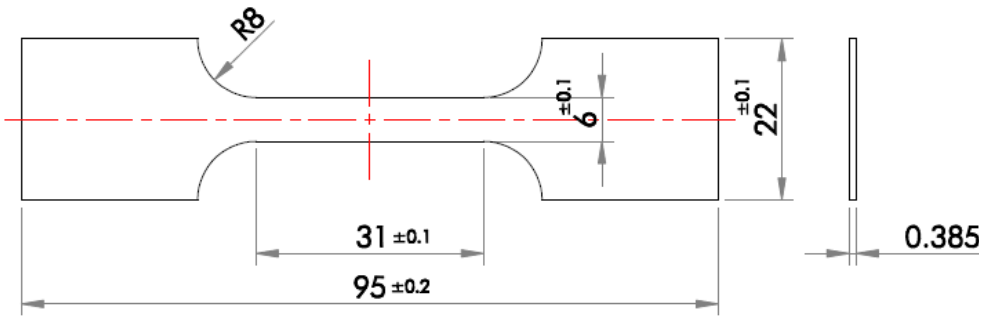

Fig. 4: Drawing of tensile specimen

Table 1: Composition of AISI 321 strip estimated through XRF

Si	Ti	V	Mn	Ni	Cu	Mo	Cr	Fe
0.5	0.55	0.05	1.15	10.31	0.25	0.142	17.31	Bal.

Fig. 5: Ferritscope arrangment with reference samples of different ferrite content for calibration

Solutionizing heat treatments were done in two ways. For one set, the specimens were rapidly heated upto 1100^0C and solutionized for thirty minutes and then were water quenched. For the second set, the specimens were put into the furnace at room temperature and heated at 5°C/min till 1100°C and solutionized for 30 mins and then water quenched. All solutionizing heat treatments were done inside a fixture of SS 316L with a continuous purging of inert helium at 5 lps till the end of quenching to prevent oxidation. The arrangment of fixture is shown in Fig. 6.

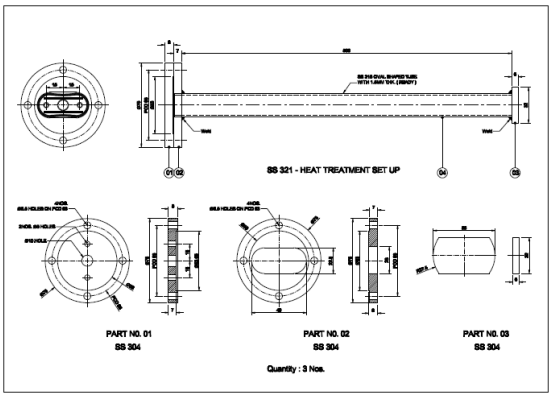

Fig. 6: Arrangement of SS fixture for heat treatment

For metallography, the samples were properly ground and polished till mirror finish and then were etched in a solution containing 3 volume parts of hydrochloric acid with 1 volume part of nitric acid. The etching time varied from one set of samples to another.

EXPERIMENTAL RESULTS AND ANALYSIS

Position in Schaffler's Diagram

The relative positions of the material in Schaffler's phase map in solutionized condition and aged condition where titanium is precipitated out were determined through nickel chromium equivalents (Fig. 7). The overall composition of the material was estimated grossly through XRF. (Table 1). The equations for nickel and chromium equivalents were calculated using the following two equations

$$Ni_{eq} = pct\ Ni + 30\ pct\ C + 18\ pct.N + 0.5\ pct\ Mn + 0.3\ pct\ Co + 0.2\ pct\ Cu - 0.2\ pct\ Al \quad (1)$$

$$Cr_{eq} = pct\ Cr + pct\ Mo + 4\ pct\ Ti + 4\ pct\ Al + 1.5\ pct\ Si + 1.5\ pct\ V + 0.9\ pct\ Nb + 0.9\ pct\ Ta + 0.5\ pct\ W \quad (2)$$

The calculated Nickel equivalent is 13.5 for the specimens that were studied. Chromium equivalent should change with dissolved titanium content, as it is suggested by equation (2). A full solutionized specimen has chromium equivalent 20.48, and with no dissolved titanium content it drops down to 18.28. Thus the stability of austenite gets hampered with dissolved titanium as per Schaffler's phase map (Fig. 7).

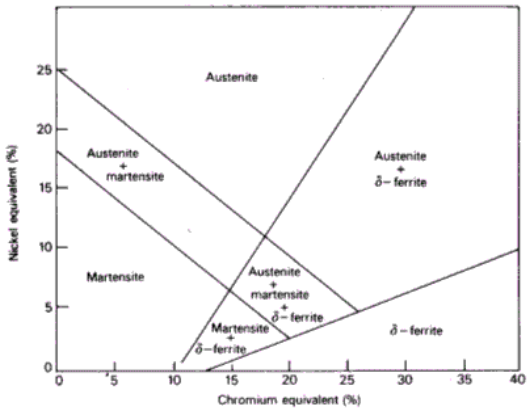

Fig. 7: Schaffler Diagram with positions of full solutionized and full precipitated AISI 321 [ref]

DEFORMATION BEHAVIOUR DURING TENSILE LOADING

The specimens in three different conditions mentioned above showed different work hardening behaviour under uniaxial tensile loading. The deformation behaviour was also observed to change with strain rates. For as received specimens, tensile test at 10^{-4}/sec strain rate showed maximum ductility and a uniform plastic elongation of 0.5 deduced from Considere criterion (Fig. 8a). Faster tesile tests decreased the uniform elongation (Fig. 8b, 8c, 8d). The work hardening behaviour did not manifest any apparent increasing work hardening peak. For solutionized sample category (b), slower tests at 10^{-4}/sec and 10^{-3}/sec showed almost same unifom elongation, while faster test at 10^{-2}/sec showed reduced ductility. (Fig. 9a, 9b, 9c). For category (c) heated slowly to solutionizing temperature, tensile test at 10^{-3}/sec strain rate showed similar ductility. (Fig. 10).

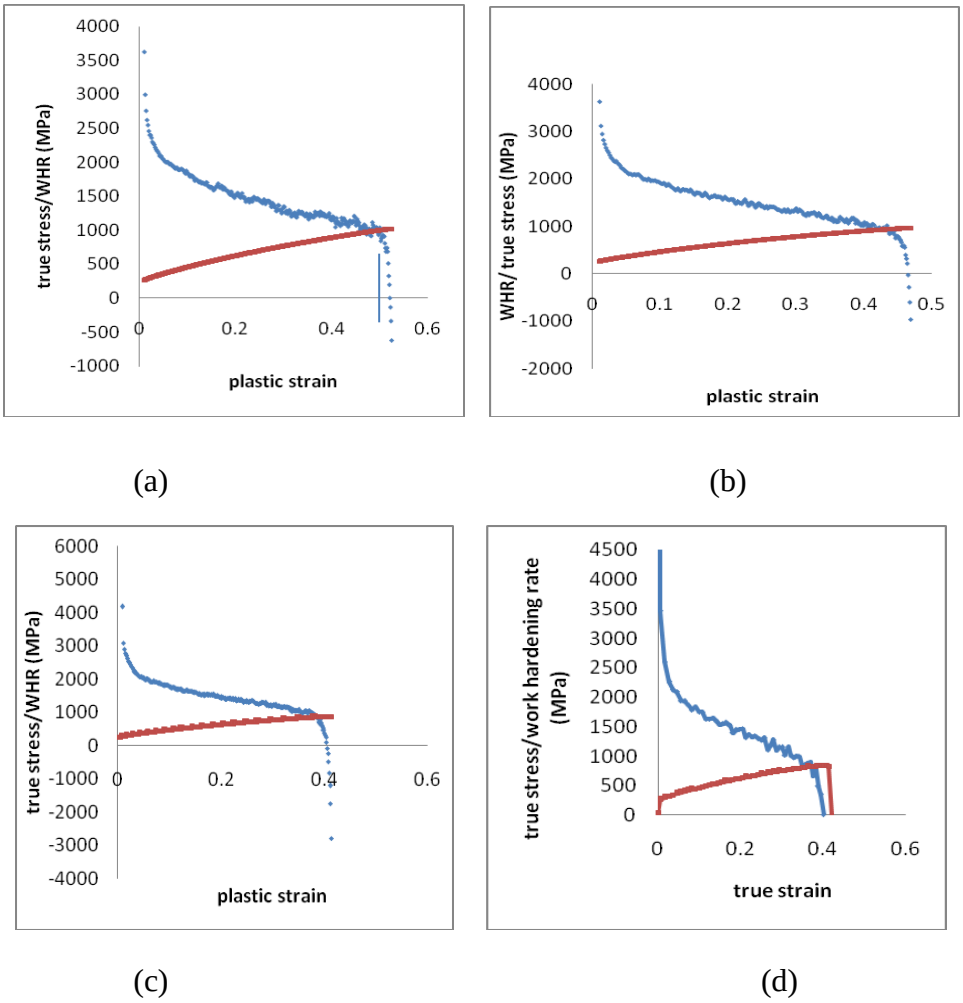

Fig. 8 (a) to (d): Tensile behaiour of as received specimens at 10^{-4}, 10^{-3}, 10^{-2} and 0.047/sec respectively.

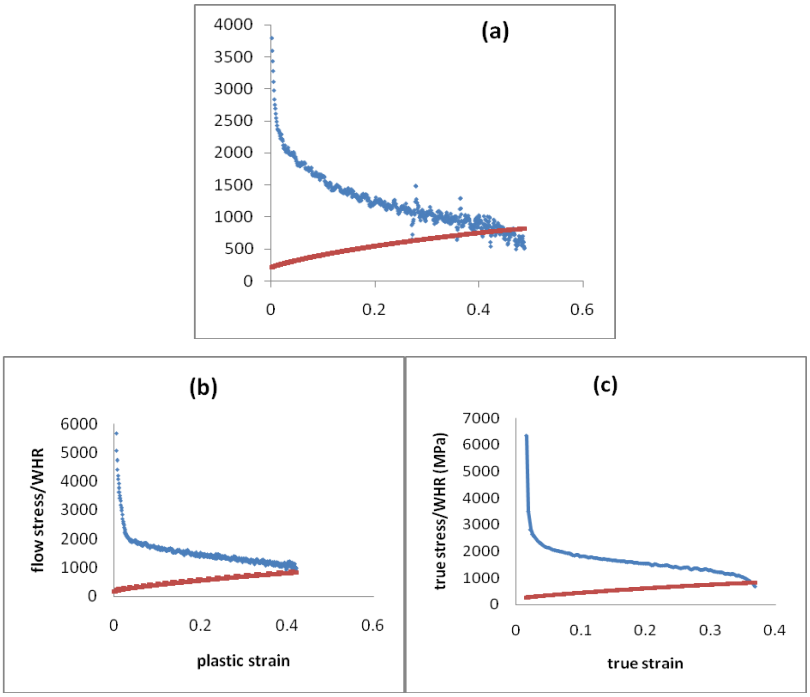

Fig 9 (a) to (c): Tensile behaviour of samples rapidly heated to 1100^{0}C and solutionized for 30 mins and water quenched at 10^{-4}, 10^{-3} and 10^{-2}/sec respectively.

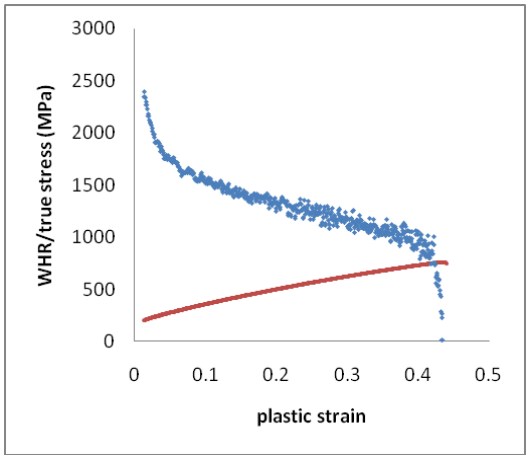

Fig. 10: Tensile behaviour of specimen heated at 5^{0}C/min to 1100^{0}C and solutionized for 30 mins and water quenched (at 10^{-3}/sec)

OPTICAL MICROGRAPH

Optical microscopy of as-received specimen showed uniform grain size with propensity of twins along with coarse precipitate. ASTM grain size of the as-received specimens as observed at 100X magnification (Fig. 11) was 6-7. An anomalous growth of grains was found in the sample heated slowly to solutionizing temperature (category (c)) (Fig. 12). ASTM

grainsize in this sample varied from 5 to 7. Samples rapidly heated to 1100^0C and solutionized for 30 mins showed coarser grainsize (Fig. 13) of ASTM 4-5 with along with visible annealed twins. No precipitate was found in the observed region. ASTM grain size and mean intercept lengths of the three categories of samples have been tabulated in Table 2.

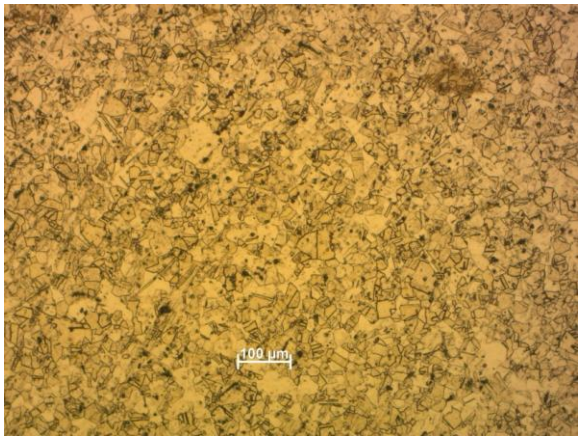

Fig 11: Optical micrograph of as-received specimen at 100X

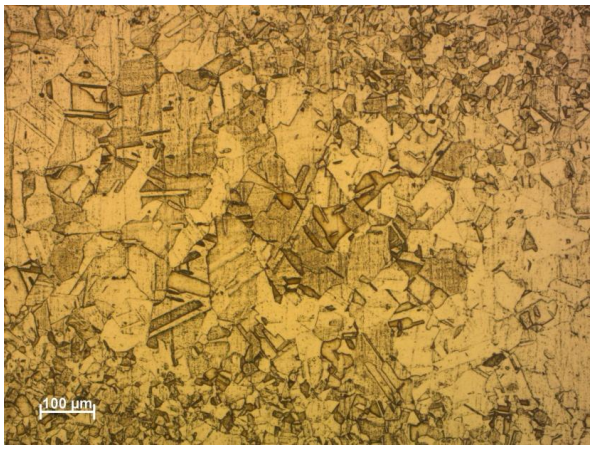

Fig. 12: Anomalous growth of grains in sample slowly heated and solutionized at 100X

Table 2: ASTM grainsize and mean intercept lengths of different specimens

Sr. No.	Specimens	ASTM grain size	Mean intercept length
1.	As received	7	15 microns
2.	Rapidly heated solutionized	4-5	57.78 microns
3.	Slowly heated solutionized	5-7	50 microns

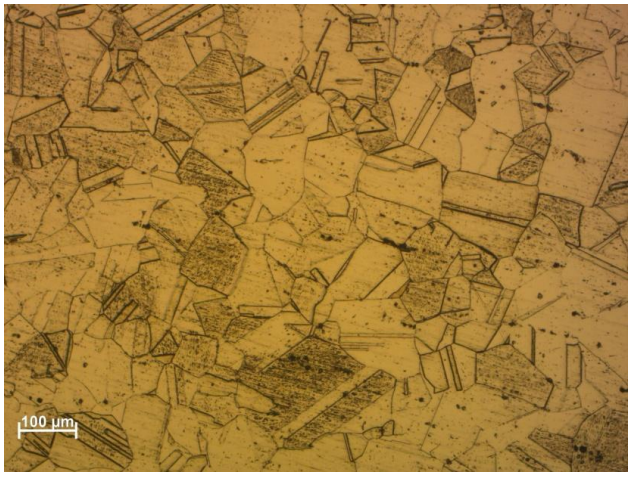

Fig. 13: Optical micrograph of sample rapidly heated and solutionized at 100X

SCANNING ELECTRON MICROGRAPH AND EDAX

Scanning electron microscopy was done on each sample to observe the morphology of grains and precipitates. Both backstattered and secondary electron images were captured. As received structure (Fig. 14) manifested clear anneals twins and presence of coarse rhomboidal precipitates of size 6-8 microns. An EDAX investigation confirmed the titanium enrichment in precipitates. The matrix essentially was devoid of any titanium content. For solutionized samples, rapidly heated and solutionized (category b) showed coarser grainsize with annealed twins with little precipitation (Fig. 15). EDAX investigation was done on 13 positions at different regions on matrix captured at a lower magnification of 100X to get an average composition of dissolved titanium content in the matrix. The same procedure was followed for the other solutionized specimen heated slowly to solutionizing temperature (category c) (Fig. 16). The average content of dissolved titanium content estimated through EDAX at several locations for solutionized samples has been tabulated in Table 3.

Table 3: Dissolved titanium in different specimens

Sr no.	**Specimens**	**Dissolved titanium in austenite**
1.	As received	-
2.	Rapidly heated solutionized	0.43
3.	Slowly heated solutionized	0.33

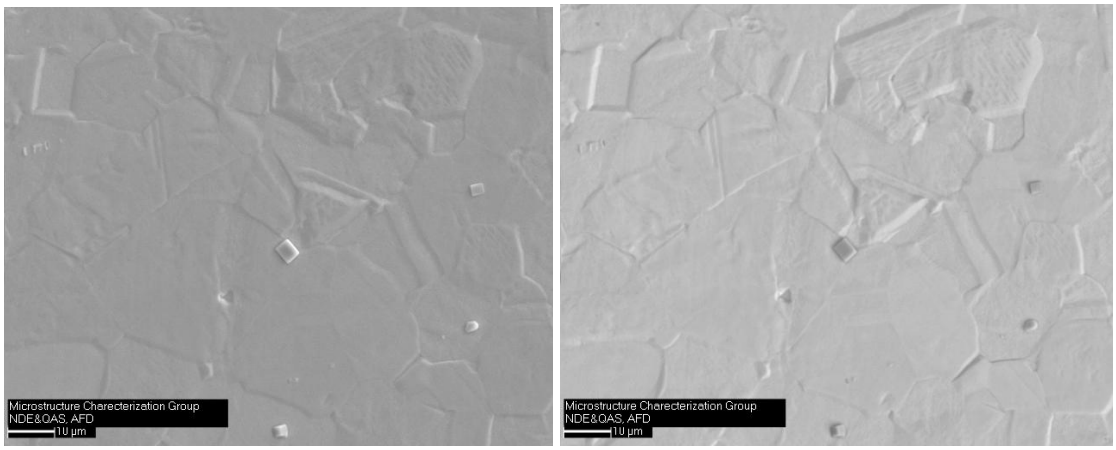

Fig. 14: Secondary electron image (left) and backscattered electron image (right) of as-received specimen showing coarse rhomboidal precipitates at 1000X.

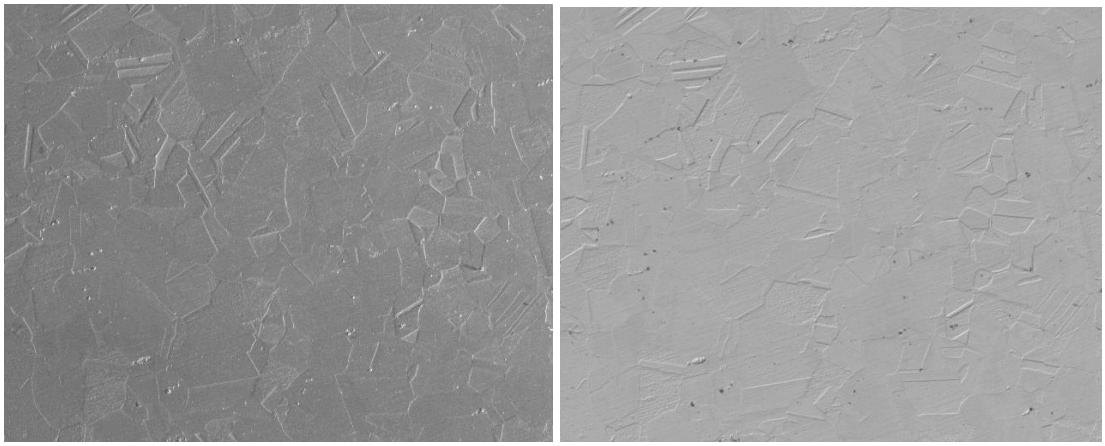

Fig. 15: Secondary electron image (left) and backscattered electron image (right) of samples rapidly heated and solutionized at 100X.

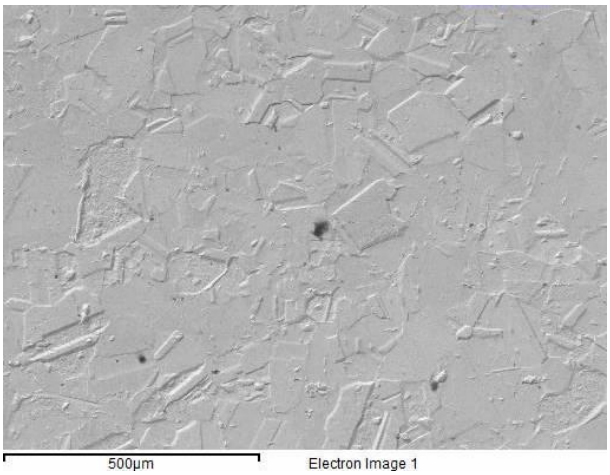

Fig. 16: Backscattered electron image of sample slowly heated and solutionized.

FERRITSCOPE MEASUREMENT

An estimate of strain induced martensite was done through Ferritscope on different regions in the gauge length of necked tensile specimens of all three categories. Ferritscope result revealed the presence of strain induced martensite on all necked specimens. The propensity of strain induced martensite was found to decrease with higher strain rate (Fig. 17). As received specimens showed least tendency to form strain induced martensite under tensile loading, whereas the propensity increased in solutionized samples. (Fig. 18).

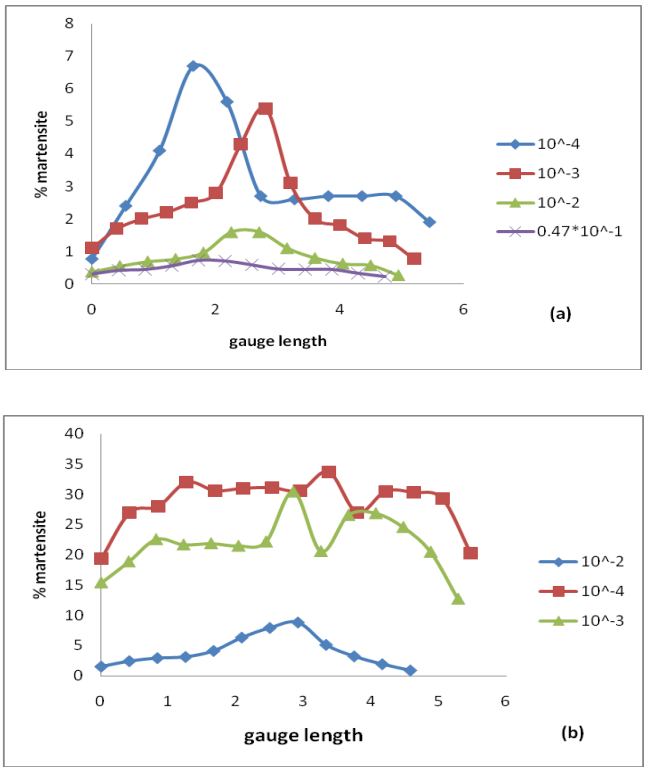

Fig. 17: Percentage martensite formed along the length of necked specimens at different strain rates for (a) as received specimen and (b) rapidly heated and solutionized specimen.

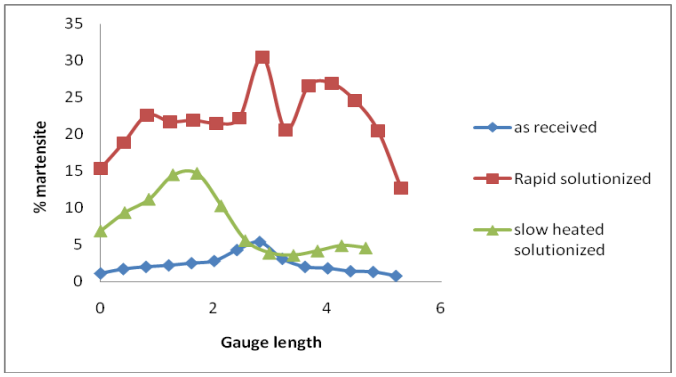

Fig. 18: Martensitic propensity in different conditions of necked specimens strained at 10^{-3}/sec.

DISCUSSION

No apparent peak in work hardening rate was observed for any of the specimens (Fig. 8, Fig. 9, Fig. 10). This may be attributed to a dynamic equilibrium that could have been established between hardening due to autocatalytic martensitic transformation and softening by dislocation annihilation on austenitic matrix, beyond a critical martensite formation for each specimen. A properly calibrated Ferritscope confirmed the presence of martensitic transformation though (Fig. 17 and Fig. 18). Figure 17 reveals that a faster tensile loading hindered martensitic transformation. This can be explained with adiabatic heating in faster tests [10]. Figure 18 shows that a greater extent of martensite was found in solutionized samples. The specimen heated instantaneously to 1100^0C and solutionized showed maximum ferrite content (martensite) in Ferritscope. Slowly heated specimen showed less volume percentage of martensite, which is an apparent inconsistency. This occured possibly because of the incomplete annealing due to erroneous heat treatment. From EDAX measurement (Table 3), mean percentage of dissolved titanium in slowly heated sample was found to be lower than its rapidly heated counterpart. Moreover from the optical micrographs, an anomaly and inhomogeneity in grain size was also found in case of slowly heated and solutionized sample, which is indicative of incomplete annealing. A measure of the thermodynamic driving force for strain induced martensitic transformation is the calculation of M_{d30} temperature, i.e, the temperature at which 50 percent of austenite would get transformed into martensite for 30% plastic deformation. The modified empirical formula by Angel by Nohara et al. [11] describes the dependence of M_{d30} on grain size. With increasing grainsize M_{d30} comes lower, which suggests, for bigger grains, strain induced martensitic transformation will be more at room temperature. The erroneous heat treatment manifesting incomplete annealing in terms of inhomogeneity in grainsize (Table 2) may have incurred local changes in driving force for martensitic transformation. Nonetheless, the propensity of martensitic transformation under tensile loading was conclusively found to have increased in case of solutionized specimens as compared to as received specimens with little or no dissolved titanium in austenitic matrix. This suggests that precipitation has hindered martensitic transformation. Marco et al. [12] in his work explained the effect of Vanadium Nitride on strain induced martensitic transformation. Although vanadium in solution should increase the stability of austenitic phase as per Schaffler phase map, they found that the strain induced martensitic transformation was favored when vanadium was in the solution. They argued, the interaction between dislocations and the strain field posed by vanadium nitride

precipitates is the reason which is why the shear stresses necessary to accomplish martensitic transformation could not be attained. The future scope of this study is to find out the effect of precipitation in terms of shape and size on martensitic transformation and to invoke a correlation between Orowan stress needed for dislocations to glide past the barriers of non-shearable precipitates and volume percentage of martensitic transformation. This shall be accomplished by aging solutionized specimens at different elevated temperatures for different time periods followed by a study of the work hardening behaviour and an estimation of martensitic transformation as a function of plastic strain for each specimen.

SUMMARY

The findings from this study can be summarized as follows:

1. A faster tensile test was found to decrease martensitic transformation. This can be explained by the adiabatic heating of material at higher strain rates. No peak in the work hardening behaviour was observed, possibly because a dynamic equilibrium was established between hardening and and softening rates beyond a critical percentage of martensite formation.
2. The martensitic transformation was favored when titanium was dissolved in austenitic phase. Specimens instantaneously heated to 1100^0C and solutionized for 30 minutes and water quenched showed maximum content of martensite in the necked specimen. As-received samples with coarser titanium precipitates and little or no dissolved titanium in austenite matrix showed least transformation in necked specimen.
3. Slowly heated sample showed inhomogeneity in grain size and a less average dissolved titanium content than the specimen instantaneously heated to solutionizing temperature. The propensity of martensitic transformation found in this sample was intermediate between as-received and fast heated specimens, which is well in agreement with the hypothesis that dissolved titanium promoted martensitic transformation.

REFERENCE

[1]. J. W. Brooks, M. H. Loretto, R. E. Smallman (1979): Acta Metallurgia, Volume 27, Issue 12, 1839-1847.

[2]. G. B. Olson and Morris Cohen (1972): Journal of the Less-Common Metals, 28, pp-107-118.

[3]. Narutami. T, (1989): Materials Transactions JIM 30 (1), 33-45

[4]. R. H. Richman and G. F. Bolling (1971): Metallurgical Transactions, 2, 2451-2462.

[5]. G. B. Olson and Morris Cohen (1972): Journal of the Less-Common Metals, 28, pp-107-118.

[6]. A. J. Bogers and W. G. Burgers (1964): Acta Met., 12, 255

[7]. Mangonon P L and Thomas G (1970), Metall. Trans., 1, 1577.

[8]. Jeom-Yong Choi and Won Jin (1997): Scripta Mater., 36, 99.

[9]. L. Remy and R. Pineau (1977): Mater. Sci. Eng. 28, 99.

[10]. C. P. Livitsanos and P. F. Thomson (1977): Journal of Material Science 12, 2209-2213.

[11]. Nohara K, Ono Y, Ohashi N (1977): J Iron Steel Inst Jpn, 63:212-222.

[12]. Macro Wendler, Benedict Reichel, Ralf Eckner, Olga Fabrichnaya, Lutz Kruger, Andreas Weib and Javed Mola (2014): Metallurgical and Materials Transactions A.

National Conference on Thermo-mechanical processing of Steels &
5th Gleeble User Workshop India (GUWI-2015),
August 6-7, 2015, pp 57-69.

Study on Flow Properties of Rotor Grade Steel

M.I.Mehta[1], B.P. Kashyap[2] and R.K.P.Singh[1]

[1] Kalyani Centre for Technology and Innovation, Bharat Forge Ltd, Pune 411036, India

[2] IIT Bombay, Mumbai 400076, India

Email: mohan.mehta@bharatforge.com, bpk@iitb.ac.in, RajkumarSingh@bharatforge.com

ABSTRACT

Compression tests were performed on Gleeble 3800 Thermo-Mechanical Simulator to study the flow properties of rotor grade steel 28CrMoNiV59. Compression specimens were deformed at a constant strain rate of 10^{-3} s^{-1}. The temperature range during tests was between room temperature and 1000 °C with an interval of 100 °C. When the normalized flow stress was plotted as a function of temperature, it exhibited three different regions. In regions I and III flow stress decreases with increase in temperature but the same increases with temperature in region II. Microstructural changes and work hardening behaviour have been studied for the deformed specimen. Furthermore, TEM analysis was also done for the samples of these three different regions (I, II & III). Strain hardening rate as a function of the normalized flow stresses decreases at larger strain and become negligible at higher temperature.

***Keywords**: rotor grade steel, flow properties, Gleeble 3800, deformation*

INTRODUCTION

In power plants, turbine rotors are subjected to high temperatures especially during start up cycle. The rotor shaft is a spinning component, on which wheels and blades are attached. Initially steam is generated in a boiler which then hits the turbine blades at elevated temperature and pressure. The steam's impact causes the rotor to start spinning. This also causes sudden changes in the temperature and transient thermal stresses are induced in the turbine rotor. So, it becomes essential to estimate the thermal stresses induced in the turbine. Recently, C. Zhang et al. [1] has analysed the steam turbine for temperature variations and stresses generated in short period of time during the start and stop of cycle.

Figure 1 shows the temperature variation for 600MW supercritical steam turbine's rotor. [1] It is observed in Fig. 1 that the temperature variation in the rotor varies from 60 °C to 542 °C within 12000 sec from the start of the cycle. In order to understand the behaviour of the rotor

shaft under the combination of the thermal as well as mechanical loads, it is important to understand the deformation behaviour of the material at different temperatures.

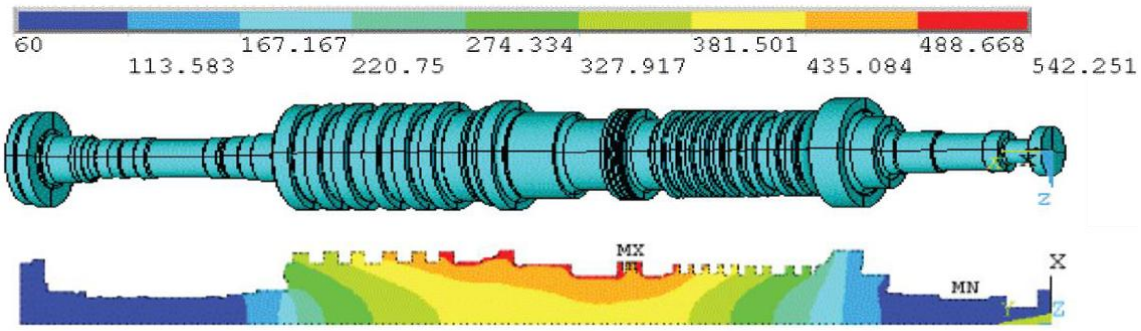

Fig. 1: Temperature variation for 600MW supercritical turbine after 12000 sec [1]

The material flow behaviour during hot deformation is complex; hardening and softening mechanisms are affected by temperature and strain rate [2-3]. In thermo-mechanical processes, material undergoes several metallurgical phenomena such as work hardening [4], dynamic recovery [5] and dynamic recrystallization [6]. The effects of these phenomena are often exhibited in the flow curves.

In the current paper, compressive deformation behaviour of rotor grade steel was studied. The test temperatures were varied up to 1000 °C. Compression tests were carried out to find out flow stress of rotor shaft for a wide range of temperatures at a constant strain rate of 10^{-3} s^{-1}. The stress- strain values obtained from tests may be used as input to the FEM analysis of the part for optimization of the design.

EXPERIMENTAL WORK

Material for experiment

In the present study, rotor grade steel (28CrMoNiV59) was selected for the experiment, as this material is used for manufacturing of steam turbine rotor shaft. The chemistry spec of material is given in Table 1. Chemical analysis was carried out on the selected rotor material to confirm the grade and chemistry of the selected steel.

Material for experiment was extracted from finished rotor shaft. This rotor shaft was manufactured using a process flow which is shown in Fig.2. The rotor shaft was forged from

ingot on 4000T hydraulic press. After forging, post heat treatments were carried out on the shaft to achieve required mechanical properties.

Table 1 Chemistry specification of material 28CrMoNiV59

Alloying Elements	C	Mn	P	S	Si	Cr	Ni	Mo	V	Al
Min (wt%)	0.25	0.3	----	----	---	1.1	0.5	0.8	0.25	---
Max (wt%)	0.3	0.8	0.007	0.007	0.1	1.4	0.75	1.0	0.35	0.008

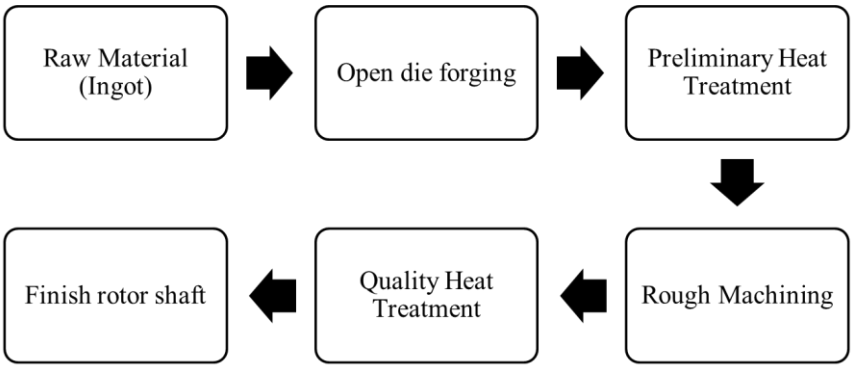

Fig. 2: Flow chart of rotor shaft

The shaft was hardened by quenching from the austenizing temperature and later it was tempered in the temperature range of 690- 750 °C.The microstructure of as received heat treated material consists of ferrite and tempered martensite. Figure 3 exhibits two different phases i.e. soft ferrite phase (bright) and hard martensite phase (dark). SEM image of the same is shown in Fig. 4. Prior austenitic grain boundaries can be observed in the SEM image.

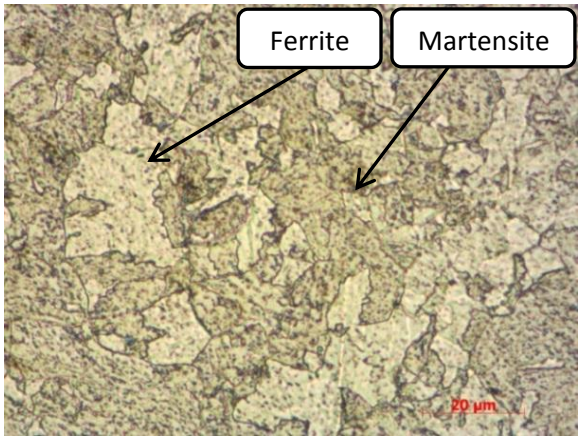

Fig. 3: Optical image of heat treated steel sample when etched in nital 2%.(500X).

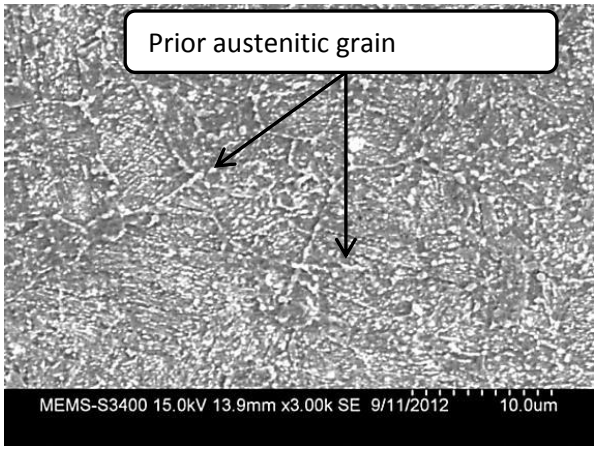

Fig. 4: SEM image of heat treated sample.

Mechanical testing

The mechanical properties of finished rotor shaft were determined by different tests like hardness test, tensile and impact test, at room temperature. Samples were taken out from rotor shaft for hardness testing. Furthermore, the oxide layers formed during heat treatment were removed by grinding. Hardness was measured using digital Rockwell hardness tester. Average value of three hardness readings at different positions was calculated. Indents were made on the polished surface using 150 kg load for HRc scale and 10 sec dwell time. For tensile tests, cylindrical specimens were prepared as per ASTM E8 standard. Tensile testing was done on universal testing machine of make Zwick / Roell.

Impact specimens (extracted from rotor shaft) were prepared as per ASTM 23. The tests were conducted on Zwick/ Roell Charpy impact test machine. Three samples were tested and average value was calculated.

Compression testing

Flow properties of rotor grade steel (28CrMoNiV59) were determined by compression test. For compression testing, test specimens were prepared from rotor shaft in longitudinal direction by maintaining L/D ration of 1.5. The specimens for compression tests were cylindrical with diameter 10 mm and height 15 mm. Compression tests were performed by using a Gleeble 3800 thermo-mechanical simulator. Figure 5 shows schematic diagram of compression testing set up. ISO-T anvils were used for compression testing. A piece of 0.125 mm thick graphite foil was used as a lubricant in the uniaxial compression testing.

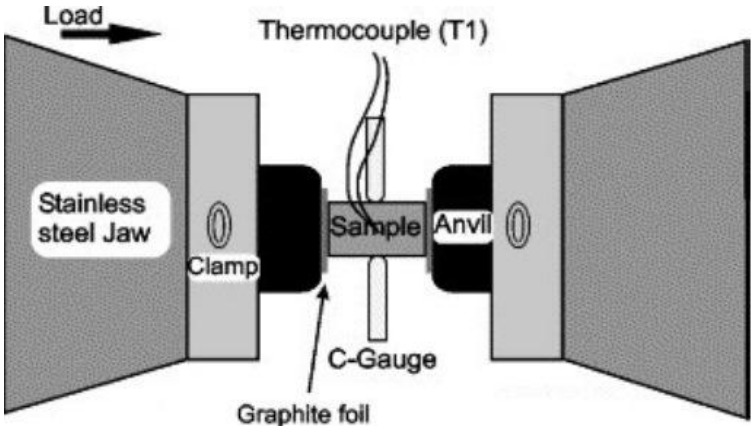

Fig: 5: Schematic diagram of compression testing machine.

Compression tests were performed with the constant strain rate of 10^{-3} s^{-1} from room temperature to 1000 °C at an interval of 100 °C. On each specimen, a K-type thermocouple was welded at the mid-span to control temperature during testing. Each specimen was heated with a heating rate of 5 °C/s up to T-20 °C where, T is the test temperature. In the temperature range from T-20 °C to T, the heating rate was decreased to 2.5 °C/s to prevent temperature overshooting. Once T was reached, 10 seconds of soaking time were given to stabilize the temperature in the sample. After the completion of test, each specimen was immediately subjected to rapid air cooling with the cooling rate of ~100 °C/s to freeze the microstructure.

Test data have been recorded during testing. True strain and stress has been calculated from eq. 1 and eq. 2 respectively.

$$\varepsilon = ln\left[\frac{h_o}{(h_o - \Delta h)}\right] \qquad (1)$$

where, ho: Initial height of a specimen,

Δh: Cross-head displacement.

$$\sigma = \frac{[F(h_o - \Delta h)]}{[S_o h_o]} \qquad (2)$$

where, F: Measured load,

So: Initial cross section.

Microstructure analysis

Microstructural analysis was carried out on compression test specimens. The optical micrographs were taken using bright field inverted stage microscope of make Zeiss. Scanning electron microscope (SEM) of make Zeiss was also used to examine specimen. For transmission electron microscopy, thin foils were prepared by thinning compression test specimen using emery paper. Final thinning was completed by jet electro polishing. Thin prepared foil was examined by transmission electron microscope operating with an accelerating potential of 100kV.

RESULTS AND DISCUSSION

High strength and ductility are the critical properties for rotor grade steel. Microstructural analysis and deformation curves obtained from compression tests are discussed here.

Chemical analysis of the material

The result of the chemical analysis is given in the Table 2. It can be seen from the results that the values are well within spec.

Table 2: Chemical analysis results of 28CrMoNiV59

Alloying Elements	C	Mn	P	S	Si	Cr	Ni	Mo	V	Al
Obtained (wt%)	0.26	0.42	0.001	0.003	0.05	1.2	0.61	0.87	0.31	0.004

Mechanical test results

The results of tensile, impact and hardness tests, carried out at room temperature, are presented in Table 3.

Table 3: Mechanical properties at room temperature

Sr No.	Yield Strength (MPa)	Ultimate tensile strength (MPa)	% Elongation	Hardness (HRC)	Impact (J)
1	660	840	12.25	24	108

Compression test results

Compression specimens of rotor grade steel material were deformed up to 50% strain at a wide range of temperature from room temperature to 1000 °C at constant strain rate 10^{-3} s^{-1}[7-8].

Figure 6 shows true stress-strain graphs of compression test at various conditions. Following can be observed from these graphs:

1. As the test temperature increases, stress required for deformation reduces.
2. The material exhibits almost same deformation behavior at temperatures 100, 200 and 300 °C.

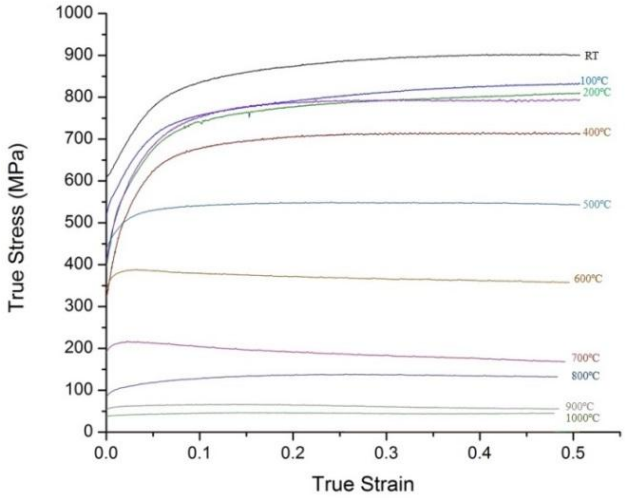

Fig. 6: True stress strain curve over temperature ranges from room temperature to 1000 °C at strain rate 10^{-3} s^{-1}.

The effect of temperature on normalized stress at different strains is shown in in Fig. 7. B. A. Latella et al. [9] has calculated the values of Young's modulus (E) at different temperature using formula as shown in eq. 3,

$$E = 216.3 - 0.0766T * R \qquad (3)$$

where, E: Young's modulus in GPa,

T: Temperature in °C,

R: Correlation coefficient. (Approx~0.999)

E values at different temperatures were calculated by using above equation. These E values were used to normalise the stress values. Figure 7 shows curves of σ/E vs. temperature which can be divided in to three different regions namely region I, II, and III as per the following observations:

1. The graph exhibits that in regions I and III, flow stresses decrease with increase in temperature.

2. In region II the flow stresses increase with increasing temperature.

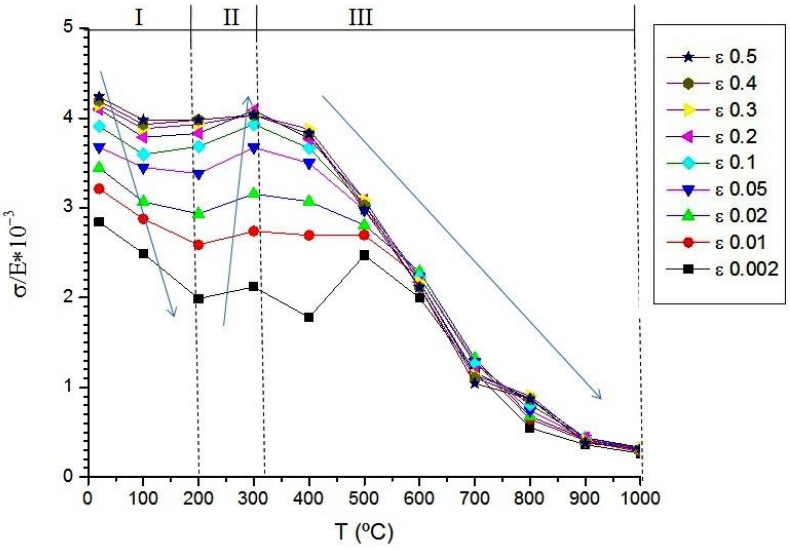

Fig. 7: σ/E vs. Temperature (at ε=0.002, 0.01, 0.02, 0.05, 0.1, 0.2, 0.3, 0.4, 0.5) at $\dot{\varepsilon}=10^{-3}$ s^{-1}.

The stresses required for deformation at lower temperatures (i.e. region I) are higher because the grain boundaries act as barrier to slip. In region III, diffusion plays a very important role which contributes to the decrease in stress with increasing temperature. In this temperature regime, diffusion helps in the movement of dislocation and thus, deformation becomes easier [10].

Microstructure analysis

The optical microstructure of specimens deformed at various temperatures was studied. No significant difference was observed in the microstructure of various deformed specimens as shown in Fig.8. It shows that there is no effect of deformation and its temperature on the microstructure of the deformed specimen. But, it is seen that the deformation stresses

increase with temperature in the region II. To find its root cause TEM analysis was carried out. In TEM analysis one specimen from each region was studied. TEM analysis results as shown in Fig. 9.

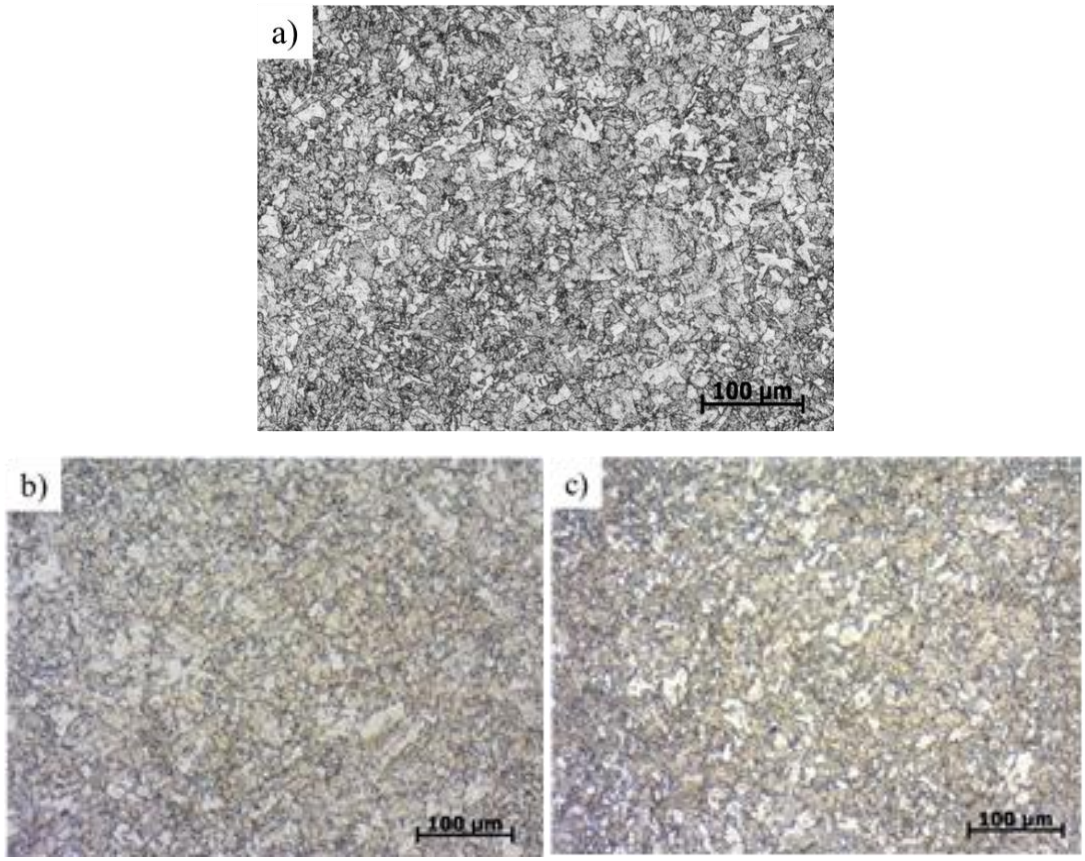

Fig 8: Microstructure of the steel after hot compression at the temperature a) 100 °C b) 300 °C and c) 1000 °C

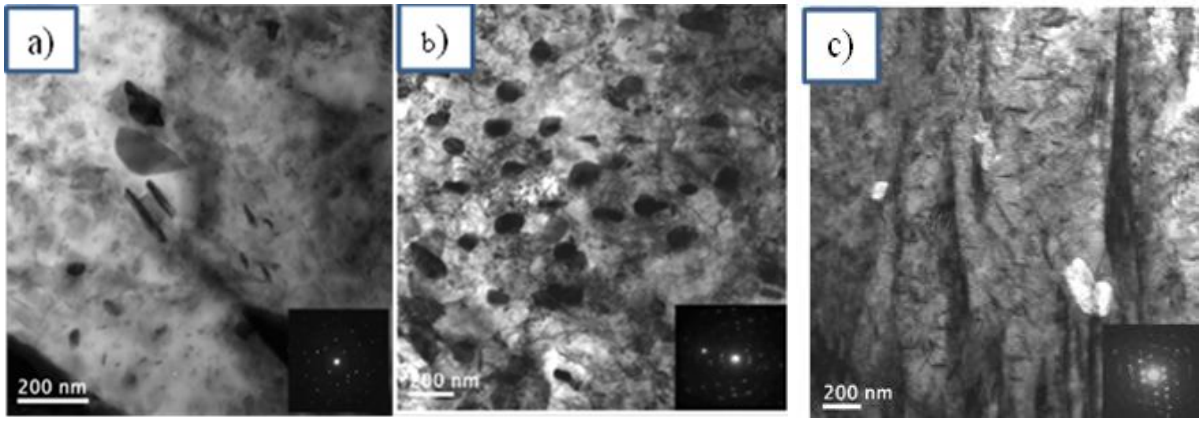

Fig. 9: TEM micrographs of specimen compressed at a) region I room temperature b) region II 300 °C and c) region III 1000 °C.

Following can be observed from the TEM results:

1. Some precipitates are observed in the samples from all the three regions.
2. The region I and III samples shows less or negligible precipitates.
3. The region II samples show fine uniformly distributed precipitates.

Energy dispersive X-ray (EDX) technique was used to identify the composition of these precipitates in region II sample. Figure 10 exhibits EDX spectra which show elements Cr, Fe. Hence, the formation of Cr carbide particle may be possible in the intermediate temperature range i.e. around 300 °C. This may be the cause for barrier to the dislocation. Thus, increasing the flow stresses required for deformation in region II.

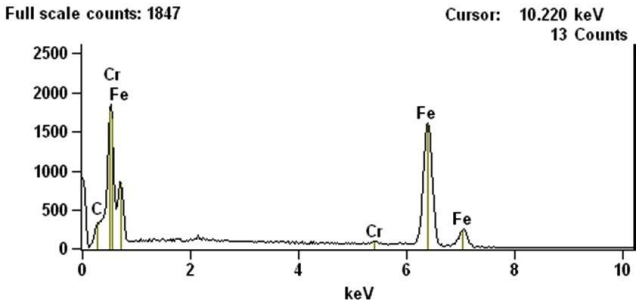

Fig. 10: EDX spectra of compress sample at 300 °C.

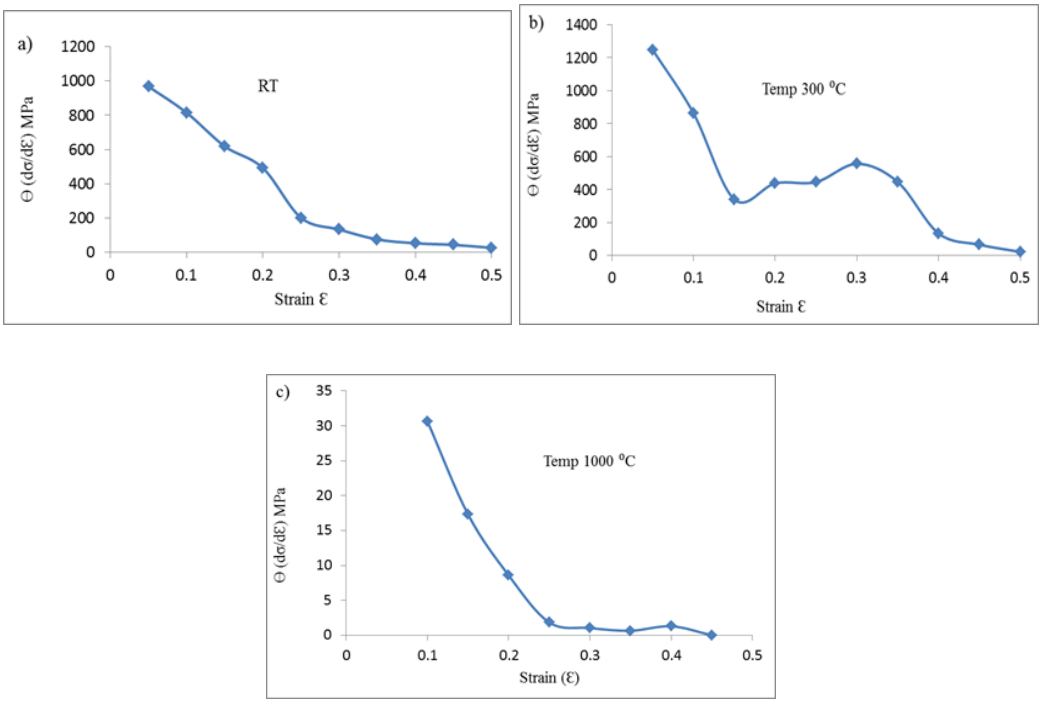

Fig. 11: The variation in strain hardening rate Θ as function of strain ε at a) room temp b) 300 °C c) 1000 °C.

For understanding the compression flow behaviour, effect of strain hardening rate (Θ) as a function of strain was studied. Figure 11 (a), (b) and (c) shows variation in strain hardening rate for room temperature, 300 °C and 1000 °C respectively. These curves show variation of Θ with respect to strain. At low and high temperature, Θ decreases almost linearly with increasing strain. But for intermediate temperature i.e. 300 °C, increase in Θis observed.

E. Isaac Samuel et al. [11] has used the variations of instantaneous work hardening rate Θas function of stress to study hardening behaviour. Similarly, for this study the strain hardening rate as a function of stress was plotted. The effect of strain hardening rate as function of normalized stress is as shown in Fig. 12. Compression test data obtained at all temperatures were analysed with respect to Θand stress but only few representative plots are presented in Fig. 12. Low (room temperature), intermediate (300 °C) and high (1000 °C) temperature conditions are consider studying the variation of Θ It can be observed that the strain hardening rate decreases with increase in strain and the same becomes negligible at higher temperature.

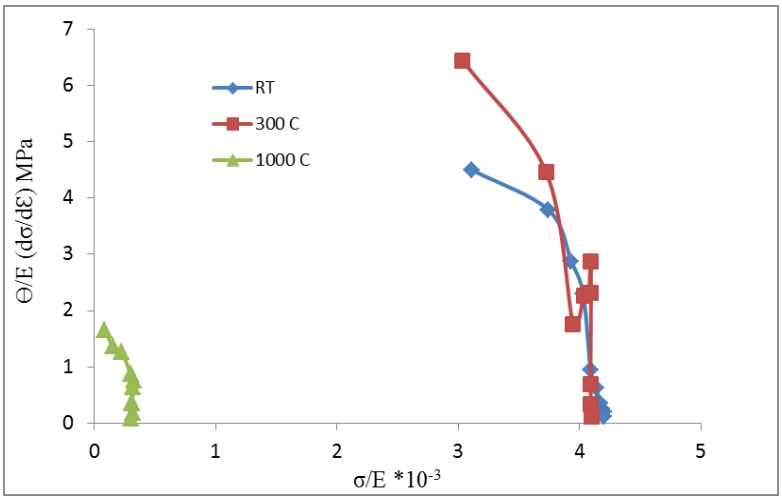

Fig. 12: The variation in strain hardening rate Θas function of stress at a) room temp b) 300 °C c) 1000 °C

CONCLUSIONS

- This investigation explored the effect of temperatures on flow properties of "28CrNiMoV59" during compression test. As the test temperature increases, stress required for deformation reduces.

- When the normalized flow stress was plotted as a function of temperature, it exhibits three different regions. In regions I and III flow stress decreases with increase in temperature but the same increases with the temperature in region II.

- In region II, the increase in flow stress with temperature can be attributed to uniform precipitation of fine carbide particles which may cause barrier to dislocation (~200 °C - 350 °C).

- The strain hardening rate (Θ) decreases with increase in strain. The same becomes negligible at higher temperature.

ACKNOWLEDGMENT

The authors would like to express a sense of gratitude towards Dr. Ilchat Sabirov (IMDEA Material Institute, Spain) and Dr. Devesh Mishra (Department of Chemical Engineering University of Louisiana at Lafayette, USA) for their sincere support.

The authors gratefully acknowledge the extended support provided to this work by KCTI (Kalyani Centre for Technology and Innovation) for providing financial funding, laboratory and library facilities. The authors also acknowledge the support provided by Bharat Forge Ltd, Pune and DSIR (Department of Scientific and Industrial Research), Govt. of India. Finally, the authors would like to express special thanks and gratitude to review committee and top management of Bharat Forge Ltd for granting the permission to publish/present the research work.

REFERENCES

[1]. C. Zhang, N. Hu, J. Wang, Qiping, Chen, F. He, Xiaoli (2010): IEEE 978-1-4244-4813-5/10/&25.00c.

[2]. W.J. Dan, W.G. Zhang, S.H. Li, Z.Q. Lin(2007): Material Science and Engineering 40, 101–107.

[3]. C. Sommitsch, R. Sievert, T. Wlanis, B. Gu¨nther, V. Wieser (2007): Material Science and Engineering 39, 55–64.

[4]. C.A.C. Imbert, H.J. McQueen (2001): Material Science & Engineering A 313, 88–103.

[5]. C. Roucoules, M. Pietrzyk, P.D. Hodgson (2003): Material Science and Engineering, A 339, 1–9.

[6]. D. Ponge, G. Gottstein (1998): Acta Materialia, 46, 69-80.

[7]. A.Yu. Churyumov, M.G. Khomutov, A.N. Solonin, A.V. Pozdniakov, T.A. Churyumova (2015): Materials and Design 74, 44–54

[8]. B.P.Kashyap, K McTaggart, K. Tangri (1988): Philosophical Magazine, Vol 57, No. 1, 97-114.

[9]. B.A.Latella, S.R. Humphries (2004): Scripta Materialia 51, 635–639.

[10].W. D. Callister, Jr. Materials Science and Engineering, 7th Edn., John Wiley & Sons, USA (1940) pp.109-112.

[11]. E. Isaac Samuel, B.K. Choudhary, K. Bhanu Sankara Rao (2002): Scripta Materialia 46, 507–512.

National Conference on Thermo-mechanical processing of Steels &
5th Gleeble User Workshop India (GUWI-2015),
August 6-7, 2015, pp 70-77.

Hot Ductility Study on High Phosphorus Containing Cu-Cr Low Alloy Steel

Gadadhar Sahoo, Vinod Kumar, Balbir Singh and Atul Saxena

R & D Centre for Iron and Steel, SAIL, Ranchi-834002, India

Email: gadadhar@sail-rdcis.com

ABSTRACT

Seven numbers of laboratory heats of 25 kg each were made using a high frequency induction melting furnace. Various elements in the steel, viz, Ni, Cu, P and Si, varied in the range of 0.01-2.0%, 0.22-0.47%, 0.12-0.19% and 0.40-0.86%, respectively. Carbon and sulphur contents were maintained low, i.e., 0.05-0.087% and 0.005-0.01%, respectively. Hot tensile test carried out using Gleeble-3500C simulator revealed reduction in area in excess of 70% at all deformation temperatures and at slow strain rate (0.005/s) testing conditions for all the experimental steels except for low Si (0.40%) and a little higher S (0.01%) containing steels. The lower hot ductility (RA value < 30%) of these steels resulted in brittle failure at 850 ^{0}C corresponding to the temperature at straightening operation during continuous casting. On the other hand, all steels exhibited good hot ductility (RA values greater than 70%) at higher strain rate (6.5/s).

Keywords: *Hot ductility, slab cracking, brittle failure, weathering steel, continuous casting*

INTRODUCTION

Copper, which is mainly contained in the scrap of cars and home electronic appliance, is problematic in mechanical workings at elevated temperatures and limits the usage of scrap iron [1]. It is enriched at steel/scale interface by preferential oxidation of Fe, which leads to liquid embrittlement or surface cracking during hot working. This type of defect is well known as surface hot shortness[1]. Cu has been also reported to give surface cracking problem including transverse cracking in continuously cast products and has been found to be detrimental to surface quality[2-4]. Broadly, two forms of hot shortness are categorised by Melford[12], (i) liquation cracking, i.e., hot shortness in the bulk of the steel and (ii) surface hot shortness. Liquation cracking is a problem associated with enriched liquid phase at grain boundaries, which occurs when relatively insoluble residual elements (e.g. sulphur) are present in steel resulting in cracking. Surface hot shortness, on the other hand is caused by the

enrichment of residual elements on the subsurface during oxidation which is liquefied and subsequently, penetrated into austenite grain boundaries.

Other than surface hot shortness generally found in Cu bearing steels, different types of cracks are also appeared in continuously cast products in low carbon, Cu bearing and mirco-alloyed steel as shown schematically in Figure 1. The most common defect found is transverse cracks, which may be formed on the broad face, narrow face, or corner of continuously cast slab. However, these are not always apparent to visual inspection unless the slab surface is scrapped or prepared for microscopic observation. These are usually associated with the depression of oscillation marks, and are predominantly found on the top slab surface. The length of the cracks can be several 10s of mm, and generally follow austenite grain boundaries. The cracks are partially oxidised with a little decarbonisation[5].

Transverse cracking occurs most frequently in steels micro-alloyed with Nb, which greatly promotes the formation of transverse cracks while V at low N levels has no effect. However, the combinations of 0.15%V and 0.02%N have been reported to lead to transverse cracking. In copper bearing steel, Burden et al.[6] have reported that surface cracks in continuously cast blooms are associated with enrichment of Cu, Ni and Sn. The work by Woollen[4] at British steel indicates that plate steels containing Nb with additions of 0.25% Cu and 0.25% Ni have a greater incidence of transverse cracking compared with similar grades without Cu and Ni additions.

Lankford[7] has reviewed the source of stresses during continuous casting which can arise from a large number of different causes. These include transformation effects, thermal effects (variable heat transfer within the mould, temperature gradients within slabs, effects of cooling water sprays, contact with rollers, etc.), friction between strand and mould, bulging of the strand caused by ferrostatic pressure, mechanical effects due to misalignment of the casting machine, and straightening strains. Out of these, straightening strains is most important. This is because large transverse cracks are observed in the final straightened slab, together with the fact that these are often most numerous on the top surface of the slab (i.e. the surface which is in tension during straightening). This suggests that there is much crack propagation induced by the stresses experienced during the straightening process. When these stresses occur in the temperature range over which ductility is poor, the appearance of transverse cracking becomes severe.

The primary objective of this study is to evaluate the effect of Si, P and Ni on crack formation in a Cu-Cr-P low alloy steel. The technique involved to evaluate cracking problem is mainly hot tensile test using a Gleeble simulator which will simulate a processing environment that leads to surface hot shortness and hot cracking during continuous casting of slab/billet, and during reheating and hot rolling of copper bearing steels.

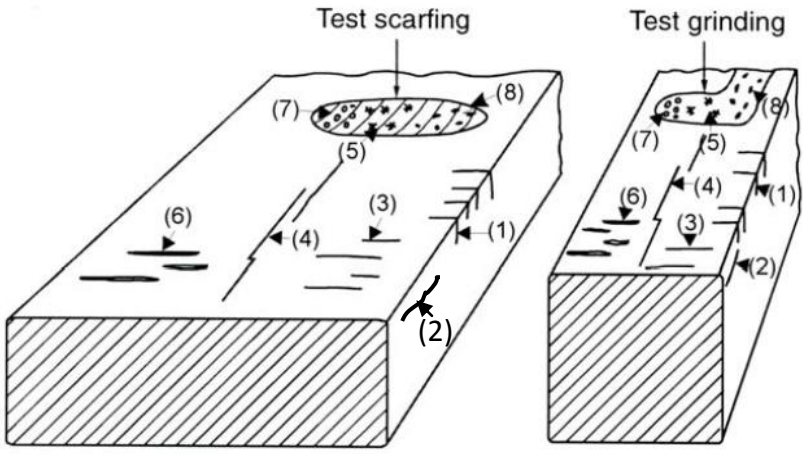

1. Transverse corner cracks; 2. Longitudinal corner cracks; 3. Transverse cracks; 4. Longitudinal cracks (broad face); 5. Star cracks; 6. Deep oscillation marks; 7. Pinholes; 8. Macro inclusions.

Fig. 1: Schematic of surface defects in continuously cast products.

EXPERIMENTAL WORK

Seven numbers of laboratory heats of low alloy steels of 25 kg each were made using a high frequency induction melting furnace. Steel scrap of C-Mn rail steel was added to soft iron (0.001 wt. % C) to balance carbon content. In order to obtain Cr, P, Cu and Ni in the desired ranges, mother alloys of Fe-P, Fe-Cr along with Cu blocks and Ni lumps were added to the liquid steel in the furnace. Aluminium in the form of shots and wire were used for deoxidation purpose. The melts were cast into 100mm × 100mm square ingots, which were subsequently hot rolled to 16 mm thick plates through five passes after soaking at 1150^0C for 2.0 hours. The chemical composition of each steel was determined using an optical emission spectrometer. Chemical compositions of experimental steels after hot rolling are given in Table 1.

Table-1: Chemical composition of different steels (in wt. %) obtained using OES after hot rolling

Steels	C	Si	Mn	S	P	Cr	Cu	Ni	Al
S1	0.059	0.82	0.31	0.005	0.12	0.36	0.41	0.13	0.017
S2	0.06	0.86	0.42	0.005	0.19	0.37	0.41	0.13	0.019
S3	0.065	0.80	0.35	0.008	0.13	0.36	0.47	trace	0.012
S4	0.068	0.81	0.38	0.005	0.20	0.37	0.47	trace	0.005
S5	0.085	0.40	0.39	0.01	0.19	0.02	0.40	trace	0.005
S6	0.087	0.40	0.42	0.01	0.19	0.34	0.40	trace	0.003
S7	0.05	0.42	0.43	0.005	0.145	0.37	0.22	0.20	0.002

To understand the surface hot cracking behaviour of experimental steels, hot tensile test was carried out using a Dynamic Thermo-Mechanical Simulator (DTMS) Gleeble-3500C. The specimens of 10 mm diameter and 120 mm length with threads at both ends were initially heated to the soaking temperatures 1300^{o}C at a heating rate of 20^{o}C/s and held for 1 min. This was followed by cooling at a rate of 5^{o} C/s to deformation temperature, viz., 1200, 1100, 1000, 900 and 850^{o}C. The deformation was allowed up to fracture with a strain rate of 0.005/s (i.e., the stroke rate is 0.125 mm/s with a gauge length of 25 mm) for S1 to S6 steels. The slow strain rate applied is similar to that occurring during straightening operation (~$10^{-3}s^{-1}$) of 240 mm thick slab on continuous casting [8]. In addition to this, deformation was also carried out at strain rate of 6.5/s (i.e., the stroke rate of 162.5mm/s) for S4 and S6 steels. Hot ductility was realized from the % of reduction in area (RA) at failure after tensile test.

RESULTS AND DISCUSSION

Hot Tensile Test and Fractography

Figure 2 shows variation in the percentage of reduction in area (RA) value with deformation temperatures after tensile test in Gleeble at a strain rate of 0.125/s in the range of 850^{0}C to 1200^{0}C. The different temperature zones of reduced hot ductility of steel related to

embrittling mechanism can be co-related to that observed in experimental steels in Figure 2. No major ductility trough is observed in any steel in any of the three expected reduced ductility temperature zones except S5 and S6 steels at 850^0C. In both cases of these S5 and S6 steels, the percentage of reduction in area (RA) value decreased to 20% at 850^0 on decreasing silicon content from 0.8 wt.% to 0.4 wt.% while it was greater than 75 % at all other temperatures. This temperature is related to zone III where phase transformation occurs. Previously reported RA values above which transverse cracks don't occur are 75%[9], 60%[10] and 30-40%[11]. Therefore, based on the present findings, it can be concluded that both S5 and S6 steels are not suitable for commercial production as there is good chance of the formation of transverse cracking during continuous casting.

As ductility trough has been directly linked to the Ar3 temperature or γ-α phase transformation[12], lowering Si content probably influenced the Ar3 temperature in S5 and S6 steels unlike to that of S1 to S4 steels where Si content is in the range of 0.75-0.86%. In addition to this, as reported by many researchers that increasing sulphur content both

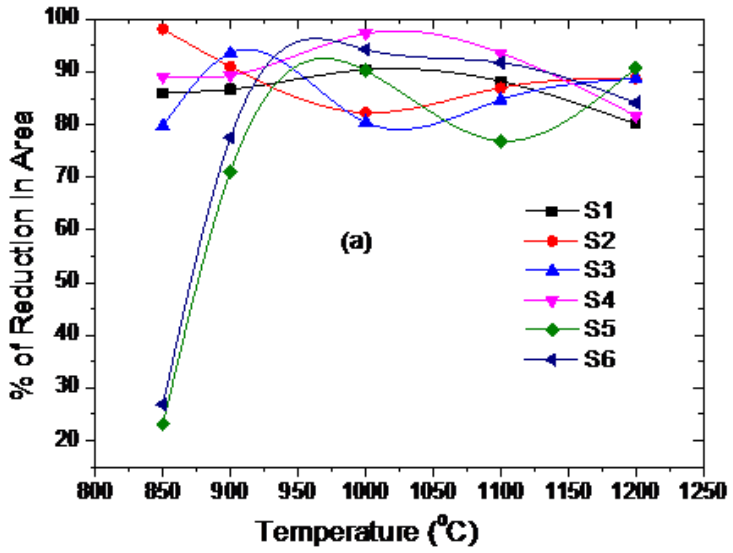

Fig. 18: Experimental steels showing variation in percentage of reduction in area (a) and maximum strength (b) with deformation temperature after tensile test in Gleeble at a strain rate of 0.005/s.

deepens[12-14] and widens[12, 15] the hot-ductility trough. Therefore, as sulphur content in S5 and S6 steel (0.01 %) is about double to that in S1 to S4 steel (~0.005%), this might have reduced the hot ductility at 850 and 900^0C. On the other hand, additions of Ni (0.13%) and Cr (0.34-0.37%) have a little effect on hot ductility of experimental steels as discussed below.

Further, in both S4 and S6 steels, the hot ductility has been improved in intermediate temperature range (900 and 1000^0C) at low and high strain rate, i.e., 0.005 s^{-1} and $6.5s^{-1}$, respectively, which is in conformity with the findings of Suzuki et. al[12].

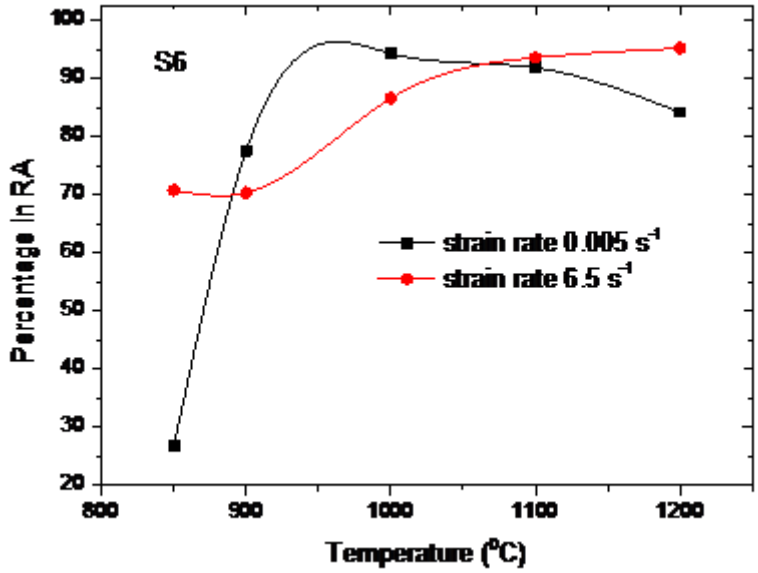

Fig. 3: Effect of strain rate on the variation of percentage of reduction in area with deformation temperature after tensile test of experimental steel S6.

CONCLUSIONS

- Seven different alloy chemistries were designed to study hot shortness and cracking effect during continuous casting. The chemistries were varied with respect to Ni, Cu, P and Si to make steel cost effective.

- All experimental steels exhibited good hot ductility at slow deformation rate (0.005/s) except S5 and S6 steel. However, S6 steel also exhibited good ductility at higher strain rate (6.5/s) and the similar result is also expected in the case of S5 steel.

- The failure of S5 and S5 steel in brittle manner at $\gamma \rightarrow \alpha$ transformation region (850^0C) is attributed to the compositional effect, especially Si and S content where stress concentration remain at the precipitates at austenitic grain boundaries at slow strain rate condition while that is distributed on whole grains during high deformation rate.

ACKNOWLEDGEMENTS

The task force members of this project are very much thankful to RDCIS, SAIL, Ranchi management for providing help and necessary support to carry out this work. Members are also thankful to all technicians who were involved during pursing this work.

REFERENCES

[1]. L. Habrakenand J. Lecomte-Beckers: Copper in lron and Steel, ed. by L. McDonaldSchetky, John Wiley &Sons, NewYork, (1982), 45.

[2]. M. H. Burdern, G. D. Funnell, A. G. Whitaker and J. M. Young, Solidification and Casting of Metals, The Metals Society, London, (1979), 279-286.

[3]. E. Anelli, A. Mollo and A. Oulhadj, Proceeding of 34th Mech. Working and Steel Processing Conf. ISS-AIME, Warrendale, PA, Vol. 30, (1993), 399-407.

[4]. G. Woollen, Personal communication, British Steel, Scunthorpe Works, (1990).

[5]. M. Hater et. al., "Results From a Curved Mould Continuous Casting Machine Making Pipe and Plate Steel", "Open Hearth Proceedings", AIME, 1973, 202-217.

[6]. M. H. Burden, G. D. Funnell, A. G. Whitaker and J. M. Young, Solidification and Castings of Metals, the Metals Society, London (1979), 279-286.

[7]. W. T. Lankford, "Considerations of Strength and Ductility in the Continuous-Casting Process", Metall. Trans., 1972, 3, 1331-1357.

[8]. K. M. Banks, A. Tuling, C. Klinkenberg and B. Mintz, Influence of Ti on hot ductility of Nb containing HSLA steels, Materials Science and Technology, 27, 2011, 537-545.

[9]. N. Bannenberg et. al., "Procedures for Successful Continuos Casting of Steel Microalloyed with Nb, V Ti and N", Microalloying 95, 83-94.

[10]. B. Mintz and S. Yue: "The Hot Tensile test For Assessing the Likelihood of Transverse Cracking During Continuous Casting of Steel", 34th Mechanical Working and Steel Processing Conference, 1992, 391-398.

[11]. Standard Test Methods and Definitions for Mechanical Testing of Steel Products, Vol. 01.01, ASTM A370 – 14

[12]. H. G. Suzuki, S. Nishimura and S. Yamaguchi, “Characteristics of Hot Ductility in Steels Subjected to the Melting and Solidification,” ISIJ Trans., (22), 1982, pp. 48-56.

[13]. W.T. Lankford, "Some Considerations of Strength and Ductility in the Continuous-Casting Process," Met. Trans., (3) , June 1972, pp. 1331-1357.

[14]. G.A. Wilber, R Batra, WF Savage, WJ Childs, "The Effects of Thermal History and Composition on the Hot Ductility of Low Carbon Steels," Met. Trans. A, (6A), September 1975, pp. 1727-1735.

[15]. F. Weinberg, "The Strength and Ductility of Continuously Cast Steels Above 800°C," Met. Trans. B, (lOB), December 1979, pp. 513-522.

National Conference on Thermo-mechanical processing of Steels &
5th Gleeble User Workshop India (GUWI-2015),
August 6-7, 2015, pp 78-91.

Identification of Favorable Hot Working Condition for Ti-6Al-4V Alloy

A.A. Shaikh[1], B.P. Kashyap[2] and A. Chauthai[3]

[1] *Kalyani Centre for Technology and Innovation, Bharat Forge Ltd, Pune 411036, India*

[2] *IIT Bombay, Mumbai 400076, India*

[3]*Bharat Forge Ltd. Pune 411036, India*

Email : Afroz.shaikh@bharatforge.com, bpk@met.iitb.ac.in, achauthai@bharatforge.com

ABSTRACT

The hot working performance of Ti-6Al-4V alloy is sensitive to its process parameters and initial microstructure. It has a very narrow range of process parameters. Therefore, to identify favorable hot working conditions, hot compression tests in the temperature range of 700 - 1000 °C and strain rate range of 0.1 - 100 s^{-1} were conducted on Gleeble 3500 thermo-mechanical simulator. The experimental results show that deformation temperature and strain rate has significant effect on the flow stresses. Flow stress increases with increase in strain rate and decrease in deformation temperature. The stress-strain curves, generated by compression test, show three types of behavior: flow hardening, flow softening and steady state flow. The activation energy for deformation was determined to be 484 kJ/mol which is much higher than that for self-diffusion in α-Ti and β-Ti (150 kJ/mol). Using Dynamic Materials Modelling (DMM) principle, the favorable condition for hot working of Ti-6Al-4V alloy has been established. Furthermore, optimum condition among favorable conditions has also been established. The same has been validated with the help of microstructural analysis.

***Keywords**: High temperature deformation, Ti-6Al-4V alloy, Compression test, Gleeble 3500 thermo-mechanical simulator*

INTRODUCTION

Titanium alloys are widely used in industries like aerospace, bio-medical, transportation, marine & offshore, petrochemical, architecture and household due to their outstanding properties, such as high strength-to-weight ratio, good corrosion resistance, high thermo-stability and good mechanical properties at high working temperature. Due to its numerous applications, research aiming towards better understanding of the manufacturing process of titanium components is of great significance for optimizing the manufacturing process.

Ti-6Al-4V is a (α+β) Ti alloy widely used in aerospace industries. The hot working performance, microstructure and texture evolution of the alloy is very sensitive to the initial billet microstructure [1] and process parameters [2, 3] and thus it has a very narrow range of process parameters. So, the knowledge of favorable hot working condition becomes important. The alloy is usually forged at a temperature which is 30–50 °C below its β transus temperature so that a fine equiaxed grain structure can be obtained and good mechanical properties can be secured [4]. Different phases in the alloy (α, β) also behave differently under hot deformation [5]. Several modeling approaches like true stress–true strain curves and processing maps are widely used to characterize the deformation behavior of titanium alloys in order to understand how to control their microstructures and optimize manufacturing processes [4].

Flow stress depends on temperature and strain rate. Flow stress curves can be obtained through hot deformation tests. But, the said tests are costly and time consuming. So, it is necessary to model the flow stresses as a function of temperature and strain rate. Wen et al. [6] proposed Artificial Neural Network (ANN) model to predict the flow behavior of Ti6Al4V using experimental data from hot compression test and compared the processing maps constructed on the basis of experimental and predicted data to verify the validity of the ANN model. J. Cai et al.[7] established a constitutive equation to predict the elevated temperature flow stresses of Ti–6Al–4V alloy. N. Park et al. [8] established a stimulation tool for prediction of deformation behavior and constructed processing maps of Ti6Al4V based on the quantitative understanding of the dynamic deformation behavior.

The maximum strain rate explored in all the mentioned studies is about 10 s^{-1}. But, minimum value of strain rate in forging is 10 s^{-1}. S. Bruschi et al. [9] has investigated the deformation behavior at 50s^{-1} but in a narrow temperature window of 880-950 °C. So, study of hot deformation behavior at higher strain rate and varied temperature range becomes important.

The objectives of the present work are: (i) to investigate the deformation behavior of Ti-6Al-4V alloy at high temperature (700-1000 ºC) and strain rate (0.1-100 s^{-1}), (ii) to develop a relation between flow stress, temperature and strain rate in the considered range, (iii) to determine favorable conditions for hot working of Ti-6Al-4V alloy and validation of the same by microstructural analysis.

EXPERIMENTAL PROCEDURE

The as-received Ti-6Al-4V alloy had a chemical composition (wt. %): 6.56 Al, 4.08 V, 0.15 Fe, 0.2 O, 0.005 N and Ti to balance. Its β transus temperature was 995 °C. The microstructure of as received material (as shown in fig. 1) consists of equiaxed α and β phases having volume fraction of approximately 62% and 38%, respectively.

Compression specimen of size Ø10 × 15 mm were machined from the as received Ti6Al-4V alloy bar. A hole of Ø 1 × 5 mm depth was drilled at mid height of sample for inserting thermocouple. The same is shown in fig. 2. Isothermal compression tests with constant strain rate were conducted in the temperature range of 700-1000 °C with an interval of 50 °C and strain rates used were 0.1, 1, 10, 100 s^{-1}. The hot compression tests were carried out on Gleeble thermo mechanical simulator. All the samples were deformed to a true strain of 0.7, which is equivalent to reduction of about 50%.

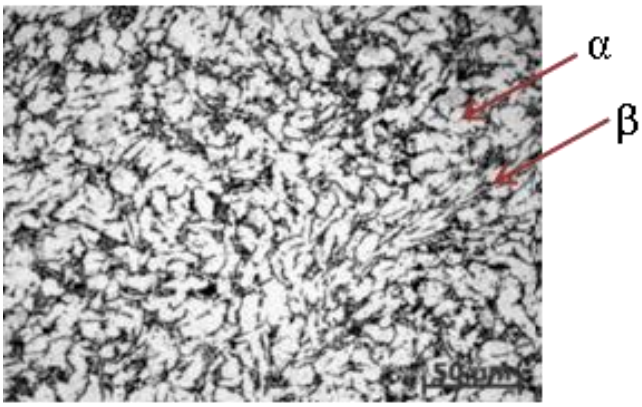

Fig. 1. Optical micrograph of as received sample

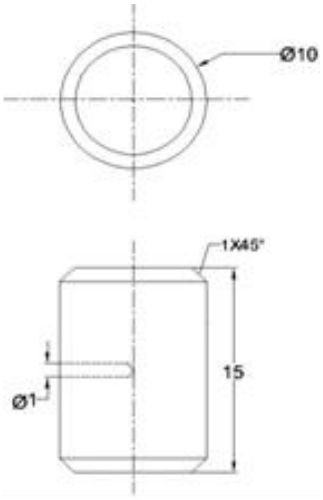

Fig. 2. Drawing of compression test sample.

In the present work, samples were heated at a constant heating rate of 5 °C/s and held at the deformation temperature for about 2 min before compression. In order to monitor the temperature, K-type thermocouple was inserted at the mid height of sample. After compression, the samples were water quenched. The deformed samples were sectioned parallel to the compression axis and the cut surfaces were prepared by the standard polishing and etching techniques for microstructure observation.

RESULTS AND DISCUSSION

Flow stress curves

To represent the flow behavior, stress-strain curves at different deformation temperatures and strain rates were generated and are shown in fig. 3. Flow stress decreases with an increase in temperature. The flow stress curves show three types of behavior namely, flow hardening, flow softening and steady-state flow. Upto a temperature of 900 $^{\circ}$C, continuous flow softening after peak stress is observed at strain rate upto 10 s^{-1}. But, at higher temperatures steady-state behavior is observed. This steady-state behavior indicates that the material flow softening is fast enough to cancel out the work hardening [4]. Flow stress increases with increase in strain rate. The same is shown in fig. 4 for temperature 900 ^{o}C.

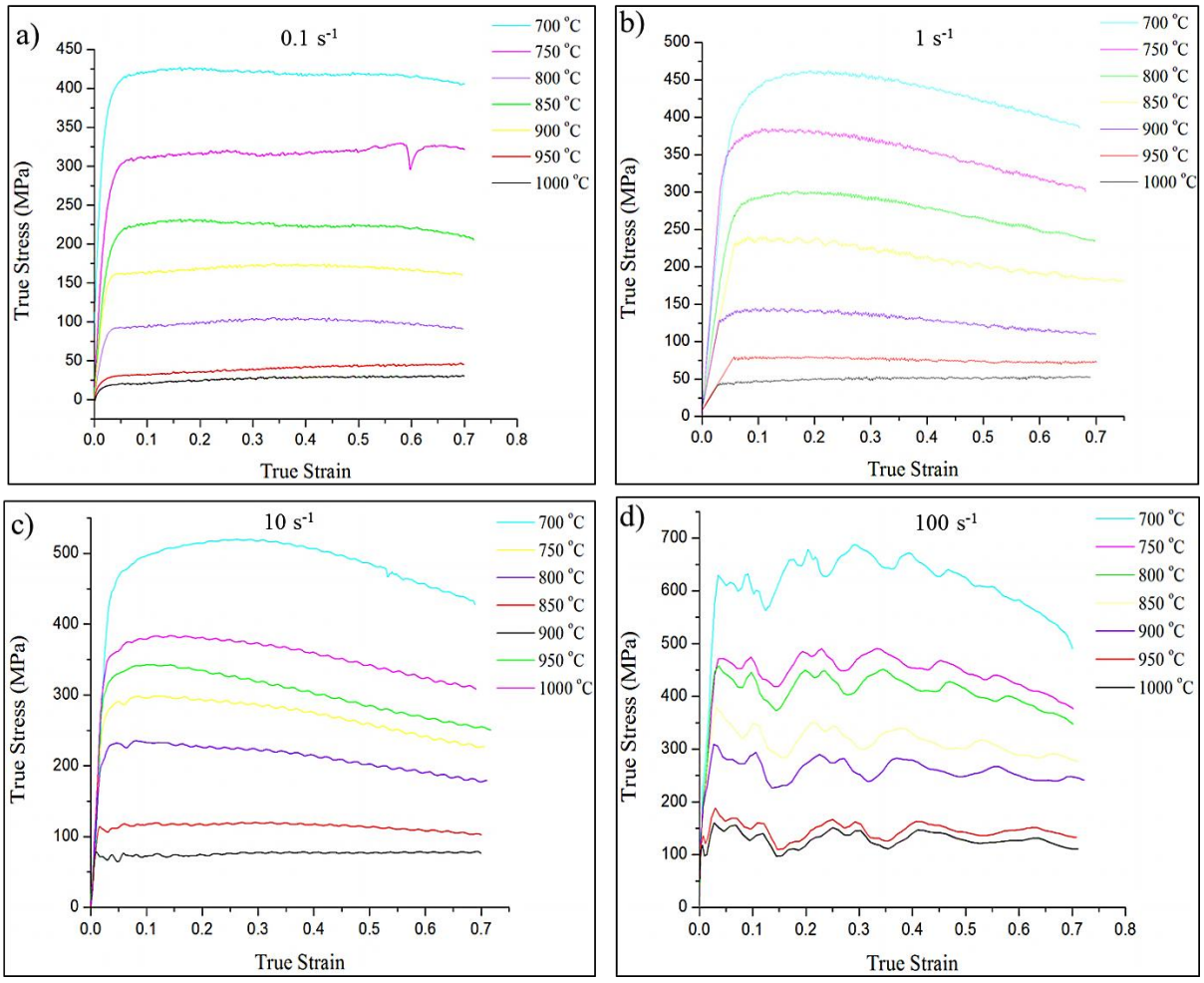

Fig. 3. True stress-strain curves at different temperatures and strain rates.
(a) 0.1 s^{-1}, (b) 1 s^{-1} , (c) 10 s^{-1} and (d)100 s^{-1}.

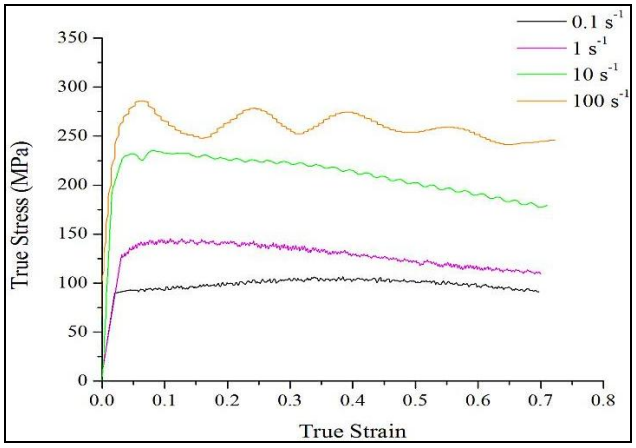

Fig. 4. True stress-strain curves at different strain rates for temperature 900 ºC.

At temperatures 950 and 1000 ºC, for the strain rate of 0.1 s^{-1}, flow hardening is observed. At strain rate of 100 s^{-1} and whole test temperature range, broad oscillations (fig. 3d) are observed. This may be due to dynamic recrystallization or flow instabilities because of deformation localization or micro-crack in the deformation process.

During tests, temperature of sample increases because of adiabatic temperature rise. So, the resulting flow stress will be lower than the actual flow stress for the desired test temperature. Thus, the flow stress from compression tests needs be corrected for adiabatic temperature rise.

Correction for friction and adiabatic temperature rise

Flow stress obtained from compression tests needs to be corrected for both friction and adiabatic temperature rise. The friction correction is done on the basis of bulging coefficient calculation. If the bulging coefficient is more than 0.9 then it is not necessary to correct the stresses for friction. Bulging coefficient of all deformed samples were calculated and were found to be more than 0.9. Hence flow stress was not corrected for friction.

The correction for adiabatic temperature rise is done on the basis of Fourier number calculation. Fourier number can be calculated by the equation:

$$F_0 = \frac{\alpha' s}{\varepsilon' l^3} \qquad (1)$$

where, α = thermal diffusivity,

s = extent of deformation,

$\dot{\varepsilon}$ = strain rate and

l = characteristic specimen dimension.

If, $F_0 < 0.01$, then the process is adiabatic in nature (flow stresses need to be corrected for adiabatic temperature rise) and if $F_0 \geq 10$, then the process is isothermal in nature. Between these two limiting conditions of F_0, the process is transitional in nature [10].

As an example, Fourier number calculation for 700 °C and whole strain rate range is presented in table 1. It is clear from the table that at strain rate of 1, 10 and 100 s^{-1}, the Fourier number $F_0 < 0.01$. So, the flow stresses corresponding to these strain rates must be corrected for adiabatic heat rise.

Table 1: Fourier number table at 700 ºC

Fourier number at temperature 700 ºC								
Strain rate (s^{-1})	Strain							$\Delta T_{adiabatic}$
	0.1	0.2	0.3	0.4	0.5	0.6	0.7	
100	1.15E-05	2.20E-05	3.08E-05	0.00003	4.64E-05	5.32E-05	5.91E-05	77
10	0.00011	0.00021	0.00030	0.00038	0.0004	0.00052	0.00058	77
1	0.00112	0.00212	0.00303	0.00386	0.00461	0.00528	0.00572	62
0.1	0.011	0.0209	0.0299	0.0381	0.0455	0.0521	0.0582	3

In the process of correcting flow stresses for the adiabatic heat rise, first step is to calculate the said temperature rise. This can be calculated by using the eq. (2).

$$\Delta T = (\eta_a \, 0.95 \int_{\varepsilon 1}^{\varepsilon 2} \sigma \, d\varepsilon) / (\rho C p) \qquad (2)$$

where, η_a is the adiabatic correction factor, ρ is the density and C_p is the specific heat. The integral part $\int_{\varepsilon 1}^{\varepsilon 2} \sigma \, d\varepsilon$ is amount of work done, which be calculated as area under the curve of uncorrected stress-strain.

The adiabatic correction factor η_a indicates the fraction of adiabatic heat rise retained in the sample after heat loss. This can be calculated by using eq. (3). This correction factor is used to get the accurate temperature rise at different strain rate conditions [11].

$$\eta_a = \frac{\Delta T\ actual}{\Delta T\ adiabatic} \qquad (3)$$

where, ΔT_{actual} is the test temperature and $\Delta T_{adiabatic}$ is the temperature measured using the thermocouple.

Accordingly, the flow stress curves related with strain rates of 1, 10 and 100 s^{-1} and whole temperature range were corrected for adiabatic heat rise. Corrected flow stresses have been used for further analysis.

Constitutive equations

It is necessary to model the flow stresses in terms of temperature and strain rate as the compression tests used to determine the stresses are costly and time consuming. The effect of temperature and strain rate on material deformation behavior can be expressed by Zener-Holloman parameter (Z) [4, 12]. So, a relation between flow stress and Z needs to be established.

The temperature and strain rate dependent flow stress in hot deformation is generally represented by kinetic rate equation:

$$\dot{\varepsilon}\, exp\left(\frac{Q}{RT}\right) = A\, sinh(\alpha\sigma)^n \qquad (4)$$

where, Q is the apparent activation energy, R is the gas constant (R= 8.3144 J/ mol. K), T is the deformation temperature, n is the stress exponent, A and α are the material constants.

Zener–Holloman parameter (Z) is represented by exponent-type equation [4, 12]:

$$Z = \dot{\varepsilon}\ exp(Q/RT) \qquad (5)$$

Determination of activation energy and material constants (α, A, n)

The value of α can be calculated by equation $\alpha = \beta/n'$. β and n′ can be calculated from the slope of the graph of σ vs ln $\dot{\varepsilon}$ and log σ v/s log $\dot{\varepsilon}$, respectively. The same are shown in fig. 5. Value of α was calculated for each temperature and the average value, 0.006412 was used for analysis.

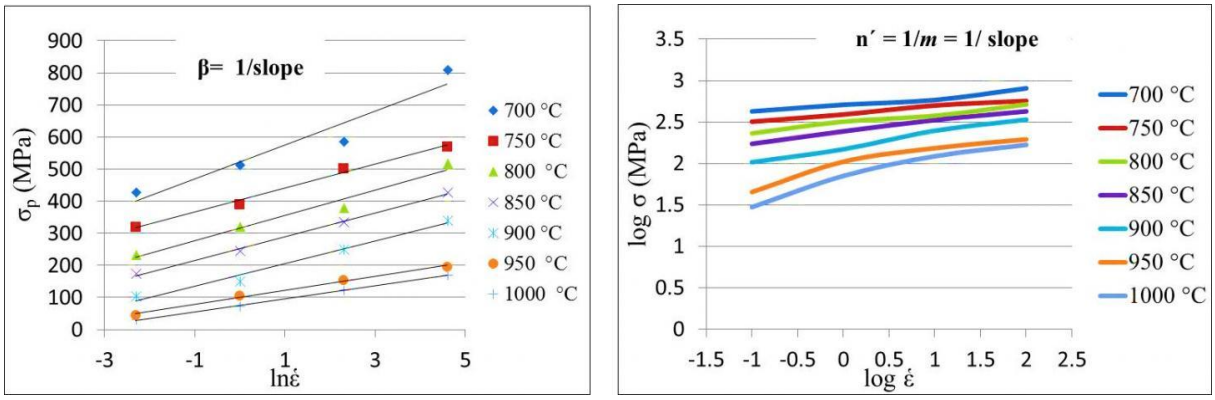

Fig. 5. (a) σ v/s ln $\dot{\varepsilon}$ for different temperatures, and (b) log σ v/s log$\dot{\varepsilon}$ for different temperatures.

The apparent activation energy, Q, is an important parameter as it indicates degree of deformation difficulty in plastic deformation.

Taking natural logarithm of eq. (4),

$$ln\ \dot{\varepsilon} = ln\ A + n\ ln\ (sinh(\alpha\sigma)) - \frac{Q}{RT} \qquad (6)$$

Activation energy, Q can be determined using the equation obtained after partially differentiating equation eq. (6),

$$Q = R \left(\frac{\partial ln\ \dot{\varepsilon}}{\partial ln\ [sinh\ (\alpha\sigma)]}\right)_T \times \left(\frac{\partial ln[\ sinh\ (\alpha\sigma)]}{\partial (1/T)}\right)_{\dot{\varepsilon}} \qquad (7)$$

Activation energy Q can be calculated with the help of eq. (7) by determining the slope of the graphs, ln [sinh(ασ)] vs ln $\dot{\varepsilon}$ and ln [sinh(ασ)] vs 1/T (Fig. 6). The activation energy calculated from graph is 484 kJ/ mol. This is in agreement with the values reported in literature [5, 7, 9]. This value is much higher than that of self-diffusion in α-Ti and β-Ti (150 kJ/mol).

The value of Z was calculated using eq. (5). In order to determine values of n and A, graph of ln Z v/s ln sinh(ασ) has been plotted as shown in fig. 7. The obtained value of n and A is 3.4453 and 5.184 x 10^{21}.

Equating eq. (4) and (5),

$$Z = A \times sinh\ (\alpha\sigma)^n \qquad (8)$$

Putting values of variables in eq. (8), relation between flow stress and Z can be established.

$$sinh\ (\alpha\sigma) = (1.9287\times10^{-22}\ Z)^{1/n}$$

$$\sigma = 155.9377 \times sinh^{-1}\ (1.9287\times10^{-22}\ Z)^{0.2929} \qquad (9)$$

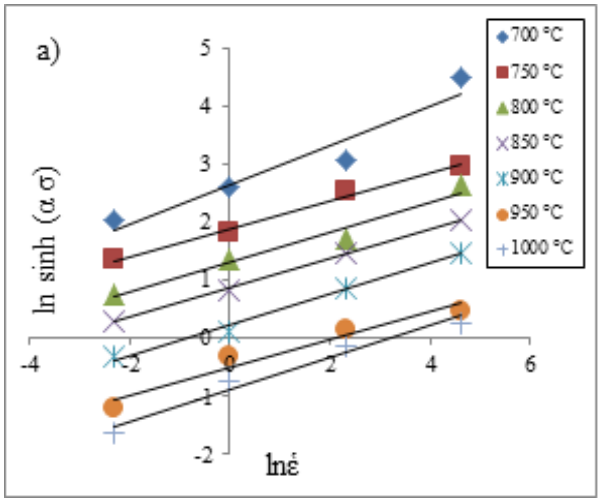

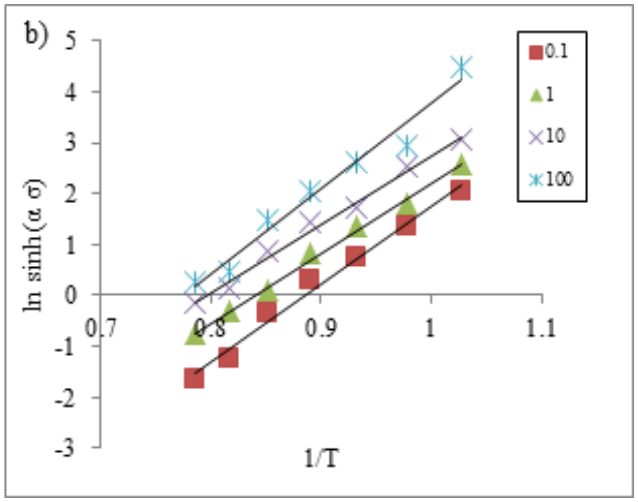

Fig. 6. Relation between (a) ln [sinh(ασ)] v/s ln ε̇, and (b) ln [sinh(ασ)] v/s 1/T.

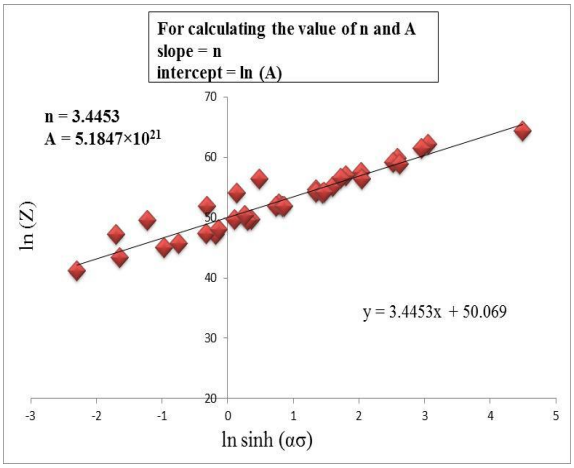

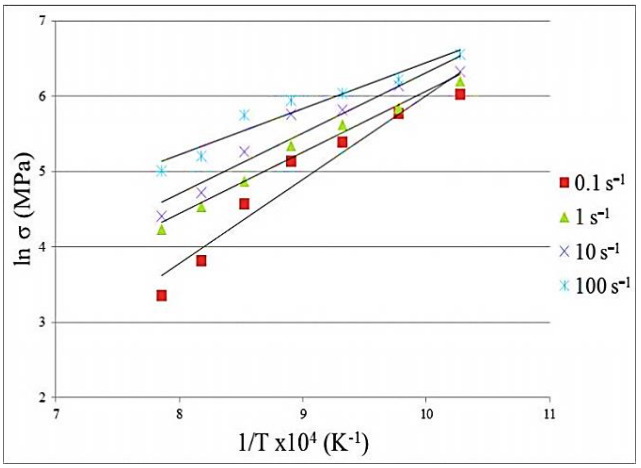

Fig. 7. Plot of ln(Z) v/s ln sinh(ασ)

Fig. 8. Plot of ln σ v/s 1/T for different strain rates.

Flow instability

To identify the stable and unstable hot working conditions of Ti6Al4V alloy the four DMM stability criteria, as proposed by J.C. Malas and V. Seetharaman[13], were used. The DMM stability criteria are as given below:

1. $0 < m \leq 1$ *(10)*

2. $\frac{\partial m}{\partial(\log\dot{\varepsilon})} < 0$ *(11)*

3. $s \geq 1$ *(12)*

4. $\partial s / \partial(\log\dot{\varepsilon}) < 0$ *(13)*

where, m = Strain rate sensitivity = $\left[\frac{\partial log\sigma}{\partial log\dot{\varepsilon}}\right]_{\dot{\varepsilon},T}$ and

s = Temperature sensitivity = $\frac{1}{T}\left[\frac{\partial\, ln\, \sigma}{\partial\, ^1/_T}\right]_{\dot{\varepsilon},\varepsilon}$.

Metals and alloys satisfy the first criterion, i.e. eq. (10), under hot deformation conditions. Negative values of m are obtained under conditions of dynamic propagation of pre-existing crack or newly formed micro-cracks in the workpiece. The second criterion, i.e. eq. (11), related to the variation of m with log $\dot{\varepsilon}$, arise from the necessity for a material system to continuously lower its total energy. So, the slope of m as a function of log $\dot{\varepsilon}$ should be negative. If fracture stress is assumed to be independent of stain rate then increasing value of m with log $\dot{\varepsilon}$ will probably lead to catastrophic failure at high strain rates. The third criterion, shown in eq. (12), is based on the extremum principle which states that the net entropy rate production for irreversible processes must be positive for stable condition. The fourth criterion, shown in eq. (13), relating to the variation of s with log $\dot{\varepsilon}$ arises from the necessity for material system to continuously lower its total energy. With increasing strain rate, the extent of adiabatic heating increases significantly. Hence, if the local strain rate increases above nominal value in any particular region of the workpiece, then it is accompanied by a reduction in the local flow stress. However, if the value of s increases with strain rate, then thermal softening will be encountered in the regime of high strain rate, which will produce flow localization and adiabatic shear bands [13].

In order to check for first two stability criteria, i.e. eq. (10) and (11), graph of m v/s log $\dot{\varepsilon}$ at given temperature and deformation (fig. 9) is plotted. The first criterion is satisfied for all temperature and strain rate range, while the second criterion is only satisfied in the strain rate range of 0.1-1 s^{-1} for temperatures 950 and 1000 ºC while the same is satified above strain rate of 10 s^{-1} for temperatures 750 and 850 ºC. In order to check third and fourth stability

criteria given by eq. (12) and (13), graph of s v/s log $\dot{\varepsilon}$, considering a constant temperature, (fig. 10) is plotted. This plot shows that third criterion is satisfied for whole temperature and strain rate range, while fourth criterion is satisfied only for strain rate range of 0.1-1 s^{-1} and above 10 s^{-1} for whole temperature range.

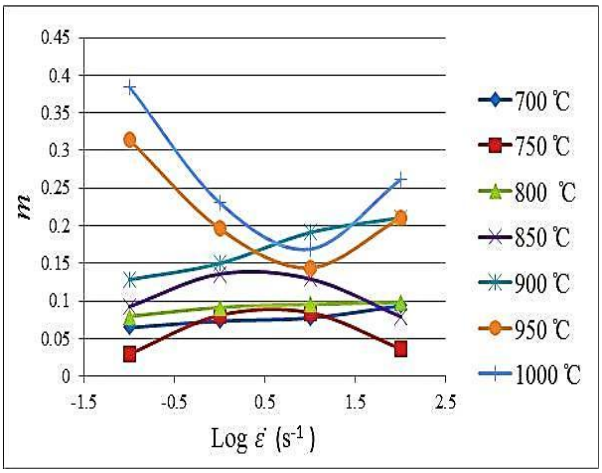

Fig. 9. Plot of *m* v/s Log $\dot{\varepsilon}$.

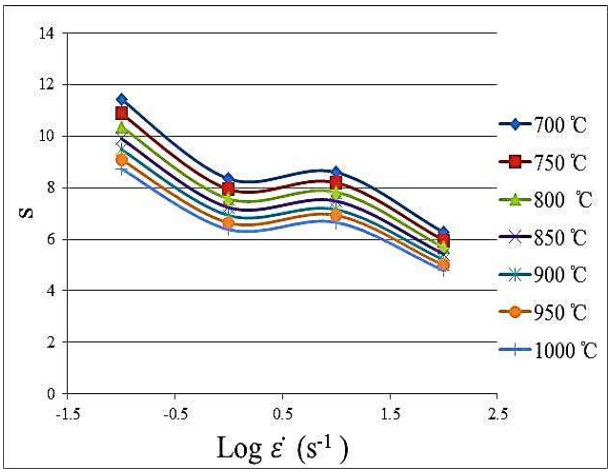

Fig. 10. Plot of s v/s Log $\dot{\varepsilon}$.

After checking all four criteria, it is found that the plastic flow is stable in the strain rate range of 0.1-1 s^{-1} for temperatures 950 and 1000 ºC as well as above strain rate of 10 s^{-1} for temperatures 750 and 850 ºC as shown in table 2.

Table 2. Stable conditions for hot deformation

The stable condition for hot deformation
950 °C, 1000 °C and 0.1-1 s^{-1}
850 °C, 750 °C and above 10 s^{-1}

For optimum condition among the stable conditions, strain rate sensitivity, m should be greater than 0.3 since, the deformation is considered to be superplastic deformation if *m* is greater than 0.3 [14]. For 750 and 850 ºC, value of m is less than 0.3. But, the same at 950 ºC and 1000 ºC is 0.32 and 0.38, respectively. At 1000 ºC volume fraction of β phase exceeds its critical value. Due to this, mechanical properties deteriorate. So, the optimum condition for hot working of Ti6Al4V alloy is 950 ºC and strain rate range 0.1-1 s^{-1}.

Microstructural observations

The favorable hot working conditions as discussed in section 3.4, have been validated through microstructural analysis. Some micrographs of samples deformed at stable and unstable conditions are shown in fig. 9 and 10. Adiabatic shear band was observed in the microstructure of sample deformed at unstable conditions of 850 ºC and 10 s^{-1} (fig. 11 a). The microstructure of sample deformed at 900 ºC and 10 s^{-1} (unstable condition) as shown in fig. 11(b) exhibits flow localization. At high strain rate, metal and alloys frequently show the narrow zone of highly localized deformation, which is referred as adiabatic shear band [4, 12]. These conditions are not good for the workability and mechanical properties of the material. These deformation conditions need to be avoided during hot working of the alloy.

Microstructure of the samples deformed at stable conditions, (750 ºC and 100 s^{-1}) and (950 ºC and 0.1 s^{-1}) are shown in fig. 12 which shows homogeneous structure with no defects.

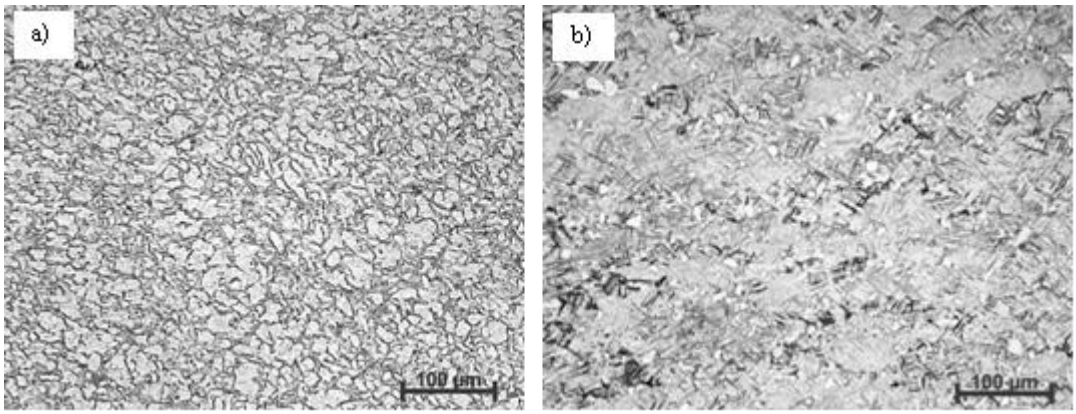

Fig. 11. Microstructure of the specimens deformed in the unstable regime (a) 850 ºC, 10 s^{-1} and (b) 900 ºC, 10 s^{-1}.

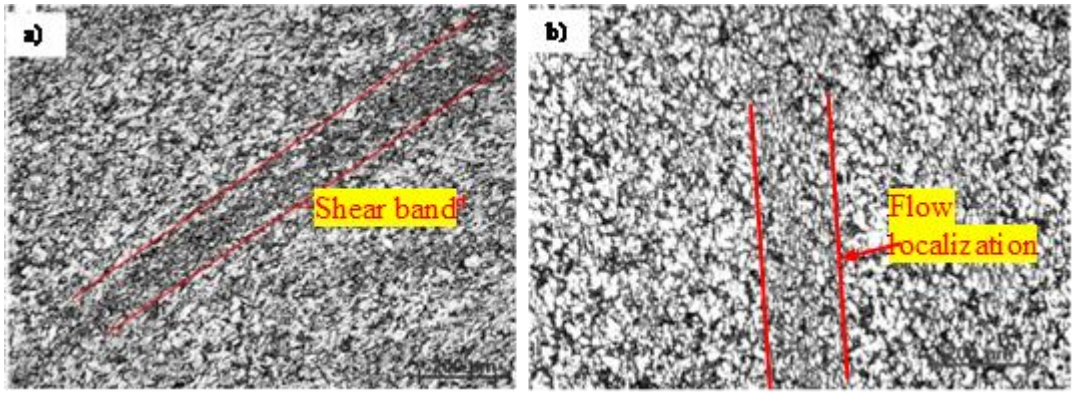

Fig. 12. Microstructure of the specimens deformed in the stable regime (a) 750 ºC, 100 s^{-1} and (b) 950 ºC, 0.1 s^{-1}.

CONCLUSIONS

Following can be concluded from the results obtained in present work:

1. Flow stresses decrease with increase in temperature and decrease in strain rate. At lower deformation temperature and higher strain rate, flow stresses exhibits continuous flow softening after peak stress.

2. The favorable conditions for hot deformation were found to be in the strain rate range of 0.1-1 s^{-1} for temperatures 950 and 1000 ºC as well as above strain rate of 10 s^{-1} for temperatures 750 and 850 ºC.

3. The optimal condition for hot working of the Ti–6Al–4V alloy is at a temperature of 950 ºC and strain rate range of 0.1-1 s^{-1}.

4. The microstructures of the sample deformed in the unstable deformation regime have the flow localization and non-homogeneous structure. Whereas the microstructures of the specimen deformed in the stable regime shows homogeneous structure.

ACKNOWLEDGEMENT

The authors gratefully acknowledge the extended support provided to this work by KCTI (Kalyani Centre for Technology and Innovation) for providing financial funding, laboratory and library facilities. The authors also acknowledge the support provided by Bharat Forge Ltd, Pune, DSIR (Department of Scientific and Industrial Research), Govt. of India and my colleague Santosh Kumar and Deepak Kundalkar. Finally, the authors would like to express special thanks and gratitude to review committee and top management of Bharat Forge Ltd for granting the permission to publish/present the research work.

REFERENCES

[1]. E. B. Shell, S. L. Semiatin (1999): Metallurgical and Materials Transactions A, 30 A, 3219-3229.

[2]. M. Arulselvan, G. Ganesan (2014): International Journal of Innovative Research in Advanced Engineering, vol. 1 issue 7, 207-212.

[3]. L. Yang, Y. Yang (2014): Transactions of Nonferrous Metals Society of China, 24, 3103-3110.

[4]. K. L. Wang, S. Q. Lu, M. W. Fu, X. Li, X. J. Dong (2010): Materials Science and Engineering A, 527, 7279-7285.

[5]. A. Momeni, S. M. Abbasi (2010): Materials and Design, 31, 3599-3604.

[6]. T. Wen, Y. W. Yue, L. T. Liu, J. M. Yu (2014): Indian Journal of Engineering and Material Sciences, 21, 647-656.

[7]. J. Cai, F. Li, T. Liu, B. Chen, M. He (2011): Materials and Design, 32, 1144-1151.

[8]. N. K. Park, J. T. Yeom, Y. S. Na (2002): Journal of Materials Processing Technology, 130–131, 540-545.

[9]. S. Bruschi, S. Poggio, F. Quadrini, M. E. Tata (2004): Materials Letters, 58, 3622-3629.

[10]. K. N. Pandey and S. Chand (2003): International Journal of Pressure Vessels and Piping, 80, 673-687.

[11]. R. L. Goetz, S. L. Semiatin (2001): Journal of Materials Engineering and Performance, Vol. 10(6), 710-717.

[12]. T. Seshacharyulu , S.C. Medeiros, W. G. Frazier , Y. V. R. K. Prasad (2000): Materials Science and Engineering A, 284, 184-194.

[13]. J. C. Malas, V. Seetharaman (1992): JOM, 44, 8-13.

[14]. A. Sołek, J. Krawczyk (2015): Materials and Design, 65, 165-173.

National Conference on Thermo-mechanical processing of Steels &
5th Gleeble User Workshop India (GUWI-2015),
August 6-7, 2015, pp 92-104.

Thermo-mechanical Simulation of Continuous Annealing and Galvannealing Process

Pranav Tripathi, I. Chakradhar, Prakash Rao and Rahul Desai

JSW Steel Ltd, Vijayanagar works. Toranagallu, Karnataka

E-mail: pranavkumar.tripathi@jsw.in

ABSTRACT

With the commissioning of CRM-II, JSW steel has started developing variety of high strength and automotive steels. These steels are processed through the state-of-the-art continuous annealing and galvanizing lines. The cold rolled steel sheets are passed through different zones including preheating, heating, soaking, slow cooling, rapid cooling, overaging and final cooling in a very short time. The galvannealing lines include multistep soaking and cooling. The strengthening mechanisms in these processes such as phase transformation, precipitation etc are a strong function of line speed and strip temperatures. Minor change in any of these parameters causes significant variations in mechanical properties. Optimization of these process parameters becomes challenging due to the associated cost involved in plant scale experimentation. To address this issue, an offline methodology has been developed for simulating these processes using thermo-mechanical simulator "Gleeble". Processing routes for the different plant cycles were converted into time-temperature plots and programmed in Gleeble for a number of steel grades such as IF, dual phase and micro alloyed. The paper explains the intelligent use of Gleeble in simulating wide range of cooling rates in multistep operations. The mechanical properties, microstructure and the phases in cold rolled strip samples simulated in Gleeble were compared with the actual plant cycles and found to be in close agreement. Off-line simulations helped in reducing the required plant trials thereby enabling faster optimization of process parameters for desired mechanical properties in different grades of steels.

***Keywords**: Thermo-mechanical simulation, Gleeble, continuous annealing, galvannealing.*

INTRODUCTION

JSW Steel Vijayanagar Works is the largest steel producer in India at a single location with an annual production of 10 MT. It has two cold rolling mills (CRM) with a combined annual production capacity of 3.3 MT. CRM-1 has continuous pickling line (CPL), compact cold mill (CCM), electrolytic cleaning line (ECL), batch annealing furnace (BAF), skin pass mill (SPM), Re-Coiling Line (RCL) and automatic packaging line (APL). Each of the unit

contributes to the total production of CRM-1. CRM-2 has Pickling Line Tandem Cold Mill (PLTCM), Continuous Annealing Line (CAL) and Continuous Galvannealing Line (CGL).

With the commissioning of CRM-2, JSW Steel has forayed into the production of cold rolled steel strips as value-added products for specific applications such as automotive exterior and interior panels and white goods demanding excellent surface finish along with stringent quality requirements. In cold rolling mill, hot rolled steel strips are pickled and cold rolled at room temperature to achieve improved surface quality and mechanical properties of the sheet. Pickling Line Tandem Cold mill is a combination of continuous pickling and continuous cold reduction of the hot rolled strip. Pickling is generally a combination of chemical reaction and mechanical separation of scales. It has the product mix of HRPO (hot rolled pickled and oiled) which goes to the end customer directly and some other coils go to further operation in subsequent units for annealing. Post PLTCM, the coils are heat treated in two separate continuous annealing and galvanizing/galvannealing lines.

The heat treatment parameters applied to the cold rolled strip during continuous annealing and galvannealing are extremely important in determining the final mechanical properties and microstructure of the coils. These parameters are highly grade specific and include the inter-critical annealing temperature, soaking duration and specific combinations of cooling rates. The continuous annealing and galvannealing lines have been divided into specific sections involving preheating, heating, soaking, slow cooling, rapid cooling, overaging and final cooling in a very short time. The strengthening mechanisms in these processes such as phase transformation, precipitation etc are a strong function of line speed and strip temperatures. Any change in these parameters causes significant variations in mechanical properties. Hence, it becomes imperative to optimize the process parameters for close control on mechanical properties of the final product.

In the present study, experiments were carried out to simulate the continuous annealing and galvannealing processes in thermo mechanical simulator (Gleeble). Cold rolled full hard material of different grades produced at CRM-2 were collected and subjected to different annealing and galvannealing cycles for strip annealing simulations. Processing routes for the different plant cycles were converted into time-temperature plots and programmed in Gleeble for a number of IF, high strength, dual phase and micro alloyed steel grades. The simulated specimens were tested for mechanical properties, microstructure and phase present to correlate the Gleeble simulations with actual plant conditions. Subsequently, Gleeble

simulations are being utilized for optimizing/improvising CAL parameters for specific auto grades.

GLEEBLE SIMULATION

Physical and Mathematical modeling has become an inevitable toll in the present day research for design development and control of steel processing. Owning to low cost and inherent limitation of experimentation in both physical simulation and mathematical simulation, both methodologies have become interdependent. Relevant data for mathematical simulation in now economically obtained from physical simulation tests. Numerous works on physical simulation have been reported for various processing operations using Gleeble which has been extensively used for simulating continuous casting, rolling, forging, heat treatment, welding, annealing etc. Gleeble provides a platform for testing samples and determine its limits of mechanical properties under various conditions. This has also been widely used for validating mathematical models. The thermo-mechanical simulator Gleeble-3800 at R&D JSW Vijayanagar works has two mobile conversion units, the pocket jaw and the hydrawedge. This machine is playing a significant role in product development and process improvement. With its continuous usage, the product development cycle has shortened along with solving many critical issues in several critical grades.

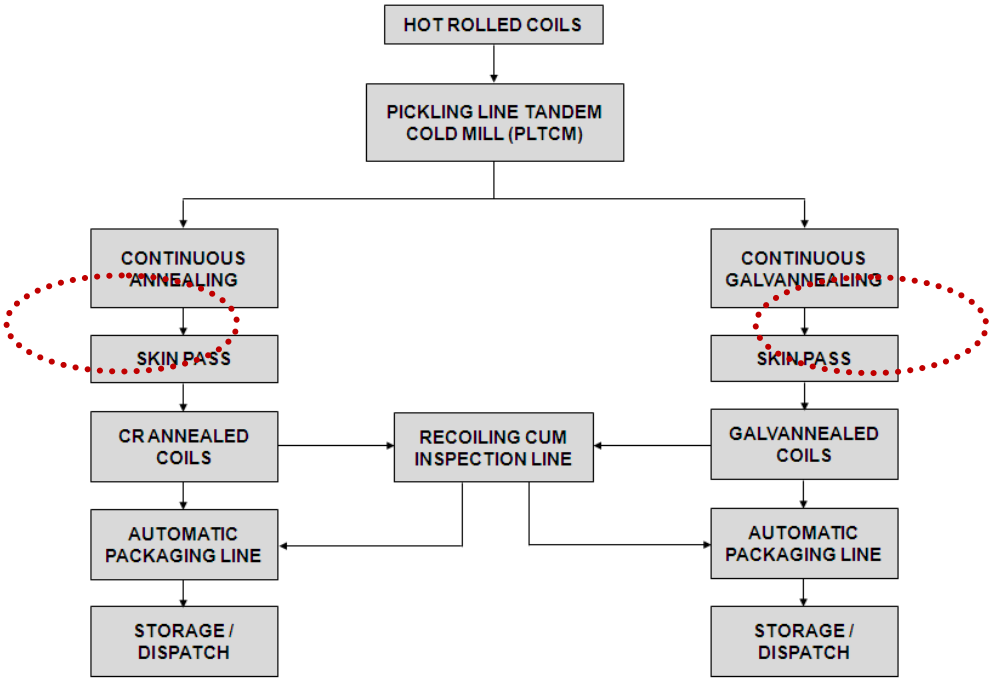

Fig. 1 : Process Flow Chart of Cold Rolling Mill-2

Gleeble Simulation of Continuous Annealing Line (CAL)

The continuous annealing line can be broadly divided into heating, soaking and cooling sections. In heating zone, the strips are heated up to the respective annealing temperatures followed by soaking for a predefined period of time. The time period for which a section of the strip is subjected to different temperature zones if primarily dependent upon the mill speed which remains constant throughout the CAL line for a single grade. After soaking, the strip enters slow cooling section which is followed by rapid heating section where major phase transformations and strengthening mechanisms take place. In the overaging section, the strip is made to cool very slowly so as to allow sufficient time for carbon diffusion. It increases the formability of the strip with a collateral decrease in the yield strength. This is followed by final cooling and water cooling zones where the temperature of the strips drops to around 50ºC. Figure 2 shows a schematic view of the continuous annealing line.

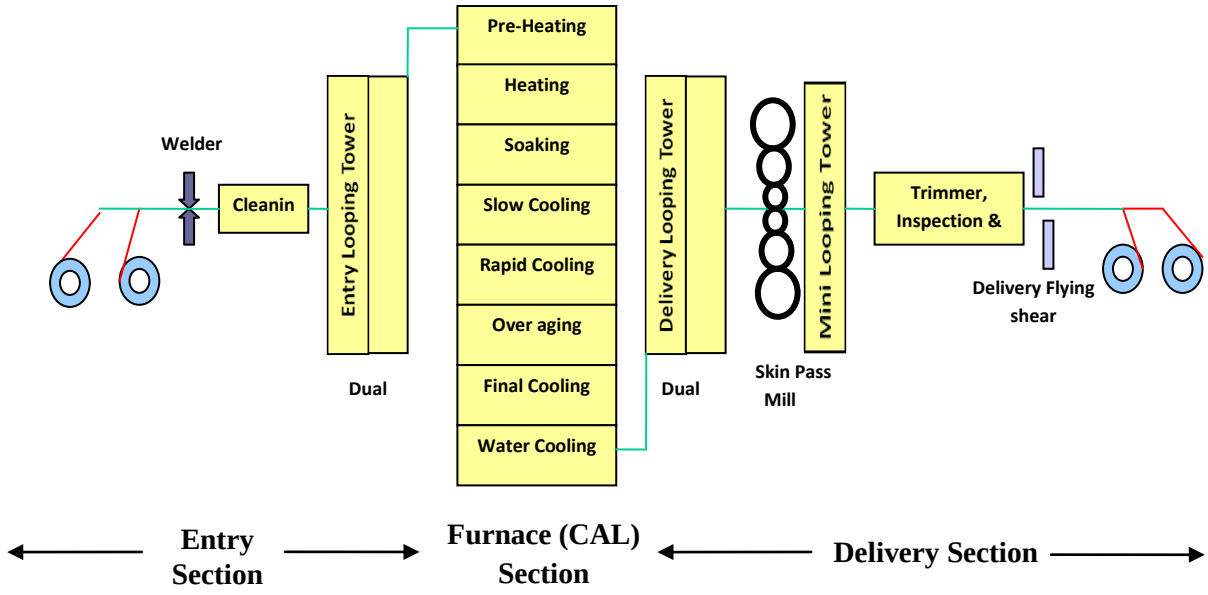

Fig. 2 : Schematic view of CAL Cycle

Gleeble Simulation of Continuous Galvannealing Line (CGL)

Cold rolled galvannealed (GA) sheet material for auto bodies requires high strength, superior formability and corrosion resistance. High strength allows for thinner gauge material, which reduces weight and increases fuel efficiency. High strength also improves the dent resistance of a material, which is important esthetically, and improves the crash resistance of the

material, important for passenger safety. The automobile manufacturers are now being forced to comply with the stringent safety and environmental norms. One way of achieving both these criteria is to increase the use of high strength steels with lower thickness. The increase in strength must be obtained without deteriorating the formability to any extent. To meet this requirement of the automobile industry, many different grades of modern galvannealed high strength steels have been developed; these include Interstitial Free steel (IF steel) and IF High Strength steel, Bake Hardening (BH) steel and High Strength Low Alloy (HSLA), Dual Phase steel (DP steel) etc. These steels are having different combination of strength-elongation properties.

Each section in the CAL and CGL has a specific zone length. Based on the line speed for different grades, the time interval in a particular section for each grade can be calculated. This way, time-temperature plots are derived which are programmed into thermal cycles for Gleeble simulations. Table 1 lists the number and type of grades for which CAL and CGL cycles have been simulated.

Table 1: Grades simulated for CAL and CGL cycles

Grade Type	Grades simulated for CAL	Grades simulated for CGL
IF Steel (A)	5	4
High Strength Steel (B)	2	2
Dual Phase (C)	3	1

EXPERIMENTAL PROCEDURE AND RESULTS

Sample Preparation

Cold rolled full hard samples were collected from PLTCM for strip annealing simulation in GLEEBLE. These samples were cut down to 240*50 mm size with 5 mm diameter holes on either side as shown in figure 3. The samples were 0.8 mm thick for IF grades and 1.2 & 1.6 mm thick for HSS and DP grades as per the operating practice.

Fig. 3 : Specimens for strip annealing simulations in Gleeble

Strip Annealing Simulations

These full hard samples are subjected to different annealing cycles depending on the property requirement. Samples were cleaned with acetone and chromel-alumel thermocouple wires were attached to the sample. Sample was fixed inside pocket jaw module with strip annealing grips. Samples were subjected to annealing as per the specific heat cycles pertaining to each grade. Figure 4 shows the arrangement for strip annealing simulation in Gleeble 3800 thermo-mechanical simulator.

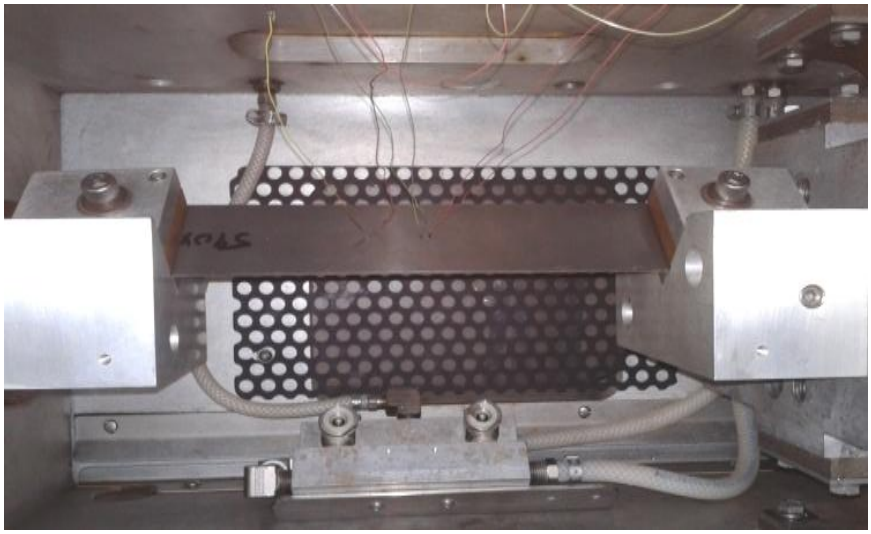

Fig 4: Strip Annealing simulations being conducted in Gleeble

After the annealing treatment, the samples were to be tested for mechanical properties, hence it was important to maintain a constant temperature zone of min. 50 mm across the strip length as per the minimum guage length required for mechanical testing. Therefore, during initial tests three set of thermocouples were attached to the sample to identify the uniform temperature zone. Figure 5 shows a sample annealed in Gleeble. A uniform temperature zone of 80-100 mm was easily achieved in all the annealed samples.

Fig 5: Strip sample after annealing

Thermal Cycle

During Gleeble simulations, the specimens were subjected to specific annealing and galvannealing cycles which were programmed into Gleeble programs. Figures 6 (a) & (b) show the typical programmed and achieved temperatures in Gleeble for CAL and CGL simulations. The figures clearly show that the plant thermal cycles have been matched exactly on the lab scale.

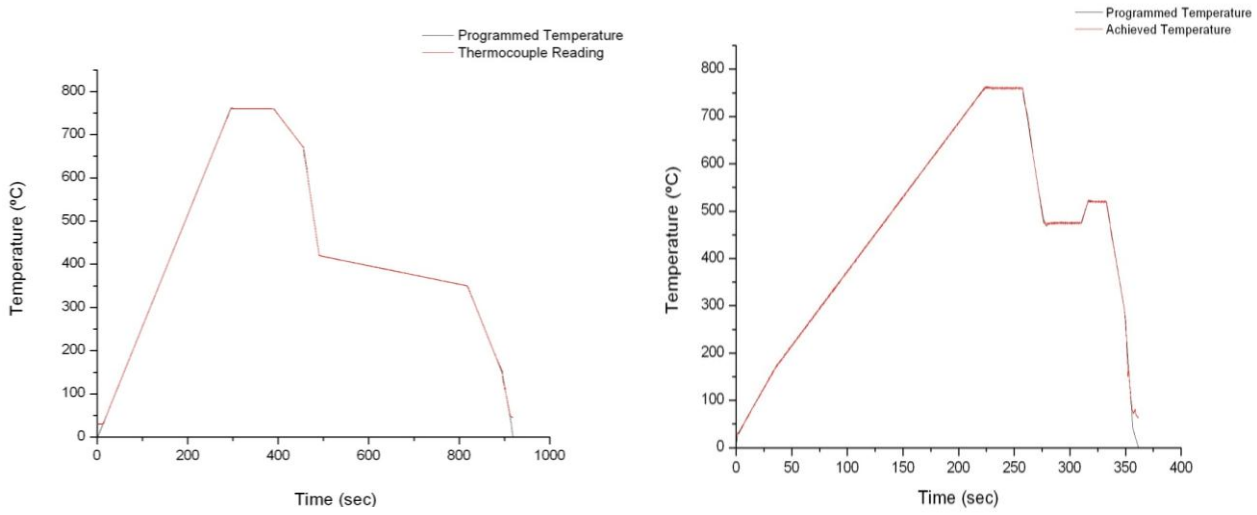

(a) **(b)**

Fig 6: Typical Time-temperature plots for (a) CAL and (b) CGL simulations

Mechanical Testing

The strip annealed samples were then subjected to tensile test with Zwick/Roell Z010 Universal testing machine to test the mechanical properties. The tensile test samples were punched out of the annealed specimen and subjected to tensile test as shown in figure 7.

Fig 7: Tensile test Specimen from Annealed sample

The mechanical properties of the grades which were subjected to strip annealing in thermo mechanical simulator Gleeble were compared with mechanical properties achieved in actual plant operations. The UTS values received in Gleeble samples were exactly matching with the plant samples. Few grades showed variation in yield stress as these samples were not subjected to skin pass rolling. This variation is due to the yield point phenomenon. As the plant grades are subjected to skin pass elongation there is no yield point phenomenon observed in those grades. However to take care of this variation the YS values were calculated using yield ratio (YS/UTS) as the yield ratio for these auto grades remains constant. Out of a number of grades simulated, for IF and HSS type grades, there was a close match between the properties of plant samples and Gleeble simulated samples. However, the properties for dual phase grades were not matching closely and needs further refinements in the simulation methodology. Henceforth, the simulation results for only IF and HSS grades are being presented and listed in tables 2 and 3 for CAL and CGL simulations respectively.

Table 2: Mechanical properties comparison of Plant and Gleeble samples for CAL simulations

Grade Type	Grade ID	Plant Properties			Gleeble Properties		
		UTS	YS	%El	UTS	YS	%El
IF Steel (A)	A1	287	142	54	286	143	54
	A2	347	182	48	345	183	46
High Strength Steel (B)	B1	444	276	37	445	270	35

Table 3: Mechanical properties comparison of Plant and Gleeble samples for CGL simulations

Grade Type	Grade ID	Plant Properties			Gleeble Properties		
		UTS	YS	%El	UTS	YS	%El
IF Steel (A)	A1	292	112	53	289	111	49
	A2	366	203	43	361	200	44
High Strength Steel (B)	B1	494	363	34	476	349	31

The typical tensile test graphs for IF and HSS grades obtained for Gleeble simulated samples are shown in figure 8. These tensile curves clearly show the occurrence of yield point phenomenon in IF and HSS grades.

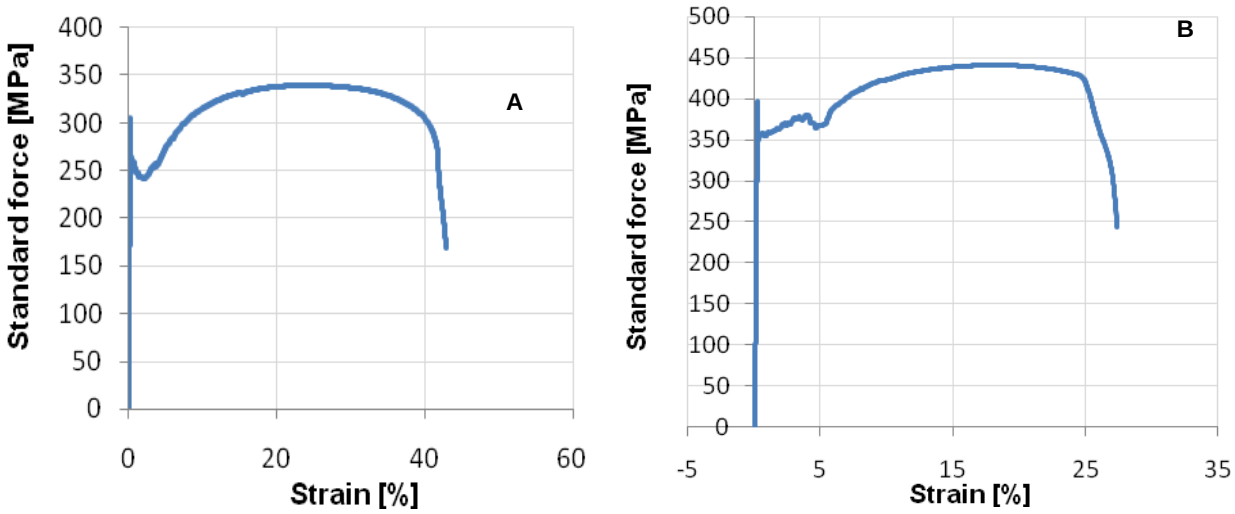

Fig 8: Typical Tensile test graphs for Gleeble annealed samples for (a) IF and (b) HSS grades

Metallography

Optical metallography samples in this study were prepared using standard techniques by grinding and fine polishing. All samples were freshly polished using 1µm diamond paste, cleaned and immediately etched with Nital to eliminate passivation due to atmospheric exposure. The optical micrographs taken at a magnification of 500X are presented in figure 9. They reveal similar mictostructures between the plant samples and Gleeble simulated samples. This reconfirms that the plant conditions have been exactly simulated.

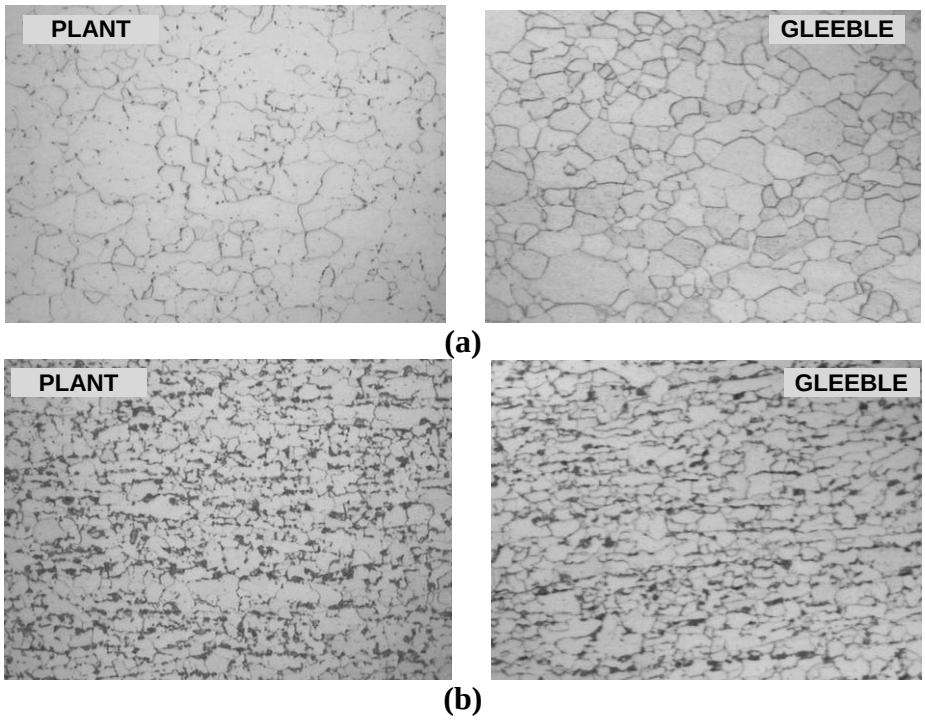

Fig 9: Comparison of micrographs for plant and Gleeble annealed samples for (a) IF and (b) HSS grades at 500X

Phase Analysis

Phase analysis through X-ray diffraction using Panalytical Empyrean was performed to compare the phases present in plant and Gleeble simulated samples. Figure 10 shows XRD analysis for a galvannealed HSS steel and confirms the presence of similar phases in both the cases. Hence, Gleeble simulations have been successful in replicating the plant conditions for these grades on a lab scale.

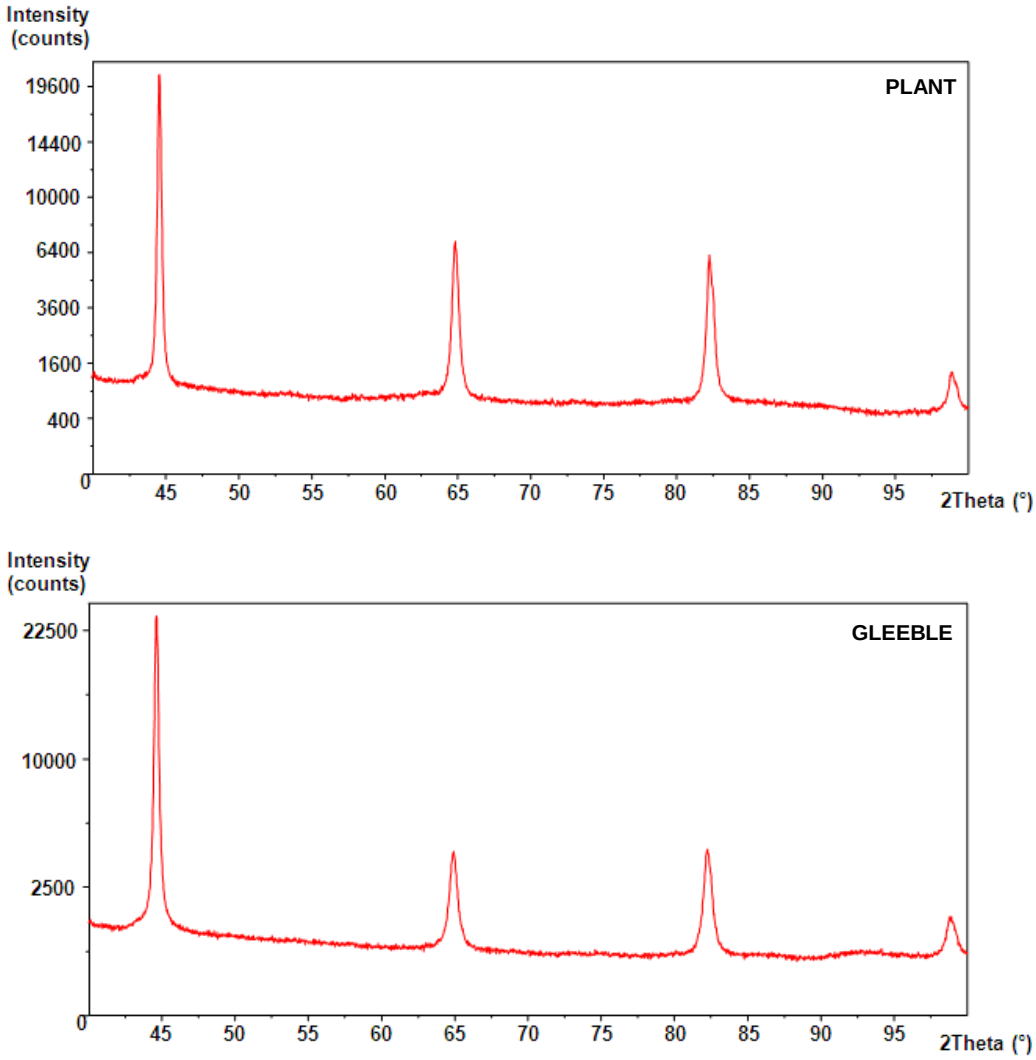

Fig 10 : Phase analysis of galvannealed Gleeble and Plant samples for HSS grade

ISSUES FACED WHILE SIMULATING CAL AND CGL CYCLES

There are a number of issues associated with the strip annealing simulations which were faced during the course of these experiments. The thickness of the strips used was 0.8 mm & 1.6 mm for CAL simulations and 0.8 mm & 1.2 mm for CGL simulations. To prevent

oxidation of the samples during the long test cycles, the experiments were performed under vacuum. As coupler is not used with hydraulic ram for strip annealing simulations, the compressive force of vacuum can be countered only by using air ram in tension. This is problematic especially during cooling cycles when thin strips (0.8 mm) are used. Some critical issues faced during strip annealing simulations are listed as under :-

- Calculating exact time-temperature plots from plant CAL and CGL cycles is of utmost importance for successful lab scale simulations. The strip temperatures are not constant during the process even in the constant temperature zones. Also, it does not cool in the entire cooling zone but only in front of the sprays. Moreover, the heating and cooling profiles in plant conditions are also not linear. Hence, the most representative time-temperature plot requires some offline heat transfer calculations to draw the precise time-temperature plots.

- The air ram pressure must be carefully set depending upon the strip thickness. As tests are conducted under high vacuum conditions; initially, the air ram pressure must be high enough to counter the compressive for generated by the vacuum. However, during cooling when air quench is used, the sample is subjected to tensile forces, hence the air ram must be switched off manually. Moreover, as CGL cycles involve reheating of the specimens, air ram pressure must be lowered manually and then it should be switch on to counter only the compressive forces generated in the specimen due to reheating (as there is no vacuum this stage). If not done so, the strips tend to get bulged.

- For both CAL and CGL cycles, the cooling cycles are very complex involving multiple combinations of high, low and very low cooling rates. To properly achieve the exact thermal cycles for each and every grade, a number of trials were required to determine the optimum quantities of air and water in the quenching mixture. Depending on the cooling rates the amount of water in the atomized spray was varied to prevent undercooling of strips and subsequent reheating through Gleeble thermal control system. Special care is needed when high cooling rates precede low cooling rates during cooling regime.

- When only air quench (Q4) is used, the system logic doesn't automatically vents off the vacuum. Hence, the same must be done manually to prevent damage to the vacuum system.

- Minimum quantities of quenching media should be used so as to avoid over quenching of the specimens. Even though Gleeble thermal system is capable of controlling the specified heating and cooling rates, several variables like radiative heat loss, thermal changes during phase transformations, strip thickness etc. are beyond any control. Hence, the quantities of the quenching media should be adjusted accordingly by taking into consideration these effects.

- High amount of quenching causes undercooling of the strip. To counter it Gleeble thermal system reheats the sample. If the underquenching is high, the heating current supplied by the thermal system can be quite high. In such a case, under the action of high air ram, thin (< 1 mm) strips start necking just ahead of the grips. This increases the resistance at these locations, further heating up and even melting the thin strips. Hence, special care regarding air ram pressure and amount of quenching media is required especially during strip annealing simulations for thin strips.

CONCLUSIONS

- A simple methodology has been developed for simulating continuous annealing and galvannealing processes in CRM line using thermo-mechanical simulator Gleeble.

- The plant cycles have been exactly simulated in lab scale with close correlation of mechanical properties obtained in industrial process and Gleeble simulated cycles.

- This off line simulation methodology helps in faster and economic product development and process optimization by reducing the requirement of online trials resulting is significant cost savings.

FUTURE WORK

The simulation methodology being established for a number of auto grades is being effectively utilized in optimizing and improvising the exiting CAL and CGL cycles. New

optimized cycles with parameters like annealing temperatures, slow & rapid cooling rates and overaging temperatures have been established on lab scale and successfully deployed in the plant scale. Further studies for optimizing process parameters for dual phase steels (upto 1000 MPa) are under progress.

REFERENCES

[1]. D. Bhattacharya, Developments in advanced high strength steels, [in] The Joint International Conference of HSLASteels 2005 and ISUGS 2005 Proceedings, Sanya, 2005, p.70.

[2]. K. Nakaoka, K. Araki, and K. Kurihara, Strength, ductility and aging properties of continuously-annealed dual-phase high-strength sheet steels, [in] A.T. Davenport ed. Formable HSLA and Dual-Phase Steels, TME/AIME, New York, 1979, p.128.

[3]. LIU Peng, JIN Xian-zhe. The development and research of automobile steel plate [J]. Shanxi Metallurgy, 1997(2): 32−33.

[4]. ZHU Xiao-dong, WANG Li. Effect of the continuous annealing parameters on the mechanical properties of cold rolled Si-Mn dual phase steel [C]//CSM 2003 Annual Meeting Proceedings, 2003:684−688.

[5]. Shuang Kuang, Yong-lin Kang, and Ren Dong Liu. Effect of Continuous Annealing parameters on the mechanical properties and microstructures of a cold rolled dual phase steel, [J]. Shanxi Metallurgy, 2008:1-6.

[6]. S. Kuang, Simulation of austenization during intercritical annealing for Fe-C-Mn cold rolling dual phase steel, J.Univ. Sci. Technol. Beijing (in Chinese), 30(2008), No.8,pg. 858.

[7]. X.D. Zhu, L. Wang, S.K. Ji, et al., Effect of over-ageing on the mechanical properties and microstructure of cold rolled low carbon Si-Mn dual phase steel sheets, Trans.Mater. Heat Treat. (in Chinese), 24(2003), No.2, p.50.

[8]. R.K. Ray, J.J. Jonas, and RE. Hook International Materials Review, Vol. 39, No. 4, 1994, and pp. 129- 172.

[9]. H. Takechi, ISIJ International, Vol. 34, No. 1, 1994, pp. 1-8.

[10]. Kei Sakata, Saiji Matsuoka and Kazuhiro Sato Kawasaki Steel Technical Report No. 48 March 2003.

National Conference on Thermo-mechanical processing of Steels &
5th Gleeble User Workshop India (GUWI-2015),
August 6-7, 2015, pp 105-114.

Hot Workability Studies on 2.7% Si Steel using Gleeble Thermo-mechanical Simulator

Kumar Aniket Anand[1], Kartik Nageswaran[1], Vinod Kumar[1] and Atul Saxena[1]

[1]*R& D Centre for Iron & Steel, Steel Authority of India Ltd., Ranchi (Jharkhand) – 834 002*

E-mail: aniketanand@sail-rdcis.com; nkartik@sail-rdcis.com; vkumar@sail-rdcis.com; atul-saxena@sail-rdcis.com

ABSTRACT

Uni-axial hot compression tests were conducted at different temperatures (1173-1423 K) and at strain rates of 0.1, 1, 10 and 100/s using Thermo-mechanical Simulator (Gleeble-3500C System) on a 2.7% Si electrical steel to understand the hot workability issues associated with this steel during hot rolling. The flow curves obtained revealed dynamic recovery as the predominant softening mechanism at majority of hot deformation conditions except at lower temperature and high strain rate where work hardening was observed. However, the work hardening was not very prominent due to ferrite structure throughout the hot deformation temperature range established by Thermo-Calc software. Strain rate sensitivity varied within a narrow range of 0.18 – 0.21 with rising tendency with an increase in temperature.

Keywords: *Silicon steel, electrical steel, hot workability, hot rolling*

INTRODUCTION

Electrical steels, also called lamination steel or silicon electrical steel, are an important category of iron–silicon alloys containing 1–5 wt % silicon and very low carbon (less than 0.005 wt %).[1, 2] Silicon significantly increases the electrical resistivity of the steel, which decreases the induced eddy currents and narrows the hysteresis loop of the material, thus lowering the core loss.[3]

Electrical steels contain generally unavoidable Mn and S after the metallurgical process. The Mn and S would even be used as alloy elements in oriented electrical steels. The Mn and S in steels would precipitate as secondary phase in the form of dispersive MnS

particles during the production processes and these particles have very important influences on the steel properties. It is generally believed, that the precipitation and coarsening of MnS particles in high grade non-oriented electrical steel could not only reduce obviously the core loss but also weaken the magnetic aging effects during the service time of the steel sheets [4] The core loss of conventional oriented electrical steels would be reduced by means of high Si content. However, large amounts of dispersive MnS particles as inhibitors are also introduced in conventional oriented electrical steels to control the matrix structure and the abnormal grain growth during the final secondary recrystallization annealing in order to obtain strong Goss texture.

However, due to high Si in such steel (2.7% Si), hot workability is adversely affected. This is reflected in form of elongated structure with high dislocation density. Presence of second phase (austenite), if any, also leads to differential flow leading to cracking thus showing poor workability. In view of this, efforts were made to study such behavior occurring during its processing stages by performing uni-axial compression tests on 2.7% Si steel.

EXPERIMENTAL DETAILS

The chemical composition of material used was ascertained by using Optical Emission Spectroscope (Model-THERMO, ARL 3460) is given in Table 1. The Fe-Si binary phase diagram determined with the help of Thermocalc 3.1® for this composition is shown in Fig. 1.

Cylindrical specimens of 15mm height and 10mm diameter were cut from the slab for hot uniaxial compression testing on thermomechanical simulator Gleeble 3500 (Dynamic Systems, Inc.). The hot deformation schematic is shown in Fig. 2. Uniaxial Compression tests were done at temperatures ranging from 1173 K to 1423 K, with a 50 K interval, so as to cover the nose of gamma phase (Fig. 1). The strain rates were also varied in multiples of 10 from 0.1/s to 100/s covering the entire processing range. All the samples were heated to deformation temperatures of 1173 K -1423 K for 1 minute and deformed to a total strain of 0.8. After the compression, the samples were air cooled in the test chamber itself. MoS was used as lubricant between the anvil and specimen, and graphite (up to 1273 K)/ tantalum foil (>1273 K) of thickness 0.1 mm was used to avoid sticking of the anvil to the specimen surface. Hot deformation software (HDS) was used to run the thermo-mechanical programming in Gleeble 3500C.

After hot deformation, samples were cut in the transverse direction and were copper mounted using hot mounting technique. They were then polished using emery papers and etched using 6% Nital solution for 15 seconds before Microstructural examination under Optical Microscope and Scanning Electron Microscope (SEM).

Table 1 Composition of the 2.7% Si Steel, in wt%

C	Si	Mn	P	S	Al
0.010	**2.72**	**0.054**	**0.010**	**0.029**	**0.011**

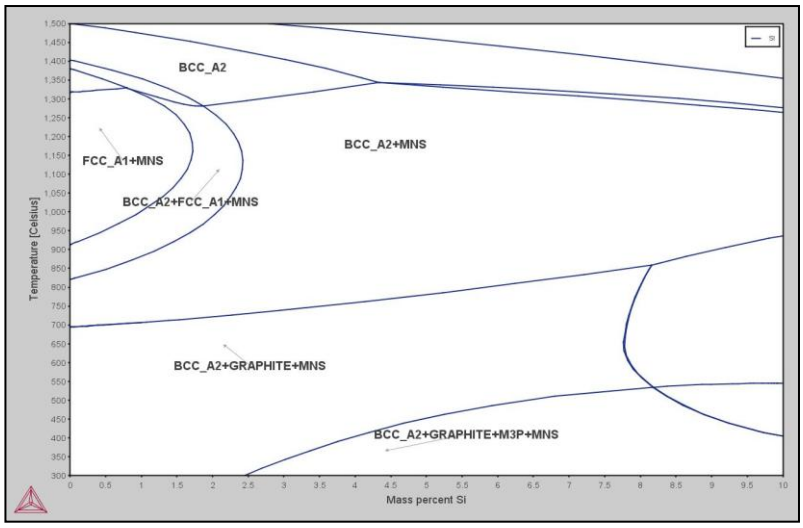

Fig. 1 Phase Diagram as determined on ThermoCalc 3.1®

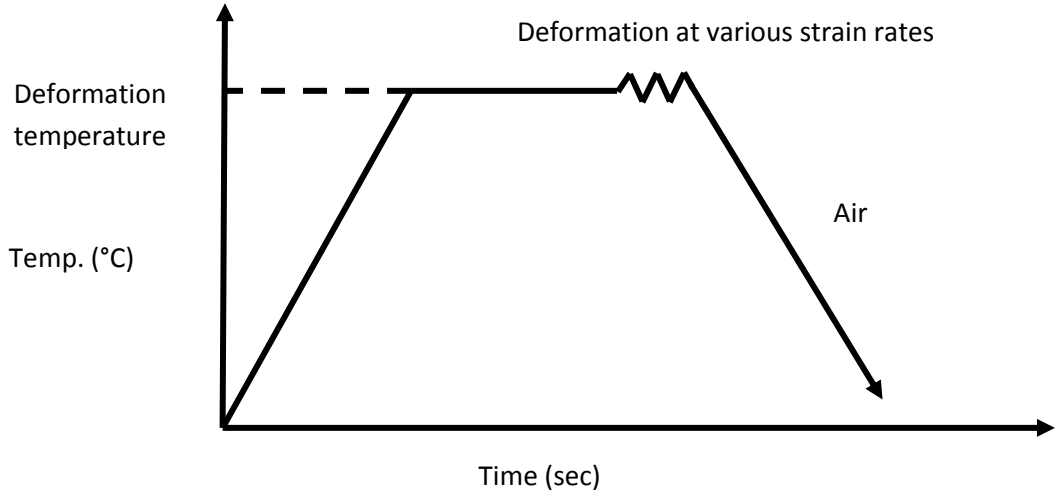

Fig. 2 Hot Deformation Schematic

RESULTS AND DISCUSSIONS

Flow stress of any material is a function of temperature, strain rate at a particular strain. The general relationship between flow stress and strain rate at constant strain and temperature is represented by Equation 1 [5]:

$$\sigma = C\,(\dot{\varepsilon})^{m}\,|_{\varepsilon, T} \qquad (1)$$

Where, σ is flow stress, ε is strain, ε̇ is strain rate, T is temperature and m is strain rate sensitivity. The strain rate sensitivity, m can be determined from the slope of the plot of log σ vs log ε̇. It represents thevariation in flow stress with strain rate at particular temperature of deformation. The variation in flow stress is large, the material is said to be strain rate sensitive and it needs to be deformed with great care. On the other hand, if the strain rate sensitivity is small, the material is supposed to be strain rate insensitive and can be deformed with comfort. Uni-axial hot compression test is the most common method to study the flow behavior of material under the influence of temperature and strain rate. Accordingly, tests were carried out to study the influence of deformation conditions (within the broad range of hot rolling of such steels) on flow behavior and ultimately to arrive at the safe rolling window.

The results obtained from uni-axial hot compression test were analyzed and correlated with microstructure examined through optical and scanning electron microscopy.

Effect of Deformation on Microstructure

Microstructural examination of samples deformed at different temperatures and strain rate were carried to study the influence of hot deformation on microstructural evolution, in general, and to identify any softening process, like dynamic recrystallization or recovery occurring during the deformation. This is important in view of the fact that high Si steels are prone to work hardening leading to high rolling load during processing. Optical micrographs of samples deformed at 1223 K and 1423 K and at two different strain rates of 0.1/s and 10/s are shown in Fig. 3. Elongated grains are observed at 1223 K and a strain rate of 0.1/s whereas some recovery observed at higher strain rate of 10/s at the same temperature. Extent of dynamic recovery improved with the increase in deformation temperature to 1423 K. At 1423 K, extensive dynamic recovery along with a small amount of recrystallization are observed at a low strain rate of 0.1/s. But, at higher strain rate of 10/s, highly recrystallized equiaxed grains are observed.

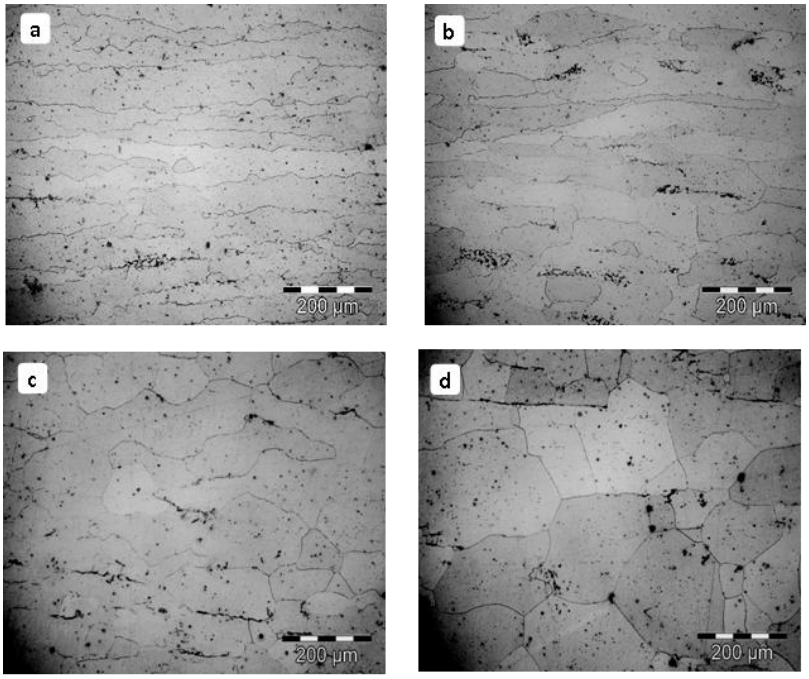

Fig.3 Optical micrographs of Hot-Deformed Samples: a) 1223 K, 0.1/s, b) 1223 K, 10/s, c) 1423 K, 0.1/s, d) 1223 K, 10/s

Microstructural examination was also carried out with the help of scanning electron microscopy to identify dislocated/ work hardened grains. A typical SEM micrograph in Fig. 4 shows both highly strained and unstrained grains simultaneously reflecting that deformation in this steel took place preferentially in some grains due to preferred orientation. Further, formation of second phase was observed along ferrite grain boundaries. Elemental analysis confirmed enrichment of C in this phase resembling austenite. It is to state that Si steel forms a gamma (austenite) loop. If silicon is low, austenite phase may form as second phase in an otherwise single ferrite phase. Formation of austenite along ferrite grain boundaries will pose problems during processing due to differential deformation and poor hot workability.

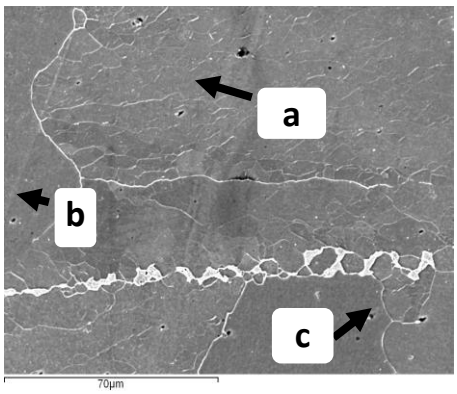

Fig. 4 SEM Image showing: a) Strained grains, b) Unstrained grains and c) Second-phase

Precipitates were also anlyzed to confirm formation of MnS in such steel which is the key to texture development at a later stage of processing. Figure 5 shows EDAX analysis of precipitate which shows presence of MnS.

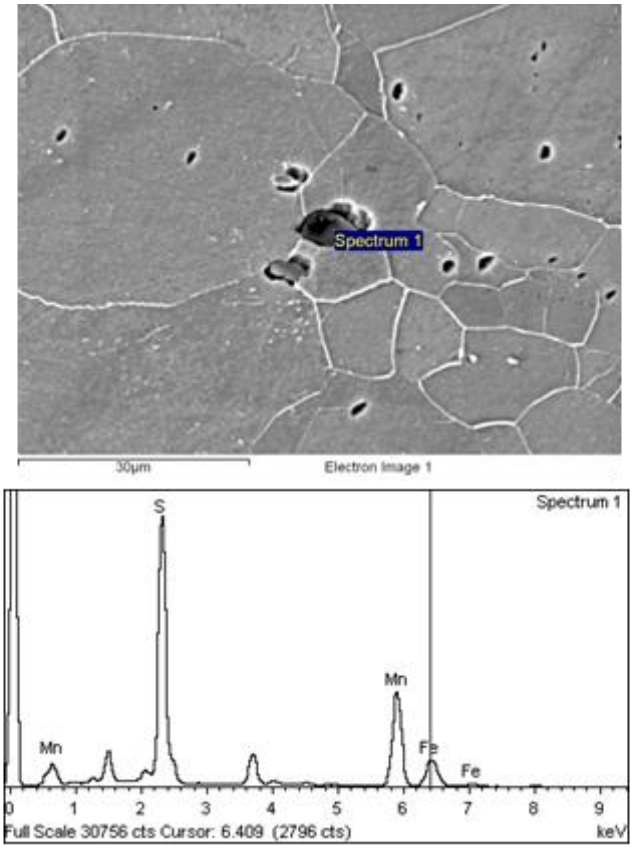

Fig. 5 EDAX Analysis Showing Presence of MnS Precipitate

Effect of Temperature on Flow Stress

A series of flow stress–strain curves obtained from isothermal compression of 2.7% Si steel at different deformation temperatures at constant strain rates are shown in Fig. 6. It is observed that the flow stress decreases with increasing deformation temperature during the isothermal compression at all strain rates. Dynamic recovery was observed at all temperatures (except 1173 K) when deformed at a strain rate of 0.1/s. At lower temperature of 1173 K, work hardening was observed continuously throughout the deformation with no sign of recovery. Work hardening was also observed at other temperatures of 1223 K through 1323 K towards higher deformation in excess of 0.4 strain. Similar trend in flow behavior was observed when deformed at a strain rate of 1/s also.

However, flow behavior changed at a strain rate of 10/s where we observed serrations in flow stress in the temperature range of 1223 K to 1373 K. The serrations were of both positive and negative nature alternatively. This may be due to precipitate – dislocation interactions in the presence of MnS precipitate confirmed by EDAX analysis (Fig. 5).

For strain rate of 100/s, we observe continuous work hardening which may be due to very less time available for dynamic recovery.

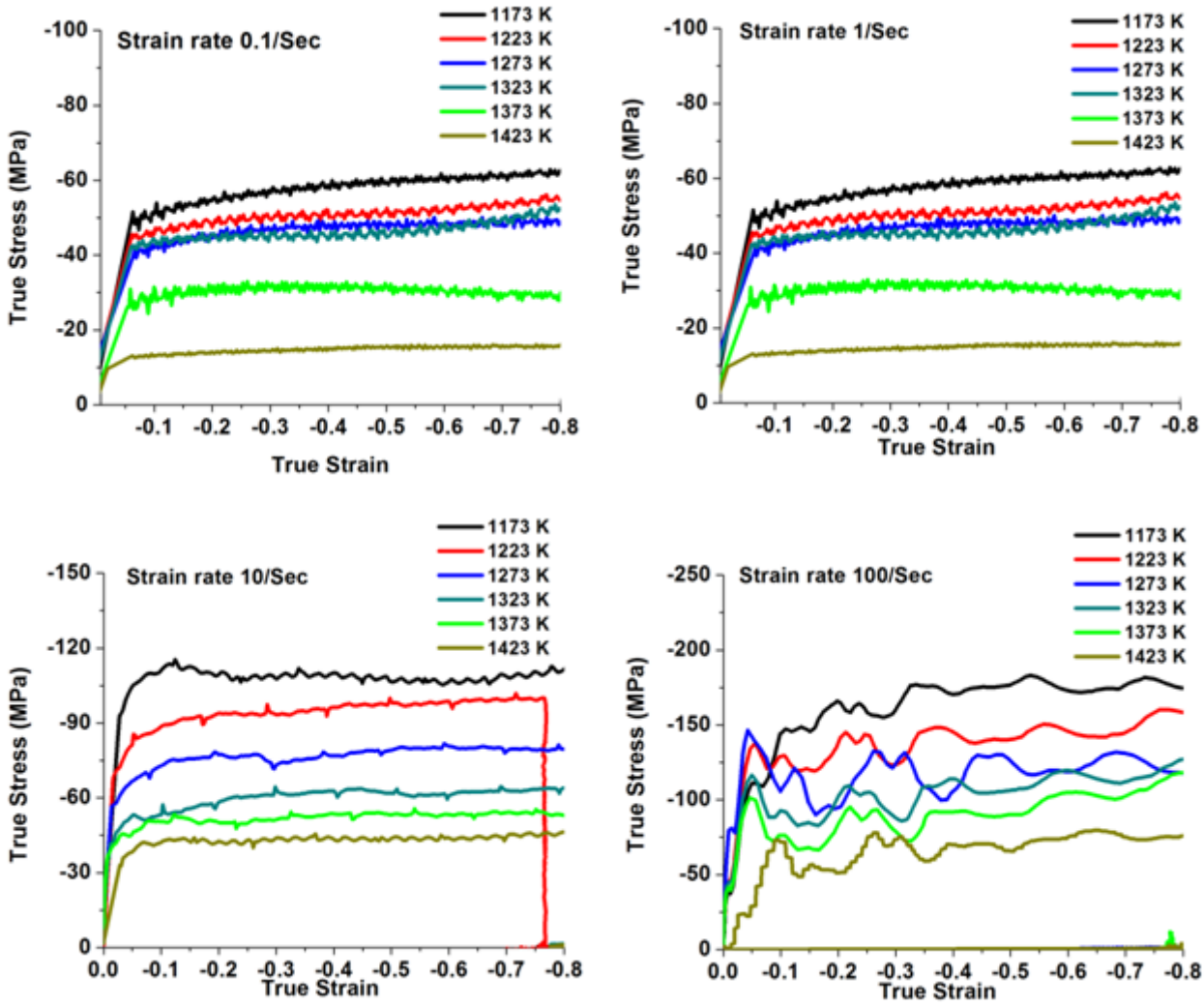

Fig. 6 Effect of Deformation Temperature on Flow Stress at Different Strain Rates

Effect of Strain Rate on Flow Stress

Figure 7 shows the effect of strain rate on flow behavior at temperatures of 1223 K and 1423 K. It is observed that as the strain rate increases, flow stress increases owing to enhanced dislocation-dislocation interactions. The optical micrographs in Fig. 3 shows recrystallization

at strain rate of 10/s at 1423 K while at strain rate of 0.1/s only a small amount of recovery is observed . Similarly at 1223 K more recovery was observed at higher strain rate even though the time available for recovery was more at lower strain rates.

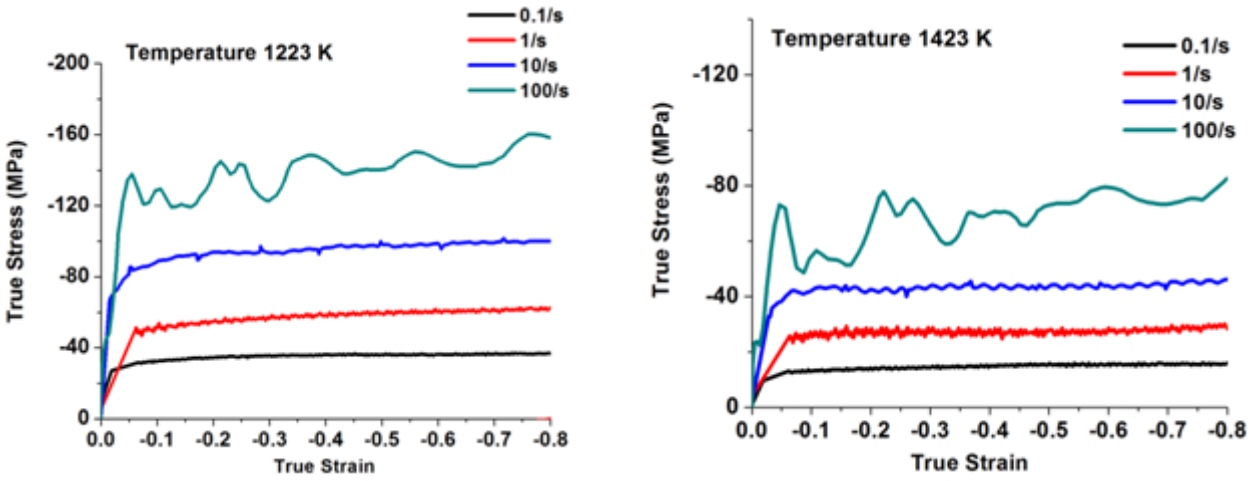

Fig. 7 Effect of strain rate on flow stress at deformation temperatures of 1223 K and 1423 K

Figure 8 shows effect of temperature on flow stress at a typical strain of 0.4 at different strain rates. It can be observed that flow stress increases with decrease in temperature and with the increase of strain rate. The increase in flow stress is gradual at lower strain rates but becomes steep as strain rate increases with lowering of temperature. This results in increase of rolling load due to which extreme care should be taken during processing of these electrical steels.

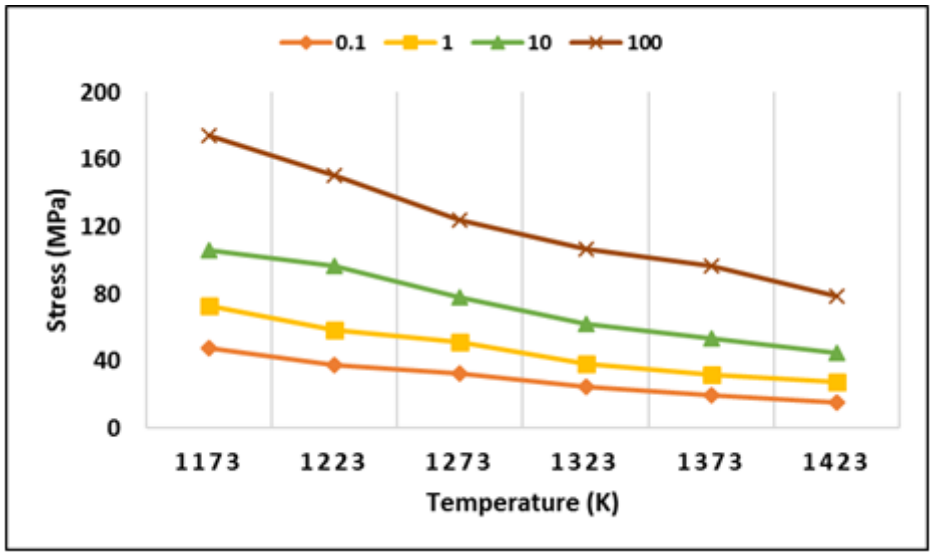

Fig. 8 Effect of temperature on flow stress at 0.4 strain for all strain rates

Strain Rate Sensitivity

The strain rate sensitivity describes the dynamic material behavior, and is, therefore, an important material property to be determined. The strain rate sensitivity is defined by its relation to the plastic flow curve, and not to the engineering stress-strain curve. Strain-rate sensitivity index is referred to as '*m*' and defined as:

$$m = \frac{\partial \log \sigma}{\partial \log \varepsilon'} \quad \textit{(At constant temperature and strain)} \qquad (2)$$

Where, σ is flow stress and έ is strain rate. [5] As can be seen in Fig. 9, strain rate sensitivity increases with temperature in general but forms a plateau in the temperature range of 1223 K to 1323 K.

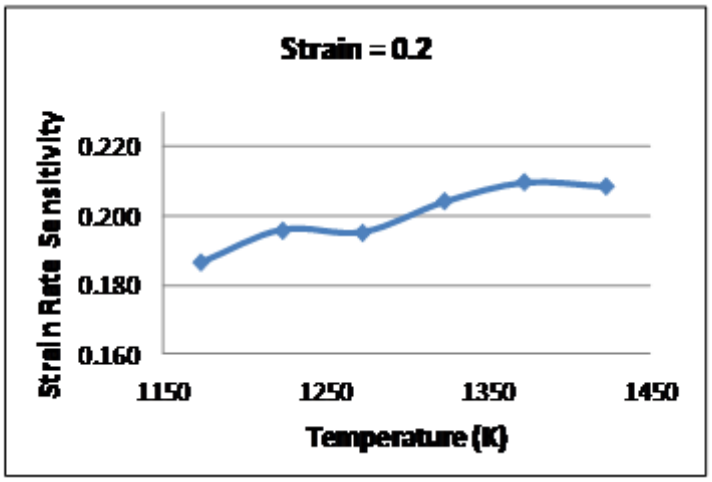

Fig. 9 Variation of Strain Rate Sensitivity with Temperature

CONCLUSIONS

- Flow stress decreased with an increase in deformation temperature and decrease in strain rate.
- Extent of dynamic recovery increased with increase in deformation temperature and strain rate.
- Recrystallization was observed at 1423 K which increased considerably with increase in strain rate from 0.1/s to 10/s.
- Preferential deformation was observed in some grains due to difference in the orientations of grains.

- The strain sensitivity of the material increased gradually from 0.19 to 0.21 with an increase in temperature from 1173 K to 1423 K .

REFERENCES

[1]. Bertotti, G.; Fiorillo, F. (1994) Grain-oriented 3 wt% silicon steels. In: Magnetic Alloys for Technical Applications, Soft Magnetic Alloys, Invar and Elinvar Alloys, vol. 19i1. Landolt-Bornstein, Group III Condensed Matter

[2]. Xia, Z.; Kang, Y.; Wang, (2008), Developments in the production of grain oriented electrical steel. J. Magn. Magn. Mater. **320** (20),p.3229.

[3]. K.H.J. Buschown et al, ed., (2001), Encyclopedia of Materials: Science and Technology, Elsevier, pp. 4807-4808.

[4]. Lyudkovsky G, Southwick P D. (1986), the effect of thermomechanical history upon the microstructure and magnetic properties of nonoriented silicon steels. Metallurgical Transactions A, 17A (8): pp. 1267–1275.

[5]. George E. Dieter, Mechanical Metallurgy, SI MetricEdn., McGraw-Hill Publishers, London, p. 297.

National Conference on Thermo-mechanical processing of Steels &
5th Gleeble User Workshop India (GUWI-2015),
August 6-7, 2015, pp 115-119.

Simulation of bar rolling in gleeble

K. Mukherjee[1], and D. K. Matlock[2]

[1]ASPPRC, Colorado School of Mines, USA; Currently in CSIR-NML, India

[2]ASPPRC, Colorado School of Mines, USA

Email : krishnendu@nmlindia.org

ABSTRACT

Simulation of bar rolling was attempted in Gleeble 3500. Entire bar rolling was simulated, i.e., roughening rolling at higher temperature and finishing rolling at lower temperature. Torsion module was used to simulate the large amount of deformation employed in bar rolling. The equivalent strains and strain rates appropriate for torsion deformation in Gleeble were calculated as per standard industrial schedule, from roughening rolling to finishing rolling. The cooling schedules between the roughening rolling and finishing rolling and afterwards was also maintained as per industrial conditions. An induction hardenable grade of steel was selected to evaluate the possibility of simulating bar rolling in Gleeble. The torsion-torque response of the Gleeble simulation indicates whether dynamic restoration processes are active during the deformation steps. The microstructure and hardness of the Gleeble simulated samples were compared with the industrially hot-rolled bar.

Keywords *:Bar rolling, torsion simulation of bar rolling, microstructural simulation, hardness of as-rolled bar.*

INTRODUCTION

Rod rolling has been simulated through laboratory torsion tests [Maccagno]. It has been reported that for a 5.5 mm diameter rod laboratory torsion tests can be useful to predict the final austenite grain size just before the start of the austenite to ferrite phase transformation. As the maximum strain rate available in the laboratory torsion machine is in the order of $10s^{1}$, while the mill strain rates can be as high as 1000 s^{-1}, the necessary adjustments required in terms of strains and interpass times during simulation is discussed by Maccagno et al. For as-rolled bars with diameter around 50 mm, thermo-mechanical simulation can be useful to predict the microstrucutre. As-rolled bars of this diameter are also used as a starting material for induction hardenable or case hardenable products.

Thermomechanical simulator Gleeble has been utilized to simulate the entire hot-rolling operation of flat steel products. Sarkar et al. simulated the hot-strip rolling process for

complex phase steel in a DSI HTS 100 hot torsion tester, while Liu et al. simulated the same for dual-phase steel. Mukherjee et al. further explored the possibility of using the torsion simulator to propose hot-rolling schedules that may result in fine-grained dual-phase steels.

The simulation of rod rolling through laboratory torsion tests and promising application of Gleeble hot torsion simulation in investigation of entire hot-strip rolling provided a motivation of exploring the applicabitly of Gleeble thermo-mechanical simulation technique for bar-rolling simulation. This study depicts the applicabiliy of Gleeble simulation technique through comparing the final microstructure and hardness with that obtained from a industrial as-rolled bar product.

EXPERIMENTAL PROCEDURE

An induction hardenable grade of steel was selected to evaluate the possibility of simulating bar rolling in Gleeble ® 3500. Torsion samples with 14 mm diameter were obtained from the mid-radius of the bars. The gauge diameter of the Gleeble torsion samples were 10 mm. The cross-sectional dimensions of the billet, of the bar after roughening rolling and finally that of the bar after the finishing passes were the important parameters to calculate the strains during the bar rolling process. The total plastic strains obtained for an industrial bar rolling schedule, $\overline{\varepsilon_p}$, was calculated to be 1.8 and 0.6, for roughing passes and finishing passes, respectively.

To convert the total strain into equivalent torsional deformation first of all the effective shear strain γ_e was calculated as per Equation 1.

$$\gamma_e = \sqrt{3}\,\overline{\varepsilon_p} \tag{1}$$

Angle of rotation, θ, for torsion were calculated using the effective shear strains (γ_e), an effective torsion sample radius a_e and gauge length of the torsion specimen, l. The effective torsion sample radius for solid tubular geometry was quantified using Equation 3, where a is the torsion specimen radius.

$$\theta = \frac{l}{a_e}\gamma_e \tag{2}$$

$$a_e = 0.724\,a \tag{3}$$

The values of a, a_e, l, γ_e and θ for roughening and finishing pass simulations are summarized in Table 1.

Table 1: Quantification of equivalent torsion deformation of bar rolling passes

Pass	a (mm)	a_e (mm)	l (mm)	γ_e	θ (radian)
Roughening pass	5	3.62	10	3.11	17.2
Finishing pass				1	5.5

The strain rates ($\dot{\varepsilon}_p$) for roughening and finishing passes for industrial bar-rolling is typically 0.5/s and 2/s, respectively [Lee]. As this strain rates are achievable in Gleeble, there was no need for correction of pass strain and interpass time as discussed by Maccagno et al. The time for the torsion deformations were calculated as per Equation 4 and summarized in Table 2.

$$t = \frac{\overline{\varepsilon_p}}{\dot{\varepsilon}_p} \tag{4}$$

Table 2: Calculation of required times of deformation for bar rolling simulation

Pass	Time t (s)
Roughening pass	3.6
Finishing pass	0.3

RESULTS AND DISCUSSION

The Gleeble simulation of bar-rolling included heating at a rate of 5 °C/s to 1200 °C, holding there for 30 min, followed by roughening rolling simulation. As per calculation of Table 1, a rotation of 17.2 radian or 986° was given to the specimen. After completion of roughening rolling simulation the specimen was cooled at a rate of 1 °C/s to the finishing rolling temperature of 1000°C. As per quantifications of Table 1, a rotation of 5.5 radian, i.e., 315° was given to the specimen next to simulate the finishing rolling. After finishing rolling simulation the specimen was cooled at a rate of 1 °C/s to 600°C from where it was naturally cooled. The torsion-torque response of this test is shown in Figure 1. The decrease in the torque value during the first rotation (roughening rolling simulation) indicates dynamic recrystallization of austenite. However, during the second rotation (finishing rolling simulation) the torque was significantly higher when compared with the first rotation. This

indicates the absence of dynamic recrystallization of austenite during the finishing rolling simulation.

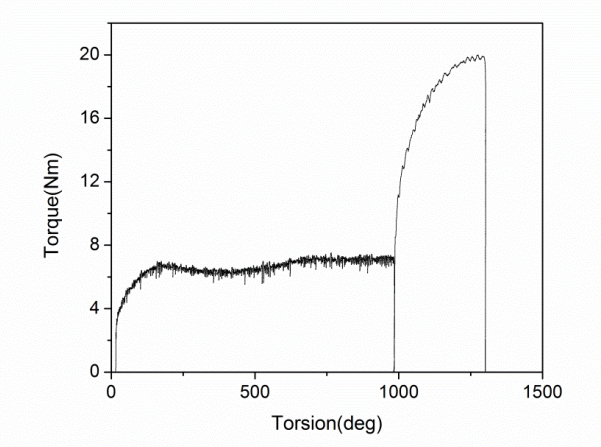

Fig. 1: Torsion-torque response of bar rolling simulation.

After bar-rolling simulation the specimen was sectioned in a plane perpendicular to its axis. The sectioning plane was at the middle of the gauge length. The microstructure and hardness were obtained within 1 mm from the surface of the specimen. The microstructure obtained from bar-rolling simulation is shown in Figure 2. The black areas indicate pearlite, while the white areas indicate ferrite. The ferrite fraction was quantified to be 23 pct. The hardness of the specimen was determined to be 245 VHN. This matches well with the ferrite fraction and hardness of the mid-radius region of the as-rolled bar (Figure 3). Further, similarity is also observed in the distribution of ferrite. In case of as-rolled bar ferrite in the mid-radius region is found to be decorating the pearlitic regions (see Figure 3b). This is also observed in Figure 2b which is bar rolling simulation.

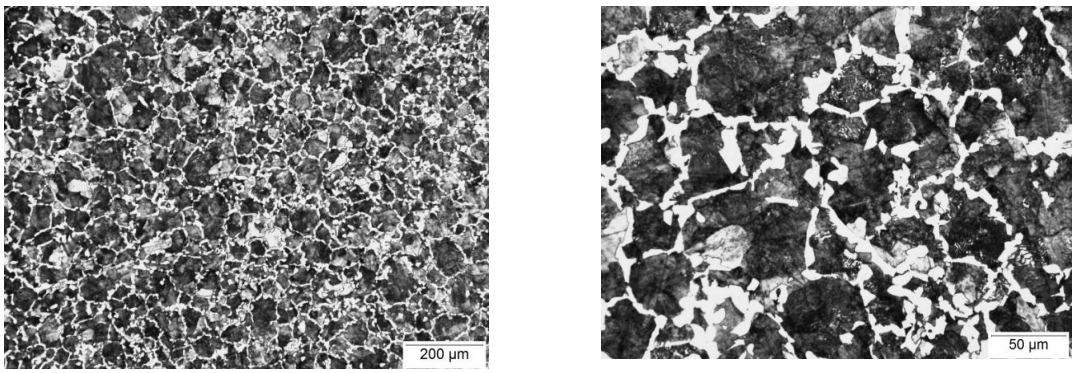

(a) (b)

Fig. 2: Simulated microstructures for bar-rolling. (a) at lower magnification, (b) at higher magnification.

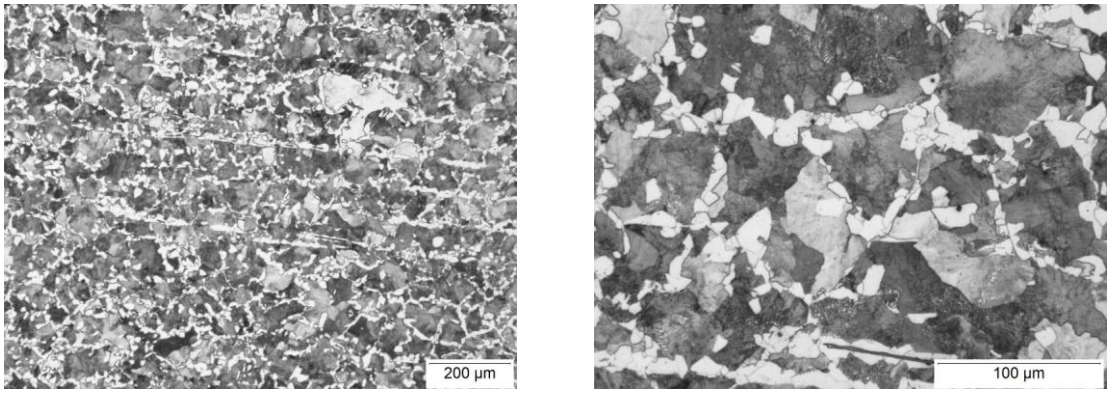

(a) (b)

Fig. 3: Microstructures of as-rolled bar. (a) at lower magnification, (b) at higher magnification.

CONCLUSION

It is shown that the as-rolled bar microstructures can be simulated in Gleeble. The simulated ferrite fractions match well with the microstructure of the mid-radius region of the as-rolled bars.

The torque-torsion response of the test indicates the presence of dynamic recrystallization during roughening rolling simulation. However, during the finishing rolling simulation it seems that any dynamic restoration mechanism is absent.

REFERENCES

[1]. [Lee] Y. Lee, *Rod and Bar Rolling: Theory and Applications*. New York: Marcel Dekker Inc. New York, 2004, pp. 339–340.

[2]. [Liu] D. Liu, F. Fazeli and M. Militzer, ISIJ International 2007, vol. 47, pp. 1789-1798.

[3]. [Maccagno] T.M. Maccagno, J.J. Jonas and P.D. Hodgson, ISIJ International, 1996, vol. 36, pp. 720-728.

[4]. [Mukherjee] K. Mukherjee, S. Hazra and M. Militzer, Metallurgical and Materials Transactions A, 2009, vol. 40, pp. 2145-2159.

[5]. [Sarkar] S. Sarkar and M. Militzer, Materials Science and Technology, 2009, vol.25, pp. 1134-1146.

National Conference on Thermo-mechanical processing of Steels &
5th Gleeble User Workshop India (GUWI-2015),
August 6-7, 2015, pp 120-130.

Development of HSLA steel with high temperature tensile properties

Prashant Pathak, Arnab Karani and M Shome

Research and Development, Tata Steel, Jamshedpur

Email : prashant.pathak@tatasteel.com

ABSTRACT

The fire safety of high rise buildings, airport structures, stadium and auditorium has become a prime importance to ensure the safety of human life and demands for the development of fire resistant steel. Steel is generally defined as fire-resistant if yield ratio for the steel is in excess of 0.5 at 600°C for a holding time of one hour. The Yield ratio of fire resistant steel is defined as the ratio between yield strength at a specified elevated temperature to that at room temperature and is usually specified to be greater than 0.5 for less critical applications and greater than 0.6 at 600°C for the critical applications. Recent developments of fire resistant steels indicate the use of higher amounts of alloying elements primarily Mo that leads to increase in the cost of steel. Therefore the present work was intended to design a low cost leaner chemistry based Fire resistant steel that can be easily processed through hot strip route. The steel was targeted to achieve minimum of 350 MPa room temperature YS in addition to the fire resistant properties.

The present work entails to Mo-V-Cr micro alloyed steel. The designed steels were characterized at room temperature and high temperature over a range of 450-600°C The high temperature properties of steel were evaluated using hot tensile facility in Gleeble 1500. It was found that the steels exhibited yield ratio in excess of 0.5, which met the desired target. This ratio was found to be higher than the equivalent plain carbon steel that has the ratio below 0.3 at 600°C. Fire resistance property of steel was attributed to the solute drag effect and the development of long range internal strain due to presence of coherent/semi-coherent precipitates of the micro alloying elements.

Keywords *: Fire resistant steel, Yield ratio, micro alloyed steels*

INTRODUCTION

The new high rise buildings require fire resistance (FR) steel structures, where the strength at elevated temperatures is of significant consideration. This requirement has already been considered for the construction of high rise buildings in Japan, Europe and North America; it is becoming important for the developing countries like India. The fire resistance steel

structures enable the inmates to evacuate the building in the event of the fire accidents. Currently the fire resistance property is achieved by applying an insulating coating (mineral fiber or vermiculite in a cement slurry) of sufficient thickness on steel structures [1]. These requirements can double the cost per ton of steel used. To qualify steel for FR high rise buildings the yield strength (Y.S) ratio, which is defined as the ratio between yield strengths at a specified elevated temperature and room temperature has been considered in the various design codes.

The Australian, European and North American design codes are based on the temperature at which the structural member loses half of its room temperature yield strength and this is typically about 500-550C for common plain carbon structural steels [1]. The Japanese codes are more conservative, where they require two thirds ($2/3^{rd}$) of the room temperature yield strength to be retained at elevated temperatures, which limits the steel temperature to about 350-450°C [2]. Traditionally, FR steels are made with high amount of Mo with other alloying elements such as Nb, V, Ti and N. Nippon steel has developed FR steels of 590 MPa tensile grade with 0.51 Mo and 0.02 Nb and carbon equivalent of (CE) of 0.43. The high CE of this steel may create issues in forming and electric resistance welding process of tube making process. Also, high Mo content will increase the cost of the product [3]. Similarly, Kawasaki Steel has developed the FR steels of 400 MPa and 490 MPa tensile grades with a common CE of 0.35 for both the grades [4]. However, the details of Mo and other micro alloying elements were not reported. Zhiwang and Qingchun [5] have reported the development of experimental FR steels of 0.5Cr-0.3 Mo and 0.6 Mo steels with 0.10 V and varying N contents of 0.0026-0.012 wt%. They have indicated that increasing Mo content results in finer and denser precipitates and concomitant improvement in the Y.S ratio. Their observation concludes that the mixture of polygonal ferrite and bainite by the suitable thermo mechanical processes is essential for high Y.S ratio at 600°C. It has been well established that the fire resistance of the steel increases proportionally with the Mo content, however the higher Mo content leads to significant increase in the cost of steel. This restricts the wide use of such steels in the developing countries like India where fire safety regulations is not very strict. Several steel manufacturing reports indicate a conservative value of alloying elements to improve the FR property which perhaps be achieved by even with leaner chemistry. However, it requires a thorough understanding and experimental findings to achieve the target properties with lean chemistry.

In view of the above, the objective of the present work was to develop low cost steel with good fire resistance property combined with good weldability

EXPERIMENTAL PROCEDURE

The steel ingots of 25 kg were produced in laboratory using air induction furnace. The cast ingot was hot forged a) to breakdown the cast structure and b) to obtain uniform and homogenized austenite structure. The forged steel ingot was subsequently hot rolled to 3.2 mm thick sheets in several passes. The forged ingots (50x50 mm cross section) were soaked at 1040°C/2 h in the first reduction and 1080°C/10 min in the final reduction. The finish rolling was performed at 900±20° C and subsequently fan cooled to 550° C followed by natural cooling.

Table 1: Chemical composition of the designed heats

Element (wt%)	C	Mn	S	P	Si	Al	Cr	Mo	V	N	CE
Heat 1	0.09	1.49	0.006	0.021	0.34	0.025	-	-	0.209	0.0068	0.20
Heat 2	0.065	0.86	0.015	0.017	0.072	0.044	0.54	0.18	0.059	0.011	0.15
Heat 3	0.075	0.94	0.014	0.017	0.082	0.008	0.37	0.150	0.148	0.012	0.149

An additional heat treatment on the as-rolled sheets was performed to understand the effect of end application temperature on the microstructure and the mechanical properties of the designed steels. The steels were heated to a temperature of 700°C and soaked for a period of 60 minutes. This is to simulate the conditions that the developed steel will experience when subjected to the event of fire. Tensile testing was performed on as rolled steel sheets and heat treated steel samples. The tensile testing was performed using the flat specimens of 200 mm total length and 30 mm gauge length as per the ASTM standard E8[6].

The high temperature tensile tests were conducted using Gleeble 1500D system, thermo mechanical simulator. Figure 1 shows the test set up employed for conducting the hot tensile tests. The right hand loading rod is stationary while the left one moves left to apply the tensile load on specimen. The tests were conducted by heating the test specimen at an elevated temperature for desired holding time followed by tensile loading until specimen failure. The data obtained from the tests i.e. force and extension were used to define the stress strain

behaviour of steel at desired temperature and yield strength was defined at 0.2% offset. Figure 2 shows the sample geometry used for hot tensile specimen.

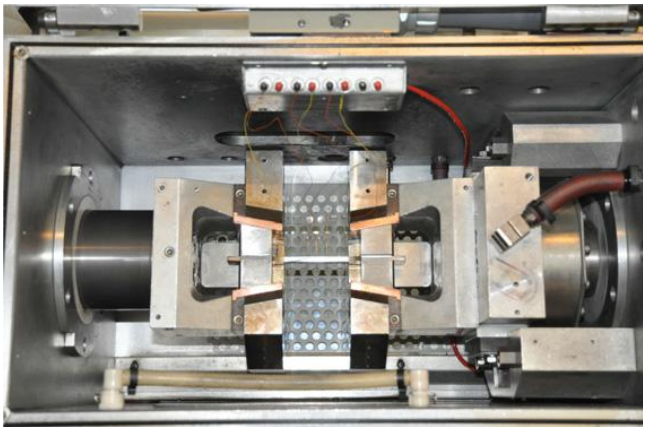

Fig.1: Shows the specimen set up for hot tensile testing in Gleeble 1500D

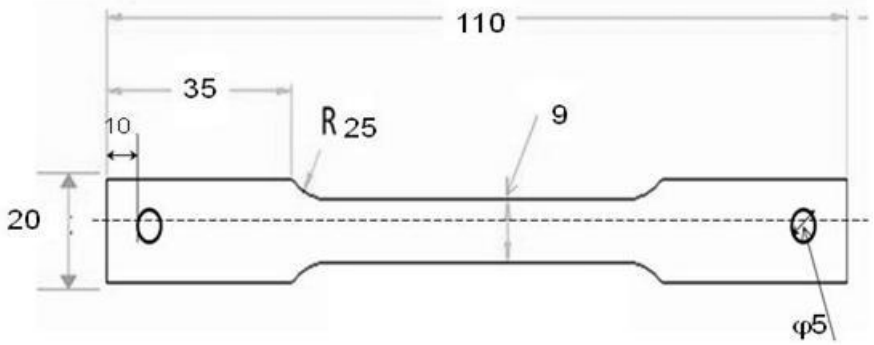

Fig 2.: Flat pin hole specimens used for hot tensile testing in Gleeble 1500D

Thin foils close to 0.1 mm thickness were prepared by slow speed diamond cutter followed by fine grinding with SiC abrasive papers. Thin foils were further subjected to twin-jet polishing and subsequently ion milled for 30 min to remove the oxide scales. Philips CM 20 TEM was used for the imaging of precipitates .The quantitative chemical analysis of precipitates was carried out using Energy dispersive spectroscopy (EDS) attached to TEM.

RESULTS AND DISCUSSION

Microstructure of steels in as rolled and heat treated condition

Fig. 3 and 4 present microstructure of the steel 1 in as rolled and heat treated condition, respectively. The as rolled microstructure reveals the ferrite and pearlite aggregate in both the conditions, but the area fraction of the second phase (pearlite) is lower in the heat treated condition than that of the as rolled condition. This is because the longer holding time just

below the AC_1 temperature results in the dissociation of pearlite phase and nucleation of new ferrite grains. Fig. 5 and 6 presents micrograph of the steel 2 in as rolled and heat treated conditions, respectively, which reveal similar microstructural features as that of the steel 1. Fig. 7 and 8 present the micrographs of the steel 3 in the as rolled and heat treated conditions, respectively. The as rolled microstructure reveals the presence of large fraction of ferrite with second phase such as pearlite and bainite. The common feature observed in all three steels are i) mixed ferrite structure and ii) refinement of microstructure in the heat treated state. The brief description of microstructural analysis for the as rolled and the steel in heat treated condition is presented in the Table 2. The refinement of grain size was attributed to the particle stimulated nucleation of intragranular ferrite. It has been well established that the vanadium precipitate formed during the late stages of transformation act as a nucleation site for the formation of ferrite in the temperature regime of 650-700°C[7].

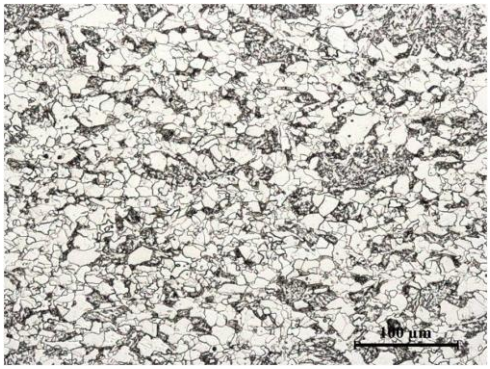

Fig.3 Microstructure of steel 1 in as rolled condition shows the ferrite with a large area fraction of second phases (40.5%) such as bainite and pearlite.

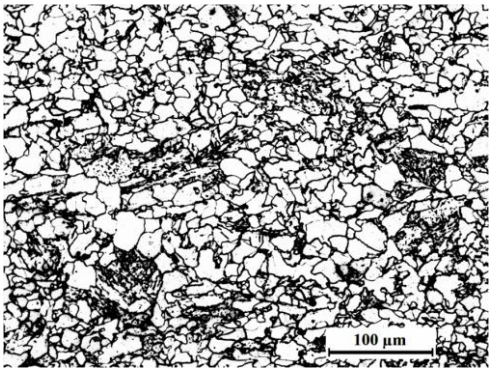

Fig. 4 Microstructure of steel 1 after heat treatment shows a decrease in the area fraction of second phase. (40.5%) such as bainite and pearlite.

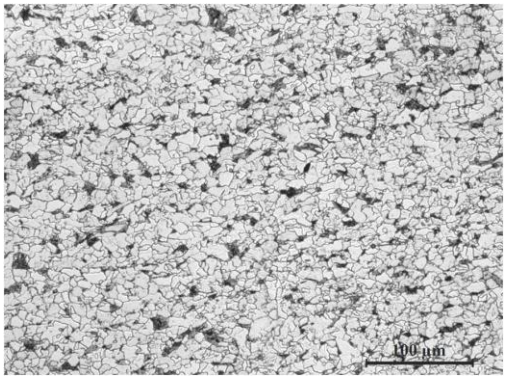

Fig.5 Microstructure of steel 2 shows the bimodal ferrite grains and pearlite (30%).

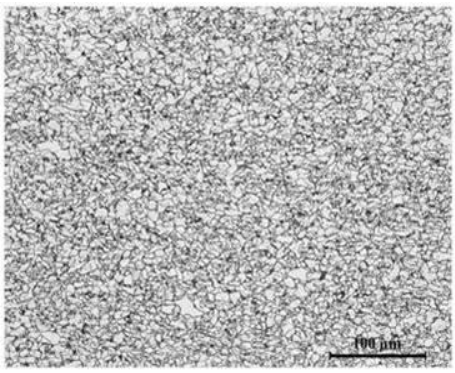

Fig.6 Microstructure of steel 2 in normalised condition showing the presence ferrite and pearlite.

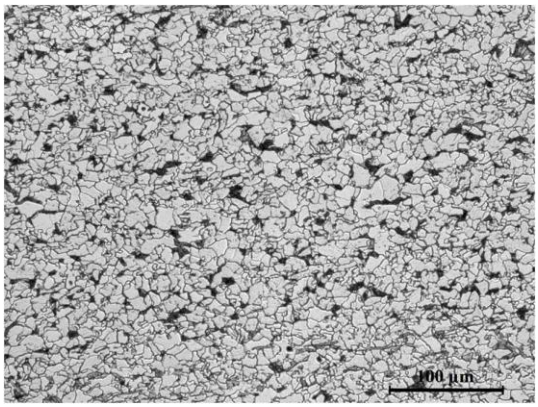

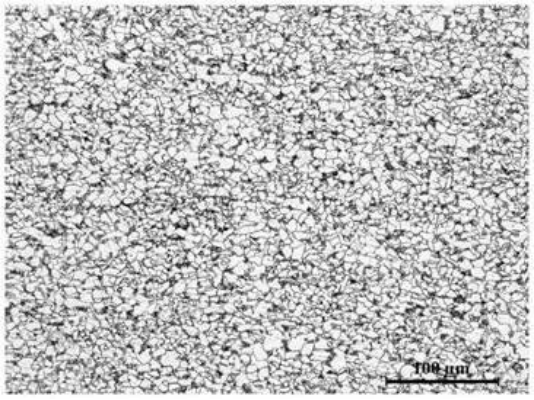

Fig.7 Microstructure of Steel 3 in as rolled condition showing a bimodal ferritic grain distribution with ~ 40% pearlite. Fig. 8 Microstructure of steel 3 in heat treated condition still showing the ferritic structure with reduced fraction of pearlite.

Table 2: Brief description of microstructure of steels in as rolled and heat treated condition

Sample ID	Grain size (µm)		Area fraction of second phase	
	As rolled	Heat Treated	As rolled	Heat Treated
Steel 1	14.30	12.03	40.5	17
Steel 2	5.23	4.5	30	15.2
Steel 3	6.4	5.6	40	29.10

Room temperature tensile properties of steels in as rolled and heat treated condition

The room temperature tensile properties of different steels in as rolled and heat treated condition are detailed in Table 3. The high tensile strength of steel 1 over the other two steels was due to the increased solid solution strengthening effect imparted by the higher manganese and vanadium content.

The common feature that was observed in all the steels was the higher strength of steels in as rolled condition than in the heat treated condition inspite of the fact that the grain refinement in the later case. The reason for the decline in the tensile strength is attributed to a) the decrease in the volume fraction of second phase (harder phase like pearlite and bainite) and b) coarsening of micro alloyed precipitates of vanadium nitride or carbo- nitrides.

Table 3: Room Temperature tensile properties of steels in as rolled and heat treated condition

Tensile property	Steel 1		Steel 2		Steel 3	
	As Rolled	Heat Treated	As Rolled	Heat Treated	As Rolled	Heat Treated
YS (MPa)	537-560	438-441	407-505	375-382	520-547	349-394
UTS (MPa)	757-797	545-546	560-608	462-477	601-608	505-510
% E	10-13	18-20	20-25	27-31	15-20	20-25

Elevated temperature tensile properties of steels

Fig. 7 presents the variation in strengths as a function of test temperature for steel 1. The yield and tensile strengths of heat 1 do not exhibit a significant variation at 500° and 550°C, but falls off rapidly at 600°C, where the similar trend has been noticed for Y.S ratio as well. The striking feature in Fig.9 is that Y.S ratio of Steel 1 is lower than that of the specification (0.5 to 0.66) in spite of significant vanadium addition. The micro alloying with V results in fine VN particles at the grain boundaries which prevent the grain coarsening during hot rolling and elevated temperature service. Moreover, the formation of V(C,N) and complex carbo-nitrides increase the resistance of thermal softening and thus retains the fire resistance property well up to 550 °C. But further rise in temperature result in the rapid coarsening of these precipitates, and as the precipitates looses coherency they no longer remain effective in suppressing the dislocation motion, grain boundary sliding and the other softening mechanism and hence the strength at higher temperature drastically falls resulting in the yield ratio of <0.5

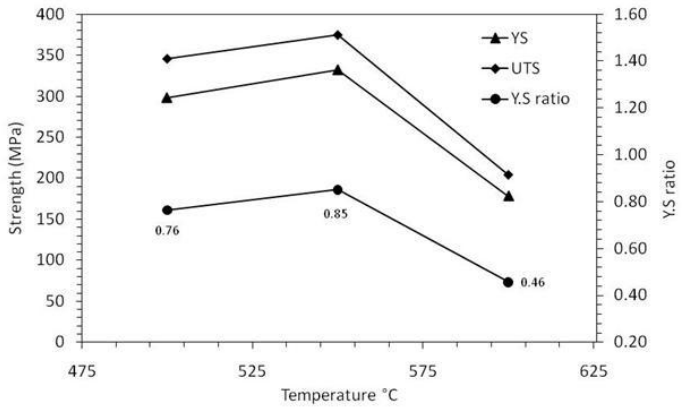

Fig.9: Variation in tensile strengths and Y.S ratio vs. testing temperature of Steel 1

Fig.10 and Fig.11 compares tensile properties of steel 2 and 3, repsetively as a function of test temperature. Figures show that tensile properties, both yield and UTS decrease as test temperature is increased, as expected. The steel 2 and 3 demonstrate a similar trend in reduction of strength up to 550°C (almost a constant slope), but steel 2 demonstrates a rapid fall in strength at 600°C compared to steel 3. The higher Y.S ratio of steel 3 in comparison with steel 2 is attributed to high V and nitrogen content, with the Mo content for these steels being comparable. The reduction in strength at elevated temperatures is assumed to be due to i) loss in preciptate strengthening due to precipitate coarsening, ii) transformation of unstable to stable precipitates. For example, the Mo_2C type precipitate in heat is non equilibrium which has transformed to equilibrium Mo_6C [8].

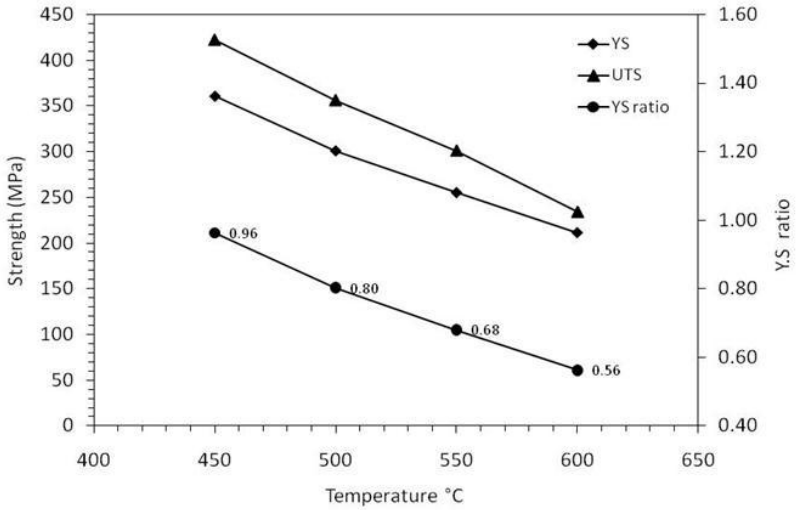

Fig. 10 Variation in tensile strengths and Y.S ratio vs. testing temperature of Steel 2

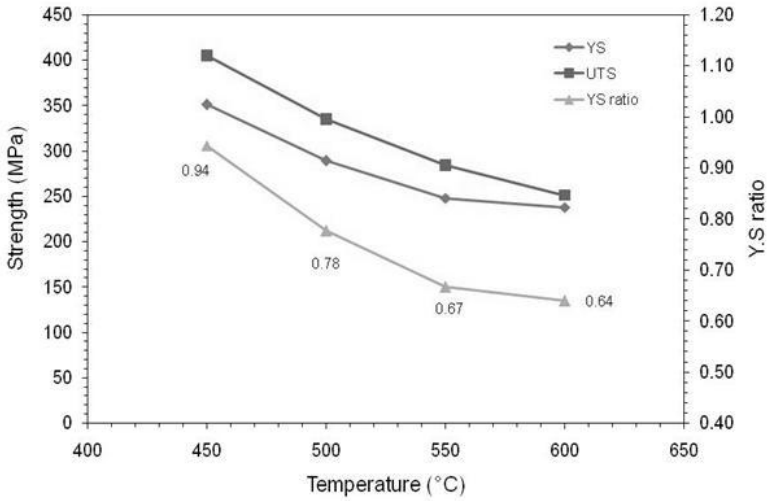

Fig .11 Variation in tensile strengths and Y.S ratio vs. testing temperature of Steel 3

Transmission Electron microscopy results

Fig 12 TEM micrograph reveals the distribution of precipitate in ferrite matrix for the Steel 1 in heat treated condition . The precipitates appears to be coarsened ,as reflected from the micrograph where the size of precipitates appears to be varying from 25-80 nm. Fig. 13 a reveals a few ten nano meters sized spherical V rich particles with elongated particles representing the Mo_2C precipitates in as rolled steel 3. Fig. 14 reveals the spherical particles inside the grain and on the grain boundary which is determined as Mo_6C using the EDS analysis. Fig. 13 and 15 suggest that heat treatment results in the morphology and composition changes of the Mo rich particles (needle $Mo_2C \rightarrow Mo_6C$)[9]. Fig. 15 reveals the spherical and elongated shaped particles at the grain interior and triple junction, where these particles were identified as V(C,N) by EDS. The high V content of the steel 3 favored the formation V(C,N). Table 4 summarizes the EDS analysis results of the particles in Fig. 12-15.

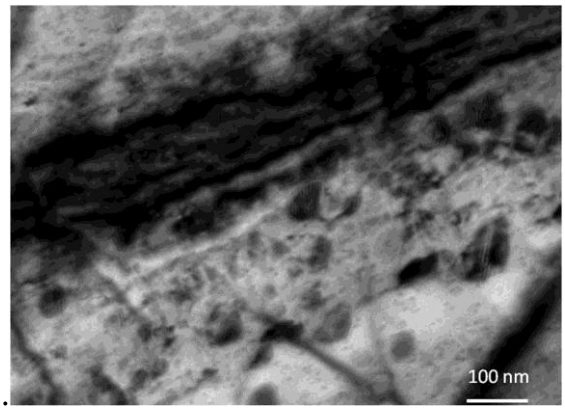

Fig. 12: Image shows the precipitates of V(C,N) in the heat treated condition for steel1

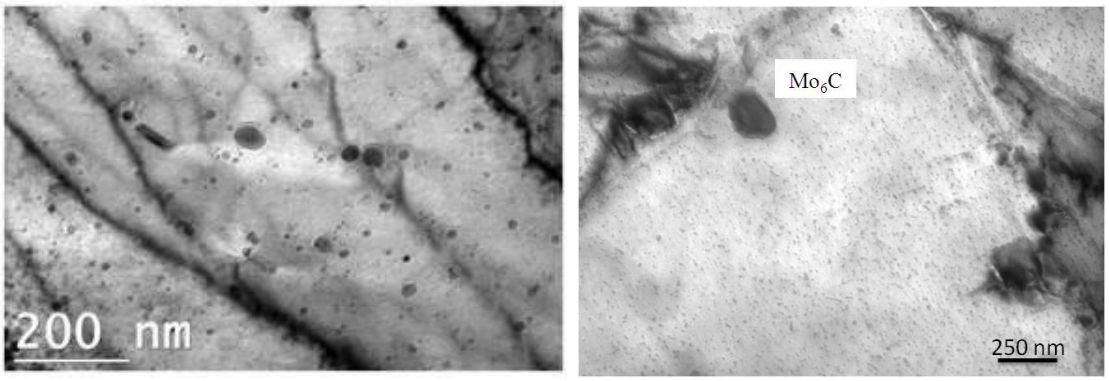

Fig 13 reveals rod like (Mo2C) precipitate and fine spherical V rich precipitates in steel 3 , and Fig 14 shows spherical Mo6C precipitate in steel 3 subjected to heat treatment.

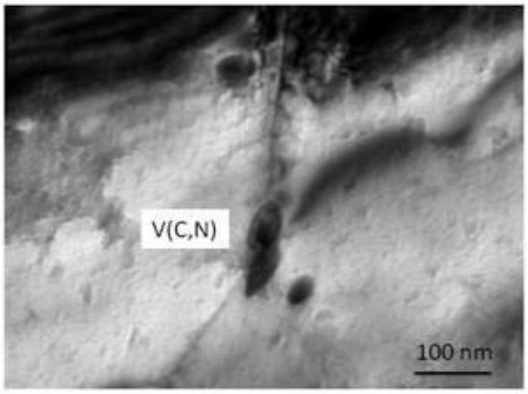

Fig. 15 Overalapping of elongated shape precipitates at grain boundary

Table 4 Chemical composition of precipitates determined by EDS detector

Figure	C	N	Cr	Mo	V	Ti	Precipitate
11, Spherical particle	62.8	26.5	-	-	10.6	-	V(C,N)
Fig.12, spherical particle	9.1	7.5	2.7	4.6	76.1	0	(Mo,V)C
Fig.13 Elongated particle	35.8	32.8	3	10.4	18	-	V(C,N)

CONCLUSION

The result of this study led to the following conclusion:

1. The heat treatment studies revealed that the presence of Vanadium based precipitates in micro alloyed steels leads to the grain refinement, when isothermally held at 700°C by the formation of intragranular ferrite.
2. Steel 2 and 3 have demonstrated the Y.S ratios of in the range of 0.58-0.64, which meets the fire resistance requirement for structural building,with the low Mo content.
3. FR steels exhibit strengthening precipitates, such as complex alloy carbides and carbo-nitrides, which contribute to the strengths at both RT and elevated temperatures confirmed by TEM results.
4. Mo and V together play important roles in attaining the fire resistance property (Steel 2&3), while V alone is not sufficient to achieve the high temperature softening beyond 550°C.

ACKNOWLEDGEMENTS

The authors thank the Staff, Research and Development Division, Tata Steel for their help in metallography and tensile testing experiments.

REFERENCES

[1]. M. Assefpour- Dezfuly, B. A. Hugaas, A. Brownrigg, Fire resistant high strength low alloy steels, Materials Science and Technology December 1990 Vol. 6

[2]. Japanese Industrial Standard JIS A-1304, 'Method of fire resistance test for structural parts of buildings', 1975.

[3]. Y. Mizutani, K. Ishibashi, K.Yoshii, Y. Watanabe, R. Chijiiwa, Y.Yoshida, 590MPa Class Fire-Resistant Steel for Building Structural Use, Nippon steel technical report no. 90 july 2004.

[4]. H. Fujino, K.Hitomi, J.Hashimoto, S.Umezhawa, Fire resistance steels for building structural use, Kawasaki steel technical report No. 29, Nov. 1993

[5]. Zheng Zhiwang, Liu Qingchun, Effect of vanadium on the microstructure and properties of fire-resistant steels, International Seminar 2005 on Application Technologies of Vanadium in Flat – Rolled Steels, pg. 96-103.

[6]. ASTM E8- Standard methods for room temperature tensile testing, ASTM standards.

[7]. S. Zajac, Extended Use of Vanadium in A New Generation of Flat Rolled Steels International Seminar 2005 on Application Technologies of Vanadium in Flat – Rolled Steels, pg-52-63

[8]. M.G. Hall, K.R.Kinsman, and H.I. Aaronson, Mechanism of Formation of Mo2C

[9]. Needles in an Fe-C-Mo Alloy, metallurgical transactions volume 3, may 1972 ,1321

[10]. M. S Bhat, W.M.Garrison, Jr., and V.F Zackay, Relationship between Microstructure and mechanical Properties in Secondary hardening steels, Materials Science and Engineering A,41 ,1979

National Conference on Thermo-mechanical processing of Steels &
5th Gleeble User Workshop India (GUWI-2015),
August 6-7, 2015, pp 131-145.

Toughness Behavior for Simulated Weld Heat Affected Zone of SA 508, Class 3 Material for Pressure Vessel Applications

Santosh kumar[1,2], Rajneesh kumar[1] and Ajoy kumar Pandey[2]

[1]CSIR-National Metallurgical Laboratory, Jamshedpur
[2]National Institute of Technology, Warangal
Email: rkgupta@nmlindia.org

ABSTRACT

SA 508 class 3 material is widely used for reactor pressure vessel and primary piping systems in nuclear power plants. Apart from strength and weldability, toughness is of paramount importance for such applications. The earlier study suggests that a huge number of failures of such material were initiated through the circumferential crack development due to lack of toughness in the Heat Affected Zone (HAZ). Present investigation aims to study toughness behavior of different regions of HAZ like Coarse Grain Heat Affected Zone (CGHAZ), Fine Grain Heat Affected Zone (FGHAZ) and Inter Critical Heat Affected Zone (ICHAZ) at Low, medium and High Heat Input conditions associated with cooling rates ($t_{8/5}$) of 10 s, 18 s, 40 s respectively by using thermo mechanical simulation technique (Gleeble: Thermal Mechanical Simulator). The maximum Impact energy of 110 J was absorbed by the LHI condition CGHAZ specimen at room temperature in comparison to 92 J for the virgin material and minimum impact energy of 8 J at low temperature of - 40 ˚C was absorbed by CGHAZ specimen simulated for HHI condition in comparison to 46 J for the base material. Results revealed that there is good balance in toughness among the HAZ sub regions for medium heat input condition (18 s of $t_{8/5}$), deleterious toughness loss at both room and low temperatures in HHI condition CGHAZ. Metallographic analysis revealed, great loss in toughness associated with HHI CGHAZ due to the presence of massive type M/A constituent. For LHI condition, maximum Impact energy absorbed in CGHAZ as it comprise tempered martensite through a mixture of bainite and martensite.

Keywords: *Toughness behavior, HAZ Simulation, Thermal Mechanical Simulator (Gleeble), SA 508.*

INTRODUCTION

Reactor Pressure Vessel (RVP) is non-replaceable major component of the pressurized water reactor (PWR) in Nuclear power plant. Low alloy SA 508 class 3 steel is widely used in nuclear components and is known as a prime candidate material for reactor pressure vessels

operating at temperatures below the creep regime (the temperature below which creep deformation is negligible). SA 508 steel forgings are used for applications in light water reactors where the operating temperature is around 300˚C. This steel is typically used in the quenched and tempered condition. There is an extensive literature available on the mechanical properties especially creep, creep-fatigue, and thermal aging behavior of SA 508 material [1-4]. The structural components of nuclear reactor systems include the pressure vessel, piping, and valves, which are fabricated from a number of different materials. The components are joined by welding, and a large reactor contains thousands of welds and many kilometers of piping. Examinations of some internal components such as core shrouds of light water reactors have revealed the presence of circumferential cracks [4] in the heat affected zone of the welds as a result of toughness loss, although the behavior of base materials has been thoroughly investigated. This was mainly due to the heat induced by welding process, HAZ microstructure gets changed and and its properties may significantly differ from the base metal in such steels. It was pointed out that the loss in toughness always happens in weld Heat Affected Zone and also the presence of circumferential cracks in the heat affected zone of the welds at near the joints [4, 5]. Several catastrophic service failures have been directly attributed to a lack of adequate notch toughness resulting from improper welding practice. To obtain a safe welded joint with no toughness loss, it is necessary to know the effect of welding thermal cycles on weld Heat Affected Zone. We need to optimize the process parameters for toughness enhancement. So the present work aimed to study the toughness behavior of sub regions of weld heat affected zone of SA 508 material with thermo-mechanical simulation technique.

MATERIALS AND EXPERIMENTAL PROCEDURE

Materials

The test material used in the present investigation was SA 508 Class 3 low alloy steel, available in the form of a pipe with 270 mm inner diameter and outer diameter of 320 mm. The mechanical properties of starting material were 591 MPa in yield strength, tensile strength of 710 MPa and 13% of elongation. For chemical composition of virgin material SA 508 steel refer table 1.

Table 1: Chemical composition of SA 508 class 3 material

Element	C	Mn	Ni	Mo	Si	Cu	Cr	Co	P	V	S
wt %	0.197	1.3	0.72	0.415	0.205	0.141	0.121	0.013	0.012	0.008	0.005

Theoretical computation for peak temperature

The distribution of peak temperatures in the base metal adjacent to the weld is obtained by using below mentioned expression [6].

$$\frac{1}{T_p - T_o} = \frac{4.13\rho C_p tY}{H_{net}} + \frac{1}{T_m - T_o}$$

where T_p is the peak temperature (°C) at distance Y (mm) from the weld fusion boundary, T_o is the initial temperature (°C), Tm is the melting temperature (°C), H_{net} is the net energy input equal to $\eta EI/v$ (J/s · mm), ρ is the density of the material (g/mm^3), C_p is the specific heat of solid metal (J/g · °C), and t is the thickness of the base metal (mm).

Theoretical computation for cooling rate

The cooling rate varies with position and time; its calculation requires the careful specification of conditions. At a temperature well below melting, the cooling rate in the weld and in its immediate HAZ is substantially independent of position. The most useful expression to determine the cooling rate on the weld centerline at the instant when the metal passes through a particular temperature of interest, T_c is mentioned below. For carbon and low-alloy steels, T_c (550°C is satisfactory for most steels) is the temperature near the pearlite nose temperature on the time-temperature transformation (TTT) diagram. The cooling rate expression for thin plate is given mentioned below [6].

$$R = 2\pi\rho k C_p \left(\frac{t}{H_{net}}\right)^2 (T_c - T_o)^3$$

where R is the cooling rate (°C/s) at a point on the weld centerline at just that moment when the point is cooling past the T_c, and k is the thermal conductivity of the metal (J/mm · s · °C).

Test Weld

Test welds were made to capture the thermal history experienced at different location from the weld centre line during welding. These thermal histories were required for use in the gleeble for thermo mechanical simulation. Due to material limitation of SA 508 material, test welding was performed with flat mild steel plates. In the present work, test welding was performed on two mild steel flat plates of 10 mm thick by submerged arc welding process (Fig. 2.), input parameters described in table 2. A single half V-butt joint, schematic view

given in Fig. 1 with root face 4 mm and included angle 45° is made by two mild steel plates having dimensions of 300 mm in length and 100 mm in wide. Thermal history was captured at three locations situated at 10 mm, 15 mm and 20mm away from center line during the welding process by inserting thermocouples. Due to experimental limitation these thermocouples could not be inserted very close to the weld center line. All the thermocouples were connected with Data acquisition (DAQ) module, which was connected to computer for online temperature measurement and recording using Labview program.

Table 2: Input parameters for Test welding (SAW process)

Voltage(V)	25
Current(I)	300
Welding speed (mm/sec)	3.33
Plate thickness (mm)	11
Heat input (j/mm)	2250
T_o (initial plate temperature)	25^o C

HAZ Simulation

Actual Heat Affected Zone (HAZ) present a complex mix of microstructure in narrow limited region and it's very difficult to predict the properties. In steels Coarse Grain HAZ, Fine Grain HAZ, Inter Critical HAZ, Sub Critical HAZ are the possible zones of HAZ and possesses different properties each. So for better prediction of properties, intricate equipment like Gleeble needed to get uniform microstructure on over a large volume for sub regions of HAZ separately. The main aim of physical simulation is to exactly reproduce the thermal and mechanical situation of the work piece material as it appears in real processing [7], and to obtain identical microstructures as well as mechanical properties of the physically simulated materials. In the present investigation Gleeble 3800 system used for studying ductility and toughness behavior of heat-affected zones of welds. Gleeble 3800 is a fully integrated digital closed loop control thermal and mechanical testing system that can simulate a wide variety of thermal/mechanical metallurgical situations [8]. In low alloy steels, the microstructure development mainly affected by the peak temperature attained, cooling rate $t_{8/5}$ is a long-established index of the cooling rate. The peak temperatures attained in sub regions of HAZ as illustrated in table 3. Simulation was carried for Coarse Grain Heat Affected Zone (CGHAZ), Fine Grain Heat Affected Zone (FGHAZ) and Inter Critical Heat Affected Zone (ICHAZ) at Low, medium and High Heat Input conditions associated with cooling rates ($t_{8/5}$) of 10 s, 18 s, 40 s respectively on standard Gleeble specimens (70mm x 11 mm x 11 mm),

thermocouple type K percussion welded at the middle to provide closed-loop temperature control. The thermal-cycle simulations were conducted with the Gleeble chamber in high vacuum of approximately 10^{-6} torr ($1.3x10^{-4}$ Pa) to limit sample surface oxidation and thermocouple detachment and a standard copper grips set was used for effective cooling.

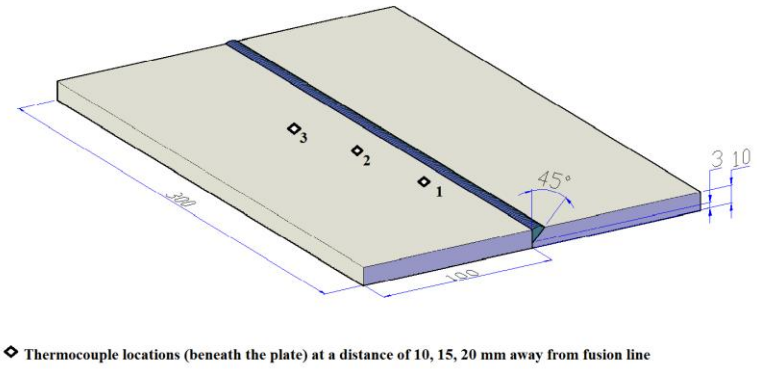

Fig. 1: Test weld schematic view

Thermal cycles used for haz simulation

The thermal cycles employed for HAZ simulation comprise, samples were resistance heated through the low-frequency (60 Hz) alternating current to the peak temperature at a linear rate of 100˚C/s and then follows exponential cooling. The exponential equation taken form Gleeble hand book is mentioned below [8].

$$\mathbf{T=T_{max}\, e^{(-0.47t/\Delta t)}}$$

Here T_{max} is Peak Temperature in ºC, Δt is Cooling time $t_{8/5}$ and t is time in sec.

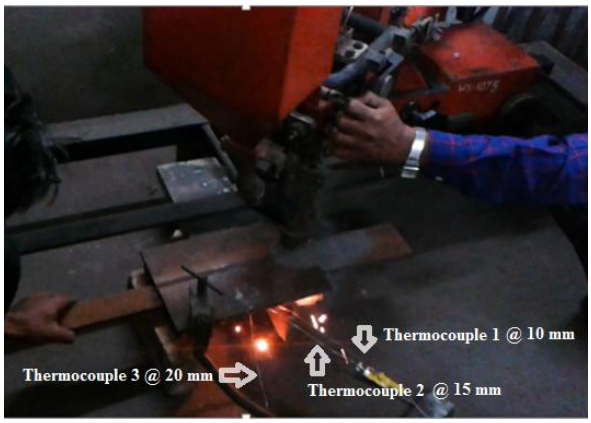

Fig. 2: Performing test welding by SAW Process

Thermal cycles, LHI condition for CGHAZ, FGHAZ and HHI condition for CGHAZ are illustrated in figure 3. The Coarse Grain Heat Affected Zone simulation for Low Heat Input condition, the weld thermal cycles follows linear heating rate of 100 ˚C/s up to peak temperature of 1200 ˚C, holding the sample at peak temperature for 2 sec and then followed by exponential cooling such that it allows a cooling rate ($t_{8/5}$) of 10 s. Coming to High Heat Input condition, the thermal cycles follow the similar trend except the cooling rate ($t_{8/5}$) as 40 s while it drops exponentially from the peak temperature as illustrated in figure 3. For Fine Grain Heat Affected Zone simulation the peak temperature attained was 1000˚C at a linear rate of 100˚C/s, holding time was 2 sec at this peak temperature and then exponential cooling such that a 10 s cooling rate ($t_{8/5}$) is attained.

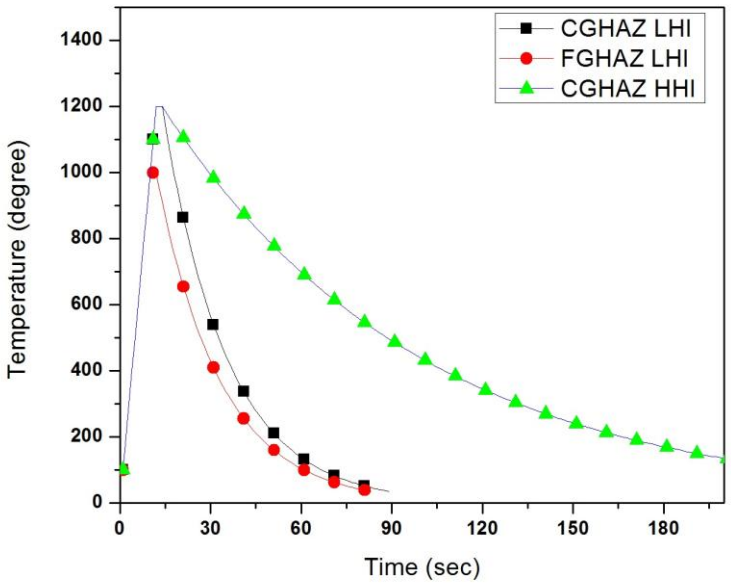

Fig. 3: Weld thermal cycles for HAZ simulation

Impact Toughness Testing

Impact tests of simulated samples generally signify a conventional test because uniform microstructure is tested where as in actual welds, non uniform microstructure prevails and also positioning of crack while making charpy block is quite tedious. However, an accurate toughness ranking was typically achieved. Full size standard Charpy-V notch specimens (Fig. 5) were prepared from the samples subjected to weld HAZs simulation (Fig. 4) in accordance with the standard ASTM Designation E 23, center notch of depth 2 mm, root radius of 25 mm and the included angle of notch is 45˚C. Charpy impact tests were carried out at a room temperature 25˚C, low temperature of -40˚C by immersing the sample in chiller machine

containing solution of Kyro 85 for 20 minutes after the required temperature achieved and then promptly tested.

Table 3: Peak temperatures in HAZ regions

HAZ Sub Regions	Location	*Peak Temperature (°C)
ICHAZ (inter critical HAZ)	Ac1□ T□ Ac3	850
FGHAZ (fine grain HAZ)	T□ Ac3	1000
CGHAZ (coarse grain HAZ)	T□ □ Ac3	1200

*The peak temperatures taken from Ref [37] with consideration of Industry experts.

Metallographic Observation complemented with Hardness Measurements

Microstructures of simulated HAZ, virgin material SA 508 were observed by LEICAD M2500 M Optical microscopy. Sectioning of simulated samples carried out by wire cut EDM Process, were cold mounted, ground on SiC papers, polished and chemically etched by 2% Nital. For analyzing the fracture surfaces, resulting from charpy impact testing was observed in NOVA NANOSEM-430 Scanning electron microscopy. Micro hardness measurement (Vickers hardness) was done using a LECO M - 400-H1 hardness testing machine with a load applied 1kg, which was in accordance with ASTM E 384-10. Brinell hardness measurement was carried out to predict the width of the simulated region on standard Gleeble specimen, to check the hardness variation along the simulated sample.

Fig. 4: HAZ Simulated samples

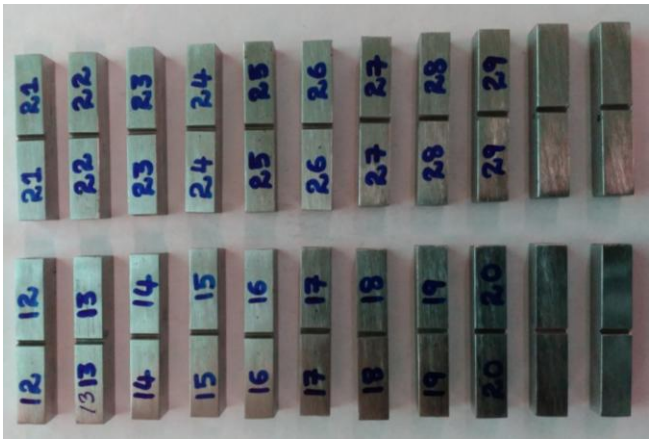

Fig. 5: Standard Charpy specimens of simulated samples

RESULTS AND DISCUSSION

Thermal Profile during Test Weld

Three thermocouples were connected to the weld coupon (on the plate with square edge) at 10 mm, 15 mm and 20 mm away from fusion line. Temperature data during welding and subsequent cooling from the thermocouples was acquired using National Instruments Data Acquisition Card and Lab View software. The time temperature plots obtained have been shown in figure 6. These plots were further used to compare peak temperature and cooling rates with the theoretical computed ones as illustrated in table 4. It was found that the computed results were in conformity with the experimental one.

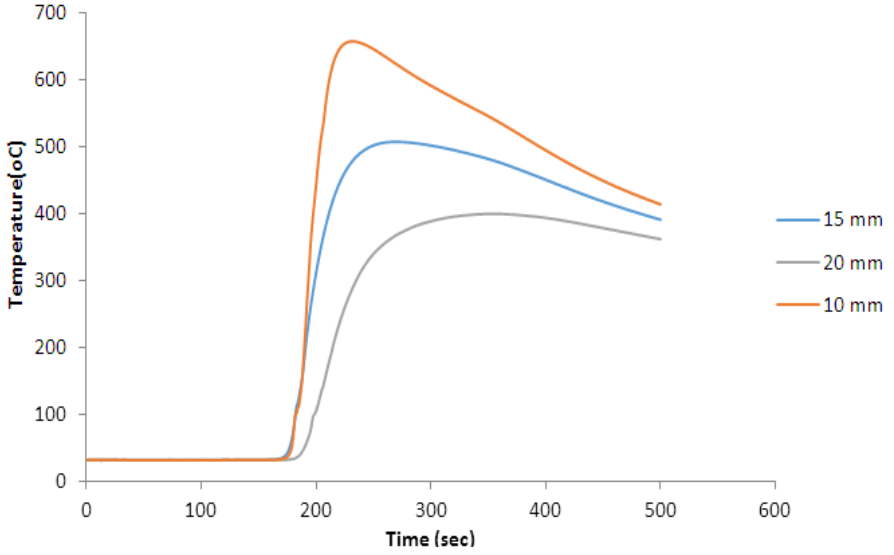

Fig. 6: Temperature profile measured during test weld.

Table 4: Calculated values of Peak Temperatures and cooling rates at different regions of weld

Distance from center line (mm)	1	2	3	10	15	20
Peak temperature (°C)	1381.784	1134.37	768.432	633.469	490.605	402.071
Cooling Rate (°C/sec)	59.850	40.710	28.934	5.370	2.406	1.278

Impact Toughness

The simulated samples machined in to standard Charpy blocks and then tested for Impact energy measurement, those results were listed in table 5. The maximum Impact energy of 110 J was absorbed by the LHI condition CGHAZ at room temperature in comparison to 92 J for virgin material and a minimum of 8 J was absorbed by CGHAZ for HHI condition at low temperature of - 40 ˚C in comparison to 46 J for base material. It was clear from results there is a deleterious toughness loss in Coarse Grain Heat Affected Zone for High Heat Input condition.

Table 5: Impact Energy measurement for sub regions of HAZ, base material

HAZ Sub region/ base material	Heat Input condition (cooling time $t_{8/5}$)	Impact energy at room temperature (25˚C)	Impact energy at low temperature (-40˚C)
CGHAZ	LHI (10 s)	110	45
CGHAZ	Medium (18 s)	70	32
CGHAZ	HHI (40 s)	23	8
FGHAZ	LHI (10 s)	88	19
FGHAZ	Medium (18 s)	40	14
FGHAZ	HHI (40 s)	43	13
ICHAZ	LHI (10 s)	33	6
ICHAZ	Medium (18 s)	104	7
ICHAZ	HHI (40 s)	72	32
Virgin material	as received condition	92	46

For LHI condition simulated samples, Impact energy plot is clearly illustrated in Fig. 7. There is similar trend in energy absorbing capacity during Impact testing for simulated samples at both room and low temperatures. Those samples tested at room temperature posse's higher energy absorbing capacity than those tested at low temperature. It is evident from results,

good balance among the HAZ sub regions for medium heat input condition in comparison to base material energy absorbing capacity. Maximum Impact energy was noticed in CGHAZ LHI condition at both test conditions (room, low temperatures). It was noticed that, decrease in the energy absorbing capacity in CGHAZ with the increasing weld heat input. In order to posses high toughness in weld CGHAZ region, it is preferable to limit the cooling rate.

Macro Hardness Measurement

In the present dissertation work Brinell Hardness measurement was used to find out the hardness variation along the center line of simulated sample (Fig. 8) and to find out the width of the simulated region in the standard Gleeble specimen (70 x11 x 11 mm^3), hardness values illustrated in table 6., also plotted in Fig. 9. The centered marked region represents the width of the simulated region was measured as 11.66 mm, the average Brinell hardness number in the simulated region was 400 HBW, 333 HBW at the interface between base material and the simulated region, an average of 210 HBW was found out in the unaffected region. The macro hardness plot for simulated sample along its longitudinal direction is given Fig. 9. It is clear that the sharp decrease in hardness measurement at the interface of simulated region, unaffected region. Thus it enables us physical simulation is an admirable tool to predict the properties of the each sub region of HAZ separately because actual HAZ presents complex district microstructure within the narrow limited region and it is very difficult to analyze conventionally.

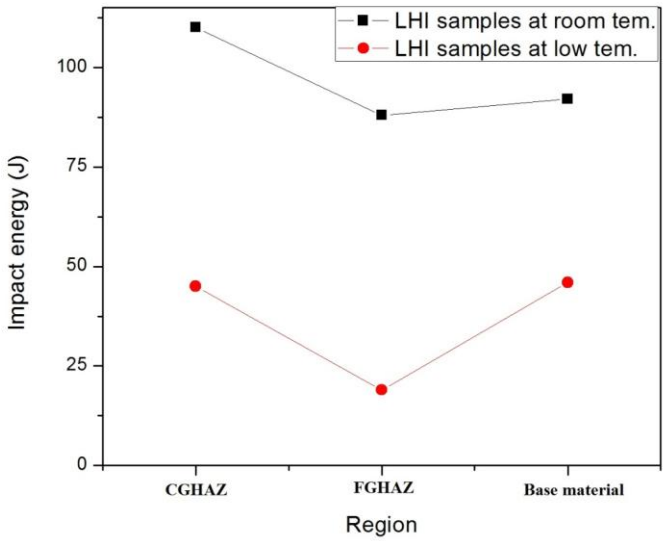

Fig. 7: Impact energy plot for LHI condition simulated samples at room, low temperatures

Fig. 8: Macro hardness variation along the simulated sample

Table 6: Brinell hardness measurement along the simulated sample

Hardness Location	Distance away from center in mm	Hardness value (BHN)
1	22.55	213
2	20.42	218
3	18.42	221
4	14.52	219
5	12.01	215
6	8.66	220
7	5.47	409
8	2.83	397
Center (9)	**at center**	**392**
10	2.00	400
11	4.87	333
12	7.11	218
13	11.43	225
14	14.16	219
15	17.41	221
16	17.43	224
17	19.55	219

Metallography

The microstructure of SA 508 low alloy steel in as received condition exhibits nearly equiaxed bainitic grains and very few ferrite grains associated with both intra and inner carbides as it shown in Fig. 10 (d). It was reported that fine Cr-carbides such as M_7C_3 and $M_{23}C_6$ precipitates primarily due to Cr concentrations and coarse M_3C type carbides mainly observed. Figure 10 (a) clears that LHI condition CGHAZ simulated sample contains predominant tempered martensite through a mixture of martensite and bainite. Typical tempered bainite and primary ferrite in the form of stringers along the prior equiaxed austenitic grain boundaries developed in FGHAZ simulated sample for LHI condition can be

seen in Fig. 10 (c). For HHI condition of CGHAZ simulated sample shows (Fig. 10 (b)) the regions of bainitic ferrite and regions of a carbon rich structure with darker grey in appearance is referred to as granular bainite associated with massive type M/A constituent and also likely to contain some martensite.

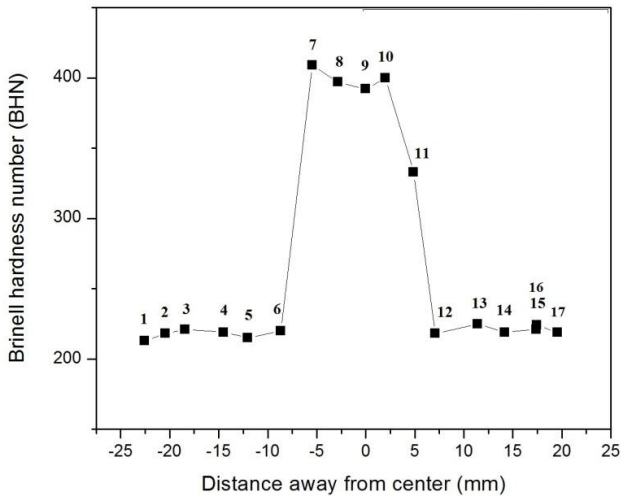

Fig. 9: Hardness plot of simulated sample.

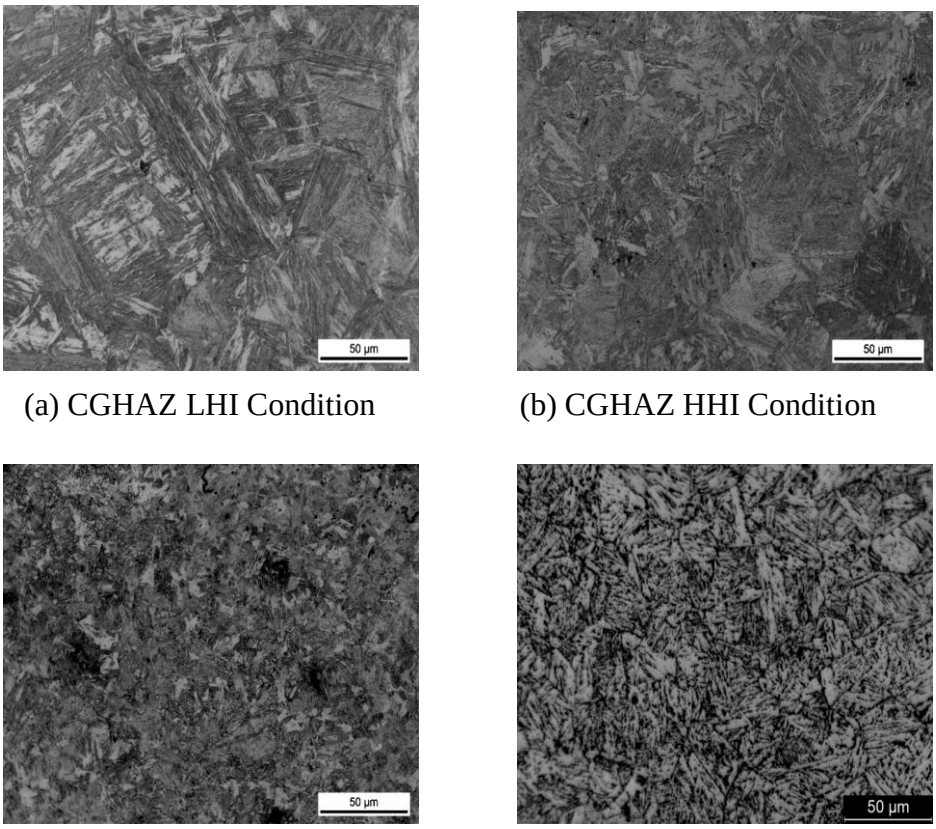

(a) CGHAZ LHI Condition (b) CGHAZ HHI Condition

(c) FGHAZ LHI Condition (d) Virgin material

Fig.10: Optical micrographs at a magnification of 1000X

Effect of m/a constituent on toughness

Toughness of the material mainly affected by the chemistry, microstructure developed as it resulting from imposed thermal cycles. It is well known that M/A constituent is hard and brittle in nature, prompt for nucleation sites for crack initiation [10]. In the present investigation HHI condition CGHAZ sample comprise of massive type of M/A constituents in morphology, mainly as a result of high heat inputs. It was observed that the morphology of M/A constituent will be transformed from bar to block and the gradual increase of its volume fraction with increasing in cooling time (Heat Input) [11]. As a result HHI CGHAZ posses deleterious toughness loss at room, low temperature test conditions. So it is advisable to avoid high heat input conditions for toughness enhancement in HAZ, especially at low temperature applications.

Fractography

The fracture surfaces of HAZ simulated specimens after Impact testing has been analyzed as in SEM have been shown in Fig. 11. The fracture surface of Impact tested sample at room temperature (25 ˚C) exhibited a ductile tearing morphology, appears to be predominantly intergranular with some grain facets can be seen in Fig. 11 (a). Thouse specimens tested at lower temperatures (-40 ˚C) exhibited dominant quasi-cleavage fracture mode, indicative of low energy fracture.

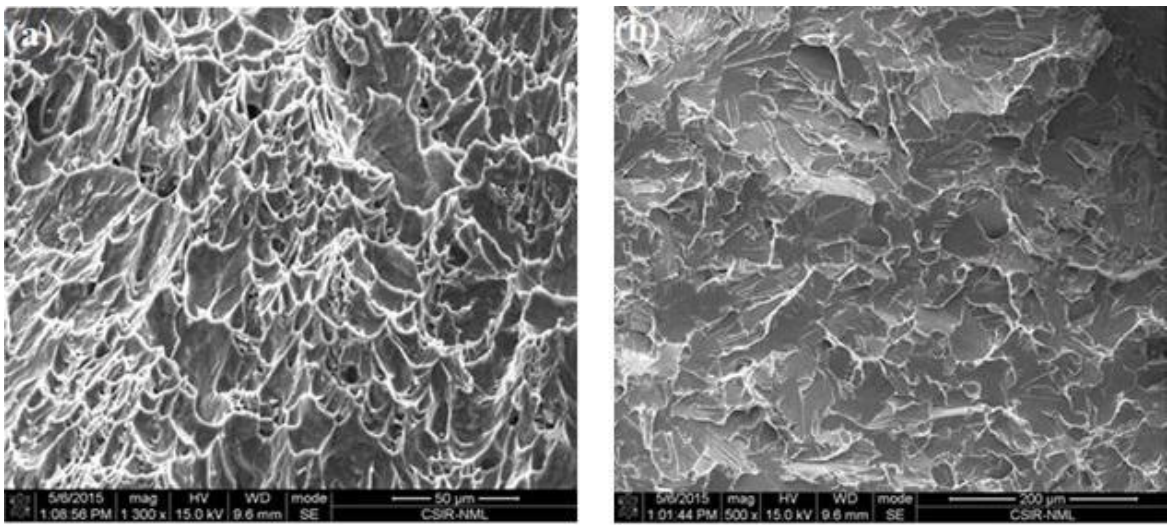

Fig.11: Fractograph of Impact tested sample at (a) room temperature, (b) Low temperature.

CONCLUSIONS

1. A test technique developed to simulate the characteristic sub regions of HAZ of RPV material SA 508 Steel using Thermo-Mechanical Simulator (Gleeble 3800).

2. A slight tougher HAZ is formed close to the fusion line with a lower hear input (10 s of $t_{8/5}$) rather than high heat input (40 s of $t_{8/5}$). It was noticed that, decrease in the energy absorbing capacity in CGHAZ with the increasing weld heat input. In order to posses high toughness in weld CGHAZ region, it is preferable to limit the cooling rate (10 s of $t_{8/5}$).

3. The maximum Impact energy of 110 J was absorbed by the LHI condition CGHAZ at room temperature in comparison to 92 J for virgin material and a minimum of 8 J was absorbed by CGHAZ for HHI condition at low temperature of - 40 ˚C in comparison to 46 J for base material.

4. Deleterious toughness loss was observed in CGHAZ for HHI condition, this remarkable decrease in CGHAZ was accompanied by the formation of M/A Constituent as result of high cooling rate.

5. Macro hardness of simulated samples revealed that the width of the simulated region was 11.66 mm on standard Gleeble specimen (70X11X11 mm^3). The average Brinell hardness number in the simulated region was found to be 400 HBW, 333 HBW at the interface and 210 HBW was found in the unaffected region.

6. Metallography analysis revealed that the maxium impact energy associated with CGHAZ LHI simulated sample is mainly because of tempered martensite through a mixture of bainite and martensite while CGHAZ HHI simulated sample shows the regions of bainitic ferrite and regions of a carbon rich structure with darker grey in appearance is referred to granular bainite and is associated with massive type M/A constituent in morphology across grain boundaries leads to posses low Impact energy.

7. The Fractographic analysis of all impact specimens tested at room temperature (25 ˚C) exhibited predominantly ductile micro void coalescence fracture while the specimens tested at low temperature (-40 ˚C) exhibited quasi-cleavage fracture.

8. Good consistency in tensile results for both samples mainly attributed to low strain rate condition of 0.000054 s^{-1} i.e with a extension rate of 0.00136 mm s^{-1}.

ACKNOWLEDGEMENT

Authors are grateful to Director, CSIR-National Metallurgical Research Laboratory to permit publishing of this work.

REFERENCES

[1]. Reddy, G. B., and Ayres, D. J., 1982,"High Temperature Elastic-Plastic and Creep Properties for SA-533 Grade B Class 1 and SA508 Materials", EPRI NP-2763.

[2]. Harris, B. L., Shah, V. N., And Korth, G. E., 1986, "Creep Rupture Failure of Three Components of the Reactor Primary Coolant System during the TMLB Accident," EGG-EA-7431.

[3]. Ellis, F. V., And Byrnum, J. E., 1990, "Creep and Tensile Properties of SA-508 Class 3 Forging Material," Damage Assessment, Reliability, and Life Prediction of Power Plant Components, PVP.

[4]. K. Natesan, S. Majumdar, P. S. Shankar, and V. N. Shah "Preliminary Materials Selection Issues for the Next Generation Nuclear Plant Reactor Pressure Vessel" September 2006, Argonne National Laboratory Argonne, IL 60439.

[5]. M. J. Gaudet, "Mechanical Behavior and Fracture Properties of the Heat Affected Zone for Dual Torch Welded X80 Steel," Ph.D, The University Of British Columbia, 2010.

[6]. C.M. Adams, JR. "Cooling Rate and Peak Temperature In Fusion Welding", Welding Journal, Volume 37 (No. 5), 1958, P 210S-215S.

[7]. Gleeble 3800 System - Product Description and Specifications, Tech. Rep., Dynamic Systems Inc., Poestenkill, NY, 2006, Pp.10-19.

[8]. Bibliography of Gleeble Papers, Tech. Rep., Dynamic Systems Inc., Poestenkill, NY 2006.

[9]. Caron, J. "Weldability Evaluation of Naval Steels" Phd Thesis, The Ohio State University, 2010.

[10]. Toyodo, M., Fracture Toughness Evaluation of Steel Welds. Osaka University. 1988.

[11]. Chen, Y.T., Guo, A.M., Wu, L, X., Zeng, J., Li, P.H., 2006. Microstructure and Mechanical Property Development in the Simulated Heat Affected Zone of V-Treated Hsla Steels. Acta Metall. Sinica 19, 57-67.

National Conference on Thermo-mechanical processing of Steels &
5th Gleeble User Workshop India (GUWI-2015),
August 6-7, 2015, pp 146-156.

Thermo-Mechanical Simulation Using Gleeble System - Advantages & Limitations

Vinod Kumar

R&D Centre for Iron & Steel, Steel Authority of Indian Limited, Ranchi – 834 002 INDIA

Email : vkumar@sail-rdcis.com

ABSTRACT

Thermo-mechanical simulation studies using Gleeble System have found extensive application in almost all spheres of metal processing industries including process optimization, development of new alloys, quality/ yield improvement and material characterization, etc. Physical simulation unlike numerical simulation being very close to the real world process can be very helpful in near exact reproduction of the process and in turn better results if carried out carefully.

However, it has certain limitations too which must be clearly understood before planning for a study. Therefoere, such studies need to be carried out with precaution to achieve desired results. Otherwise, the simulated results may not find appreciation with actual processing. These limitations can be machine specific or understanding specific. For example, thermal gradient along length is advantageous for HAZ or continuous casting simulation but it limits the scope for hot tensile test due to low uniform temperature zone across gauge length.

Similarly, most of the research papers published on hot compression to understand the hot workability or development of processing map are based on on-heating experiments involving heating the material to deformation temperature followed by deformation at different strain rate and temperature. The results generated are sometime used to optimize an industrial process which involves different thermal cycle of reheating the material to high temperature, soaking followed by cooling to deformation temperature and are unable to produce desired results.

Keywords*: Thermo-mechanical simulation, Gleeble, process optimization*

INTRODUCTION

Research in steel has traditionally been centered around understanding materials behavior during processing, process optimization, materials characterization leading to new product development, reduction in cost of production, and quality/ yield improvement. Steel

production involves a large number of processes starting from continuous casting to hot rolling, post cooling, annealing (in case of cold rolled products), heat-treatment (in case of quench & tempered products), etc. Proper alloy design is another important aspect for new product development.

Any change in the process parameters or change in chemistry for a new alloy requires a thorough understanding of materials behavior as above. Moreover, it is highly time consuming and costly affair if carried out at a plant scale. Sometime, it is not even possible or affordable. In addition, flexibility for study is limited resulting in fewer numbers of experiments. This leads to slow pace of development or limited development and in turn, a very long product development cycle making it non-profitable or techno-economically non-feasible. However, it can be shortened significantly if the process parameters can be optimized using a Thermo-mechanical Simulator before undertaking plant scale trials. Moreover, it also helps in understanding materials behavior under different processing conditions leading to quality improvement of existing products and solving materials defect leading to yield improvement. Details of various Gleeble based thermo-mechanical simulation studies and the results thereof can be found elsewhere [1-10].

However, it has certain limitations too which must be clearly understood before planning for a study. These limitations can be machine specific or understanding specific. The present paper provides an account of the advantages of thermo-mechanical simulation studies using Gleeble in materials research and its limitations in achieving desired results.

APPLICATIONS AND LIMITATIONS

Continuous Casting

Casting has been studied for several decades and the first major application to a production process was done by H. Suzuki at Nippon Steel, Japan in the late 1970's. Increasing importance is being attached to the study of cracking in continuously-cast (CC) slabs, and to their hot workability during hot rolling, in order to increase the use of continuous casting and accomplish hot direct rolling as a means of reducing the consumption of energy and the number of processes involved in the manufacture of steel products. Producing crack-free slabs is the key requirement for the success of the in-line reduction technique. This requires a study of the temperature region where the embrittlement occurs, the factor that govern the embrittlement, and the strain rate dependence of the embrittlement. A castability map can

then be developed combining all these factors to arrive at the safest casting route to be followed to produce defect-free slabs. Continuous casting simulation finds wide applications to study surface cracking during casting, directional solidification, mushy zone processing/ semi-solid processing, segregation, etc.

Gleeble Thermo-mechanical simulator provides unequal opportunity to conduct continuous casting simulation studies due to its unique heating system wherein steep thermal gradient can be generated. This helps in raising the temperature in the centre of the specimen while the ends remain at low temperature. This leads to melting the material in the centre wherein it can be held back within a quartz tube of adequate size.

Continuous casting simulation is generally done using 10 mm dia. cylindrical specimens enclosed in a quartz tube of inner dia 10.25 mm. The steel is heated at fast rate up to a little below melting point of the material and then slowly heated till its starts melting. The steel is kept for a while so that sufficient liquid metal is formed and homogenized. This is followed by cooling it at the desired rate to the test temperature. Separate sample is used to determine tensile properties, like tensile strength and reduction in area at these test temperatures. A plot of reduction in area verses the test temperature provides the ductility troughs as mentioned earlier which can be used for fine-tuning the casting parameters.

However, it is to note that diameter of the sample increases as per coefficient of thermal expansion of the material under study. In view of this, if the coefficient of thermal expansion is high for certain materials, like stainless steel, the overall expansion in diameter may increase beyond the inner diameter of the quartz tube and ultimately may break it (Fig. 1).

Fig. 1 Quartz Tube broken during Heating Due to Excessive Thermal Expansion

Fig. 2 Cracked Samples During Heating

Table 1 summarizes thermal expansion of a 10 mm dia. sample of different alloys at different temperature. It may be noted that thermal expansion is more than 0.25 mm for different stainless steel grades, like SS 304, SS 310 and SS 316.

In view of this, precaution needs to be exercised while planning continuous casting simulation studies on materials with high coefficient of thermal expansion. Higher inner diameter quartz tube may be used but the molten material may come out of the tube due to excessive gap. Otherwise, little lower diameter sample may be used to compensate for the expansion.

In any case, diameter of the specimen remains same at 10.25 mm after melting and this vale may be used for calculation of reduction in area or tensile strength instead of diameter measured at room temperature which may be entirely different. This will give a fairly good idea of the hot ductility.

Table 1: Thermal Expansion of Different Alloys for a 10 mm dia. sample

Steel	Coeff. of Thermal Expansion (10^{-6} m/mK)	Thermal Expansion at Different Temperature, mm				
		1100 ºC	1200 ºC	1300 ºC	1400 ºC	1500 ºC
C-Mn Steel	11.7	0.16	0.17	0.18	0.20	0.21
SS 304	17.3	0.24	**0.25**	**0.27**	**0.29**	**0.31**
SS 310	14.4	0.20	0.21	0.23	0.24	**0.26**
SS 316	16.0	0.22	0.24	**0.25**	**0.27**	**0.28**
SS 410	9.9	0.14	0.15	0.16	0.17	0.18
SS 430	11.0	0.15	0.16	0.17	0.18	0.20
3% Si Electrical Steel	15.3	0.21	0.22	0.24	**0.26**	**0.27**

Hot Compression

Hot compression is the most common test in Gleeble to study the hot deformation behavior of metals and alloys. It can successfully be used to study flow softening behavior due to recrystallization and recovery, flow stress determination, hot rolling simulation, forging simulation, determination of no-recrystallization temperature, stress-relaxation studies,

understanding the influence of deformation on microstructural evolution, hot workability studies, edge cracking, and so on. Hot compression studies can be divided into two categories, (i) uni-axial flow stress compression and (ii) plane strain compression depending upon the stress condition. Both these tests find different applications: whereas, uni-axial compression is more close to forging operation, plane strain condition is experienced in hot rolling.

In a steel industry, hot rolling is the main finishing mill. It involves reheating of slab at high temperature, multi-pass deformation at high temperature in the roughing stand, multi-pass deformation at lower temperature in the finishing stand followed by post-cooling and coiling in case of hot strip mill. Selection of parameters for each of these steps is normally done based on some previous knowledge either from the literature or from practical experience. However, optimization of these steps is must to utilize the mill to its fullest extent in producing quality products with desired properties. Some of the common problem encountered during hot rolling is the mill load, edge cracking, formation of undesired microstructure, and poor mechanical properties. Gleeble System can be effectively used to study and overcome these problems. For example, mean flow stress determination under temperature-strain-strain rate conditions can be used to predict rolling load, crack susceptibility studies during hot working through SICO (stress induced crack opening test) and flow stress deformation (upsetting test) can be used to study the edge cracking problem and to suggest safe working zone, microstructural evolution as influenced by hot deformation schedule can be used to predict evolution of different types of microstructure. As detailed above, Gleeble System can be utilized for the determination of various critical temperatures, like no-crystallization temperature (Tnr), austenite to ferrite start (Ar_3) and end temperature (Ar_1) under deformed condition. All these are very important to design rolling schedule.

To make effective use of hot compression studies, following precautions need to be exercised.

Selection of Heating Cycle

Hot compression studies can be carried out using (i) on-heating thermal cycle where the test specimen is heating to the deformation temperature and compressed or (ii) on-cooling thermal cycles where the specimen is heated to high temperature soaking followed by cooling to a pre-decided deformation temperature (Fig.3). On-heating hot compression testing is easier to perform and can be done at any hot compression device, on-cooling hot compression

testing requires good control over cooling rate possible with a Gleeble System. Whereas, the on-heating testing can be of academic interest, on-cooling testing is the real hot deformation simulation during an actual processing. Both produce entirely different flow behavior as depicted in Figure 4.

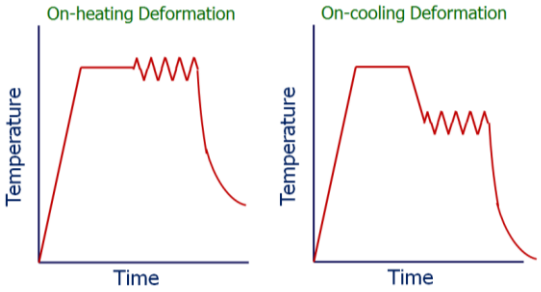

Fig. 3: Thermal Cycles Adopted During On-heating and On-cooling Test

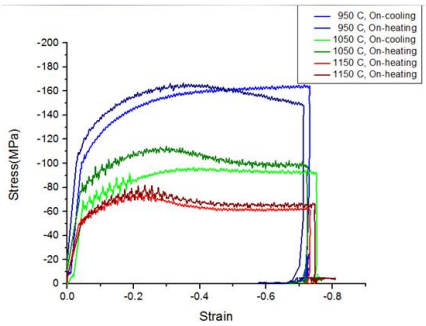

Fig.4: Flow Behaviour Under Different Thermal Cycles

Selection of Soaking Temperature

Selection of soaking temperature depends upon the alloying elements present, their solubility temperature, etc. Improper selection of soaking temperature will lead to wrong conclusion. Figure 5 shows the influence of soaking temperature on the flow stress in multi-pass hot rolling simulation study on a Nb-microalloyed steel. Higher soaking temperature resulted in higher flow stress values owing to higher dissolution of Nb into austenite.

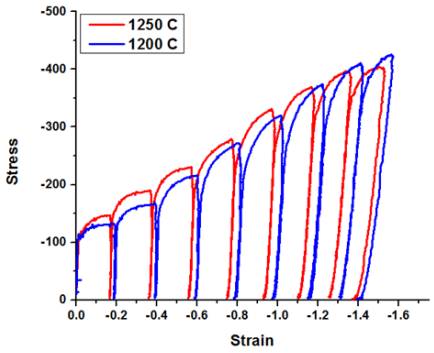

Fig. 5: Influence of Soaking Temperature on Flow Stress

Different types of specimens are used for different studies. For example, 10 mm dia. x 12/15 mm height cylindrical specimen is used for uni-axial compression and 10 mm x 15 mm x 20 mm rectangular specimens are used for plane strain compression. Heating rate is generally restricted to 5C/sec and deformation can be programmed as desired simulating actual

conditions. Only limitation lies in the total deformation that can be given on a single specimen. Minimum thickness of the deformed specimen in plane strain compression can not be less than 3 mm. In other words, 12 mm height specimen can be deformed to 75% only, whereas 15 mm height specimen can be deformed to 80%.

However, in uni-axial compression following limitations are applicable on maximum deformation (Table 2). 15 mm height sample can be deformed upto 72% only for 10 mm standard dia. whereas it can be deformed upto 80% if diameter is reduced to 8.5 mm. These calculations are based on using 19 mm dia Tungsten Carbide ISO-T Anvils. Similarly, for 12mm height sample can deformed upto 71.7% for standard 10 mm dia. sample whereas it can be little more upto 75% if diameter is decreased to 9.5 mm. There is a restriction on reduction in diameter as sample tends to twist or bend during compression and it may not deform uni-axially.

Table 2: Maximum Deformation Possible for Different Sample Dimensions During Uni-axial Compression (For 19 mm dia Tungsten Carbide ISO-T Anvil)

Original Diameter, mm	Original Height, mm	Final Height, mm	Reduction, %
15.0	10.0	4.2	72.0
15.0	8.5	3.0	80.0
12.0	10.0	3.4	71.7
12.0	9.5	3.0	75.0

In view of the above, entire hot rolling process cannot be simulated on a single specimen. Enough care, therefore, should be exercised while predicting microstructure for the entire hot rolling process. If a situation demands to simulate the entire hot rolling process, hot torsion may be used instead of Hydrawedge wherein unlimited amount of strain can be imparted. However, there is a restriction on strain rate and cooling rate.

Strip Annealing

Annealing involves heating to a suitable temperature, holding at that temperature followed by cooling at an appropriate rate. The annealing treatment is given to achieve on or more of the following: (i) softening of the material, (ii) facilitating cold working or machining, (iii) improving mechanical, electrical or forming properties, and (iv) improving dimensional stability.

Annealing process can be divided into three broad categories depending upon the temperature range over which it is imparted. For example, sub-critical Annealing where maximum temperature involved is below the lower critical temperature Ac1. In case of inter-critical annealing, the temperature is above Ac1 but lower than upper critical temperature (Ac3) whereas in case of full annealing, it is above Ac3.

In a steel plant, strip annealing of cold rolled sheets is carried out using batch annealing process or continuous annealing line. The annealing cycle depends upon the type of grade under development, properties required, etc. The simple annealing cycle involving only one step may be reproduced/ studied using a conventional furnace but a complex cycle involving several heating, holding and cooling steps cannot be simulated using conventional techniques.

Gleeble System offers an excellent platform to simulate any complex cycle involving multi-step heating and cooling cycle. An accurate temperature control makes it the most effective tool to study the microstructural evolution during the annealing process and ultimately optimize it to achieve the desired microstructure and properties. Exact annealing cycle can be reproduced with the help of a QuickSim Table Program – an in-built feature and wide range of cooling options. Any number of thermal steps using any heating and cooling step can be generated making it very close to the real world situation. The sample size is also large enough to carry our further studies, like tensile testing or formability testing. The sample for such study is typically 200 mm long x 50 mm wide. Other sizes can be used depending upon the type of study planned after strip annealing simulation studies.

This is to mention that Gleeble System can be employed only for continuous annealing line simulation and it cannot be applied for box annealing involving very long annealing cycle. Further uniform temperature zone is limited during strip annealing simulation study though efforts have been made to increase the uniform temperature zone. In view of this, formability study which is a measure of forming capability of the material may not be possible on simulated strip sample. However, other studies like, hardness, tensile properties evaluation, Microstructural characterization, etc. can be accomplished which gives a fairly good idea about the influence of annealing parameters on the above properties.

Strip annealing studies may be carried out in a very simple way in the absence of a simulator or due to lack of experience. This follows heating the material at a linear rate to annealing temperature followed by soaking for a desired period before cooling at different rate (Fig.

6a). However, it does not take care of actual annealing cycle followed during continuous annealing process involving step heating and cooling due to obvious reasons (Fig. 6b). Enough care, therefore, should be taken to ensure that the actual annealing cycle is followed to achieve desired result.

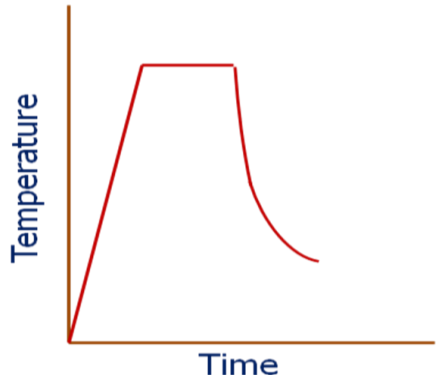

Fig. 6a: Conventional Annealing Study

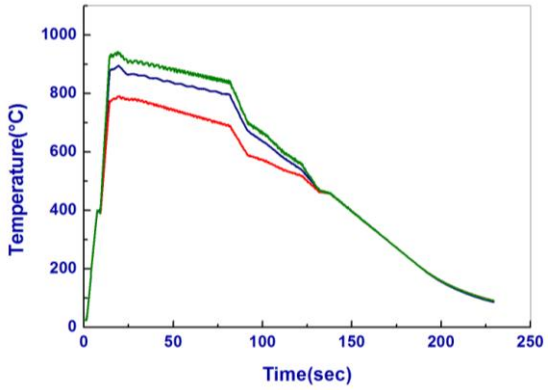

Fig. 6b: Simulated Annealing Study

Welding

Welding cycle can be easily reproduced on a variety of samples using extra-ordinary thermal capability of Gleeble System (heating rate as high as 10,000ºC/s and temperature control within ±1°C). As detailed elsewhere, a number of in-built welding simulation program are available to choose from close to the real-world situation. The user can also develop his own welding simulation cycle. The sample can be a standard Charpy specimen (10x10x55 mm) or a 10 mm diameter cylindrical specimen, which can be used for toughness or tensile properties measurement afterwards. Single-pass as well as multi-pass welding simulation studies can be carried out using flat or round sample (Figs. 7a & 7b).

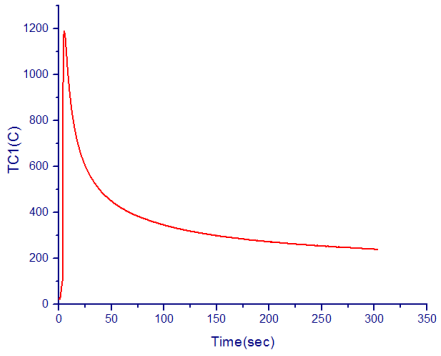

Fig. 7a Single-pass Welding Simulation

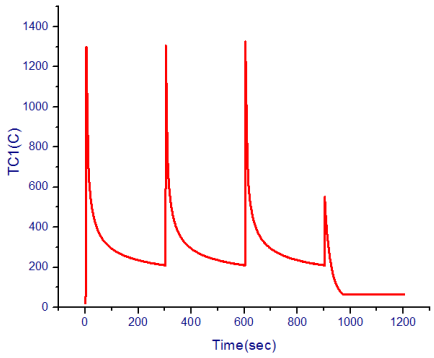

Fig. 7b Multi-pass Welding Simulation

Though, Gleeble thermo-mechanical simulator was primarily developed for welding/ HAZ simulation studies and it remains most useful for such studies today, it does not provide any support to study the influence of welding electrode or any filler material on the weld quality or HAZ properties.

CONCLUDING REMARKS

The thermo-mechanical simulation studies can be effectively utilized to study a wide range of metallurgical processes such as continuous casting, hot rolling, strip annealing, forging, welding, etc. However, such studies need to be carried out with precaution as highlighted above to achieve desired results. Otherwise, the simulated results may not find appreciation with actual processing.

REFERENCES

[1]. Vinod Kumar, S. K. Shukla and Dr. S. K. Chaudhuri, "Simulation and Optimization of Thermo-mechanical Controlled Processing of Nb/ Nb-V Micro-alloyed Steels", Proc. Int. Conf. on "Thermo-mechanical Simulation and Processing of Steels" (SimPro'04), 21-23rd September 2004, Ranchi, pp. 147-158.

[2]. P. P. Sengupta, S. Rath, G. K. Sinha, Vinod Kumar, and B. Krishna, "Optimization of Process Parameters for Increasing Production of CRNO Hot Band Steel in the Hot Strip Mill, Rourkela Steel Plant", Steel India, Vol. 28, No.2, October 2005, pp. 93-97.

[3]. Vinod Kumar, " Thermo-mechanical Simulator – Technique and Applications", Steel India, Vol.30, No. 1, Sept'07, pp.56-62

[4]. S.K. Thakur, Vinod Kumar, S. Rath, G.K. Sinha, A.K. Marik & A.P. Singh, "Effect of Rapid Annealing Cycle on the Recrystallisation Behaviour of low Carbon Steel", Steel India, Vol.32, Issue 1, Sept'09, pp. 49-53.

[5]. S.K. Mohapatra, A. Deva, Vinod Kumar, A.P. Singh & D. Rai, "Optimization of Galvanizing Line Speed through Annealing Simulation", Steel India, Vol.33, Issue 1, April 2010, pp. 67-74.

[6]. S. Patra, S. Roy, Vinod Kumar, A. Haldar and Debalay Chakrabarti, "Ferrite Grain Size Distribution in Ultra-fine Grained High-Strength Low-Alloy Steel After Controlled Thermomechanical Deformation", Metallurgical and Materials Transaction A, Vol. 42A, No. 9, September 2011, pp. 2575-2590

[7]. Vinod Kumar, D. Sarvanan, Santosh Kumar, Atul Saxena, S. Sisodia and B. K. Jha, "Optimization of Hot Rolling and Annealing Process of Low Ni Stainless Steel Using Simulation Studies", Materials Science Forum, Vol. 710 (2012), pp.471-476

[8]. Dipti Samantaray, Sumantra Mandal, Vinod Kumar, S.K. Albert, A.K. Bhaduri and T. Jayakumar, "Optimization of processing parameters based on high temperature flow behavior and microstructural evolution of a nitrogen enhanced 316L (N) stainless steel", Materials Science & Engineering A, 552(2012), 236-244

[9]. R. K. Gupta, Bhanu Pant, Vinod kumar, Vijaya Agarwala and P. P. Sinha, "Deformation behaviiour of $\gamma+\alpha 2$ Ti aluminide processed through reaction synthesis", Materials Science & Engineering A, Published online 23 August 2012, 559 (2013) 49-67

[10]. Sudipta Patra, Suman Neogi, Vinod Kumar, Debalay Chakrabarti and A. Haldar, "Refinement of Ferrite Grain Size Near to the Ultra-fine range by Multi-pass Thermo-mechanical Compression", Metallurgical and Materials Transaction A, VOLUME 43A, NOVEMBER 2012, pp. 4296-4310.

National Conference on Thermo-mechanical processing of Steels &
5th Gleeble User Workshop India (GUWI-2015),
August 6-7, 2015, pp 157-167.

Dynamic recrystallisation of API X80 grade microalloyed steel during hot deformation

Sudhir Kumar[*1,2], Tipu Kumar[1], Ajeet Kumar[1,2], V C Srivastava[1], G K Mandal[1]

[1]CSIR-National Metallurgical Laboratory, Jamshedpur, Jharkhand

[2]M. Tech. Student, Birsa Institute of Technology, Sindri, Jharkhand

Email: gopi@nmlindia.org

ABSTRACT

The development of advanced high strength microalloyed steel for linepipe (API) applications is one of the major focus areas for the steel Industries. The critical applications of these linepipe steels are governed by the available mechanical properties such as strength and toughness. These properties can be considerably improved by proper selection of chemical composition and thermo-mechanical controlled processing route. In the ferritic grade steel, one of the most important strengthening mechanisms is grain refinement, which improves both strength and toughness. Final grain size in steel can be reduced by suitable thermo-mechanical processing (TMP) parameters as final microstructure is largely governed by the prior austenite grain size just after hot deformation. Therefore, high strength and toughness can be achieved not only by suitable adjustment of microalloying elements but also by controlling thermo-mechanical process parameters during hot deformation process.

A comprehensive understanding of the recrystallisation kinetics of these grades of steel will be very much helpful in precisely controlling the hot deformation schedule in order to obtain the desired mechanical properties. In the present investigation, a microalloyed steel having composition akin to API-X80 grade was taken. Experiments were designed to examine the effect of hot deformation conditions on the flow behaviour of this microalloyed steel. Based on the given composition, presence of microalloying elements such as Nb, V and Ti can retard the recrystallisation of austenite by combining with C and N to from precipitates of carbide, nitride or carbonitrides. The presence of these fine precipitates influences the recrystallization mechanisms during and after hot deformation, which in turn control the final microstructure and product properties. To attain higher level of strength, Mo is generally added to this steel, which has significant effect during all stages of the hot rolling as Mo acts directly as a solute and indirectly influences the behaviour of other microalloying elements. The investigation also highlights the influence of Nb on the austenite recrystallisation behaviour.

Keywords*: API X80, hot deformation, dynamic Recrystallization, thermo-mechanical processing*

INTRODUCTION

High strength microalloyed steels are widely used for various special applications such as automobiles, bridges, line pipes etc. The development of advanced high strength microalloyed steel for linepipe (API) applications is one of the major focus areas for the steel Industries. The critical applications of these linepipe steels are governed by the available mechanical properties such as high strength, ductility, low temperature toughness, weldability and lower ratio of yield to ultimate tensile strength. These properties can be considerably improved by proper selection of chemical composition and thermo-mechanical controlled processing route[1]. It is also noted that pipe line steels generally contains low carbon particularly to improve the weldability[2,3]. Microstructure of these steels mainly consists of ferrite. In these ferritic grade steels, one of the most important strengthening mechanisms is grain refinement. It is obvious that decrease in grain size improves both strength and toughness[4]. Final grain size can be reduced by suitable thermo-mechanical processing (TMP) route as final microstructure is largely governed by the prior austenite grain size just after hot deformation. Therefore, high strength and toughness can be achieved not only by suitable adjustment of microalloying elements but also by controlling thermo-mechanical parameters during hot deformation process.

The most commonly added elements in API steels are Mo, Nb, V and Ti etc.[4-7] The microalloying elements, such as Nb, Ti and V can retard the recrystallisation of austenite by forming precipitates such as carbide, nitride or carbonitrides[8]. These fine precipitates play a major role in recrystallisation mechanisms during and after hot deformation[9] to control the final microstructure and hence the product properties. To attain higher level of strength, Mo is generally added along with Nb, V and Ti [6]. It is reported that addition of Mo to microalloyed steels has significant effect during all stages of the hot rolling, as Mo acts directly as a solute and indirectly influences the behaviour of microalloying elements such as Nb, Ti and V [5]. Many of the investigators reported that Mo could decrease diffusivity of the carbide forming species and thus delay the precipitation mechanism[6, 10-11]. Recrystallisation mechanisms play an important role in the control of the final microstructure. Therefore, an improved understanding of the hot deformation kinetics and precipitation behaviour is essential to develop an advanced high strength API steel. A comprehensive understanding of the recrystallisation kinetics of this grade steels will be very much helpful for precise control of hot deformation schedule in order to obtain the desired mechanical properties. Before hot deformation, material should be reheated to a temperature high enough to take all or most of

the alloying elements into the austenite solid solution so as to achieve better control due to precipitate strengthening. During hot deformation, the activation energy of DRX can be very high due to the retardation of dynamic recrystallisation (DRX) by the elements such as Nb, V, Ti, and Mo[12]. The microalloying precipitation is often enhanced during hot deformation and plays an important role in the microstructural and mechanical design of the steels. In the early stages of recrystallisation, strain induced precipitation in austenite can effectively pin the grain boundaries and inhibit their migration[8, 13-17].

For better understanding of the dynamic recrystallisation phenomena during hot deformation in microalloyed steels, the present investigation deals with the high temperature deformation studies emphasizing the role of microalloying elements. In the present investigation, a microalloyed steel having composition akin to API-X80 grade was chosen. Experiments are designed to examine the effect of hot deformation conditions on the flow behaviour of this microalloyed steel. The investigation also emphasizes the influence of Nb on the austenite recrystallisation behaviour. This study will augment the understanding for various stages of thermomechanical processing for precise design of hot deformation schedule to develop an advanced high strength API steel.

EXPERIMENTAL PROCEDURE

A microalloyed steel having composition akin to API-X80 grade was used as the starting material. The chemical composition of this material is shown in Table 1. The as-cast specimen was hot forged and hot rolled to the thickness of about 12 mm. The hot rolled plate was machined to prepare the plane strain compression specimens with dimensions of 20 mm length, 15 mm width and 10 mm height. The flow behavior of these hot rolled microalloyed steel plates has been investigated by conducting hot deformation test by varying deformation temperature and strain rate with strain up to 1.0 in Gleeble 3800 system.

Table 1: Chemical composition (in wt%) of API-X80 steel with remainder being Fe

C	Si	Mn	S	P	Al	Ti	V	Cr	N	Mo	Nb
0.06	0.32	1.50	0.007	0.028	0.06	0.010	0.050	0.10	0.008	0.19	0.04

These specimens were first heated with constant heating rate of 5^{o}C/s to the homogenization temperature to ensure complete dissolution of Nb(C,N). The soaking temperature of 1200°C was chosen based on the thermodynamic calculation using simulation software package Thermo-Calc. Figure 1 shows the variation of calculated volume fraction of austenite and

ferrite phases with temperature. The austenite start and finish temperatures are about 680°C and 870°C, respectively. The predicted volume fraction of Nb and Ti based carbonitrides (Precipitate 1 & 2, respectively) in austenite is shown in Fig. 2. It is observed that the dissolution of Ti based carbonitride (Precipitate 2) is very high (more than 1450^{o}C). The figure also shows that the predicted dissolution temperature of Nb based carbonitride (Precipitate 1) is less than 1150°C. Based on these calculations, it can be concluded that all the Nb(C,N) will be dissolved after soaking at 1200°C for sufficiently long time. Therefore, the specimens are soaked at 1200°C for 300s to dissolve all the Nb based carbonitrides.

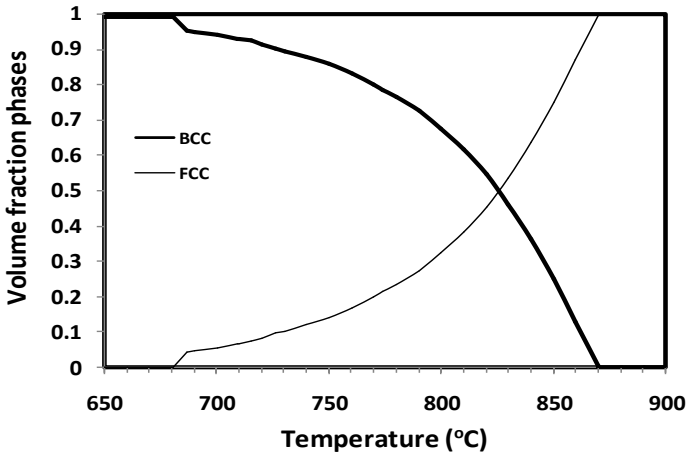

Fig. 1: Variation of estimated volume fraction of austenite and ferrite with temperature

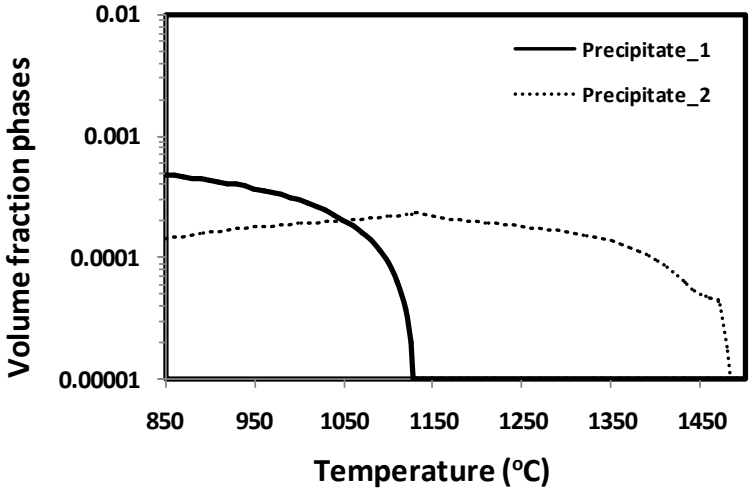

Fig. 2: Predicted volume fraction of Nb and Ti based carbonitrides in austenite (Precipitate 1 & 2, respectively)

After homogenization, the specimens were cooled to the deformation temperature at a constant cooling rate of 20°C/s. After holding at deformation temperature for 2s (mainly for temperature homogenization), plane strain compression test was carried out with varying deformation temperatures of 950, 1050 and 1100°C and strain rates of 0.1, 0.5 and 1 s^{-1} at strain up to 1. A pictorial view of the plane strain compression specimens before and after deformation is shown in Fig. 3.

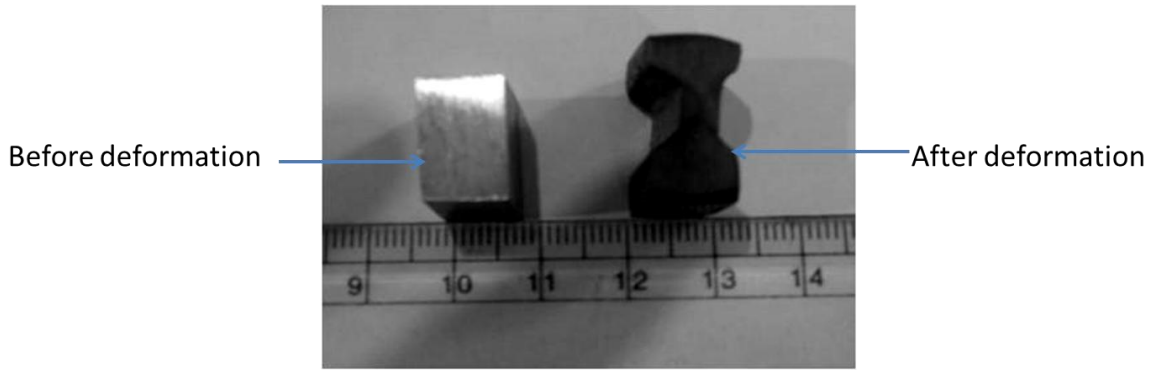

Fig. 3: Pictorial view of the plane strain compression specimens before and after deformations

After deformation, all the specimens were cooled to room temperature with a constant cooling rate of 20°C/s. These experiments were mainly carried out to examine the effect of hot deformation conditions on the recrystallisation behaviour of this material. Some of the above mentioned hot compression tests were repeated after holding the specimen at deformation temperature for 300s. These tests were performed mainly to see the effect of Nb precipitation on the recrystallisation behaviour. A schematic diagram of time-temperature schedule of hot compression test, carried out at varying deformation conditions, is shown in Fig. 4.

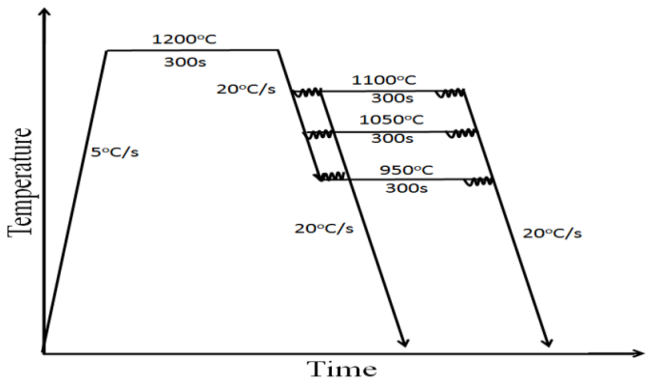

Fig. 4: Schematic diagram of time temperature schedule of hot deformation

RESULTS AND DISCUSSION

The longitudinal section of the hot rolled plate used for the plane strain compression test is shown in Fig. 5. Optical micrographs reveal the presence of polygonal ferrite in the microstructure with variation in ferrite grain size. A non-homogeneous grain size distribution is most commonly observed in Nb containing microalloyed steel. The average ferrite grain size of the starting material is about 11 μm. However, the grain size shows a wide size distribution ranging from 5-40 μm.

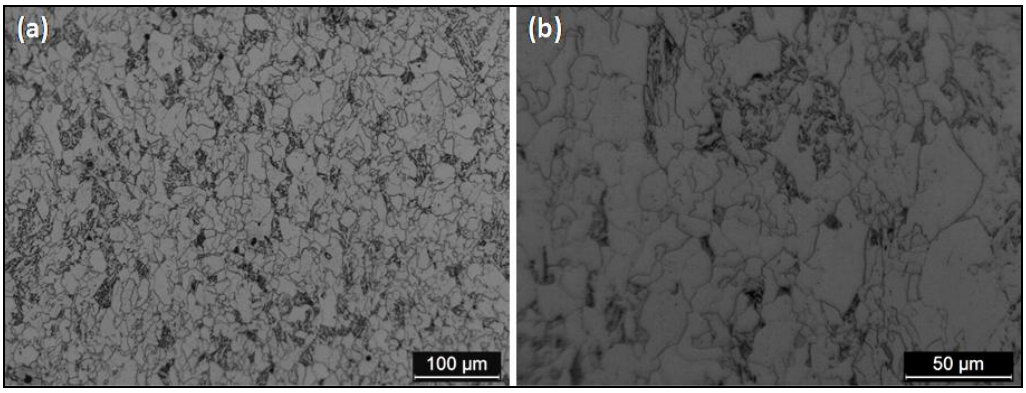

Fig. 5: Initial optical micrographs of starting material

Figure 6 shows the effect of deformation temperature on the flow behaviour of the specimen deformed with constant strain rate of 0.1 s^{-1}. As expected, flow stress decreases with increase in deformation temperature. At higher deformation temperatures of 1100^{o}C and 1050^{o}C, flow curves reveal the classical DRX behaviour. At initial deformation, flow stress increases with strain and reaches to a well defined peak stress with increasing strain. Thereafter, it decreases and a steady state region is attained at higher strain value. Flow behaviour of the specimen deformed at 950^{o}C is also similar, which shows the presence of clear peak stress followed by a work softening. However, steady state region is not observed under this deformation conditions.

In all these experiments, specimens were held at deformation temperature either for 2s or 300s before performing the hot compression test. The figure also depicts that for the higher deformation temperatures (1100 and 1050^{o}C), there is no significant difference in flow behaviour for both the specimens deformed with holding times of 2s and 300s. However, flow stress is quite high for the specimen deformed at 950^{o}C after holding for 2s in comparison to the specimen deformed at the same temperature after holding for 300s. The estimated critical and peak values for the occurrence of DRX are also plotted in the figure.

However, it is difficult to find any correlation of critical and peak values, at fixed deformation temperature, and the holding time.

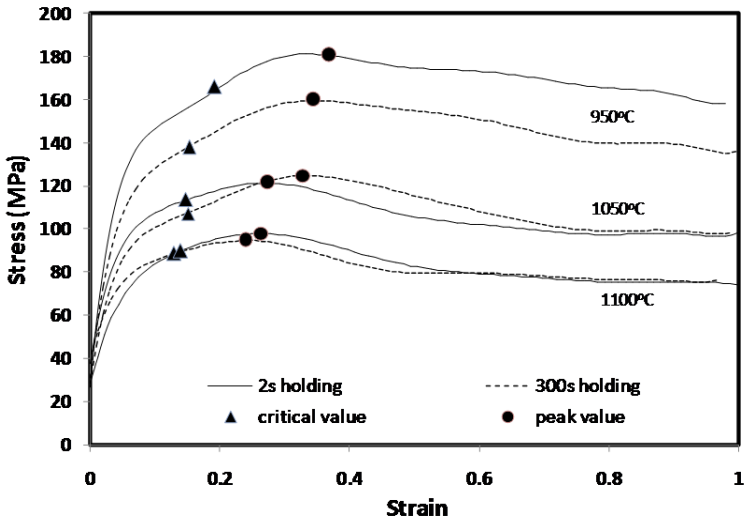

Fig. 6: Effect of deformation temperature and holding time at deformation temperature on the stress-strain curves for the specimens deformed with constant strain rate of 0.1 s^{-1}

The appearance of a peak in the flow curve indicates the occurrence of DRX during hot deformation of the specimen under isothermal and constant strain rate conditions. However, DRX initiated at lower stain and stress values in comparison to peak stress and corresponding peak strain values. These stress and strain values for the initiation of DRX are known as critical values. Both these critical and peak values depend on steel chemistry, grain size prior to deformation and deformation schedule (temperature and strain rate). The critical strain and stress values for the initiation of DRX can be estimated from microstructural characterisitcs. However, this method required analysis of large number of specimens and it is also difficult to decide the nature of some of the new grains. Ryan and McQueen[18] developed a method based on flow curve analysis in which the critical strain was defined as the strain where the experimental flow curve deviates from the idealized dynamic recovery curve. In the present study, critical stress for the initiation of DRX is estimated from the behaviour of work hardening rate with respect to true stress[19-23]. Work hardening rate ($\theta=\delta\sigma/\delta\varepsilon$) was calculated by differentiating the stress with respect to strain using a smooth stress-strain curve obtained by fitting higher order polynomial (9^{th} order) in the experimental stress-strain curve. Figure 7 shows a comparison between the flow curves obtained by raw experimental data and the smoothed curve produced by polynomial fit. The figure reveals that the smooth curves fit well with the original data.

In order to examine the effect of holding time at the given deformation temperature, the measured critical and peak stress values as a function of Zener Hollomon parameter (Z) are shown in Fig. 8. The Z value is calculated based on the activation energy (Q_{def}), which was found to be 457.5 kJ/mol. The value of activation energy is obtained based on experimental data and is well in agreement with reported value for low carbon Nb-Mo steel[12,24]. Critical stress for the initiation of DRX and peak stress increase linearly with logarithmic of Z. It is also observed that both critical and peak stress values are less for the specimen held for 300s than the specimens deformed after holding for 2s. The difference in critical and peak stress values with holding time of 300s and 2s is higher with increase in Z. Whereas, for lower Z value the differences are negligible.

It can be concluded that the influence of holding time on critical and peak stress values, for small Z values, is not much at higher deformation temperatures. However, significant difference in stress values is observed at higher Z parameter. This observation strongly signifies the role of Nb in controlling the recrystallisation mechanism.

It is expected that for the present steel composition grain coarsening will not take place at the reheating temperature below 1300^{o}C, particularly due to the presence of Mo [6]. Grain coarsening is expected to occur in Mo free Nb containing microalloyed steel at around 1200°C. This increase in grain coarsening temperature for Nb-Mo steel is due to the strong effect of Mo, when it is in solution. Therefore, in the present study it is expected that grain size variation for the specimen, held for 2s or 300s, will be effectively similar at a given deformation temperature, which may have negligible effect on DRX mechanism.

It is well known that precipitate formation and dissolution kinetics depend on time and temperature. At higher deformation temperatures (1100^{o}C), the mobility of the boundaries and of the solutes is high enough to eliminate the retardation of the initiation of DRX. At low temperature (950^{o}C), the precipitates of Nb may not be completed during 2s holding of specimen at deformation temperature. The precipitation of Nb(C,N) may be enhanced by the hot deformation and can play an important role in effectively pining the strain free grain boundaries and inhibit their migration. However, during 300s holding of specimen at deformation temperature, precipitation of Nb(C,N) may be completed before deformation and precipitate size may be coarser, which does not delay the initiation of dynamic recrystallisation at lower deformation temperature.

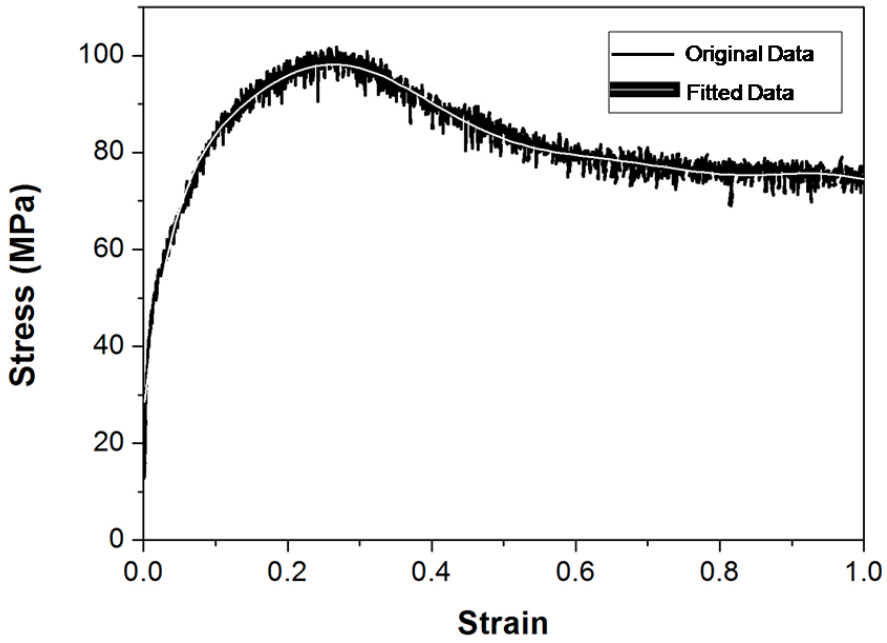

Fig. 7: A comparison between the flow curves obtained by raw experimental data and the smoothed curve produced by polynomial fit

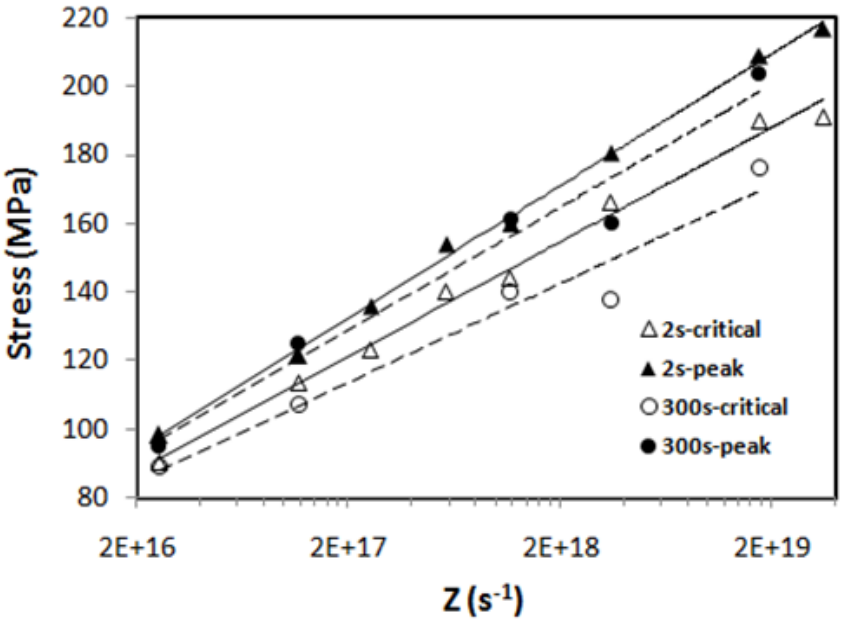

Fig. 8: Variation of critical (σ_c) and peak (σ_p) stress values with Zener–Hollomon parameter (Z)

SUMMARY AND CONCLUSIONS

The effect of hot deformation conditions on the flow behaviour of API X80 microalloyed steel was studied. At higher deformation temperatures of 1100^{o}C and 1050^{o}C, flow curves reveal the classical shape of the occurrence of DRX, when the specimens were deformed with

constant strain rate of 0.1 s^{-1}. The flow behaviour of the specimen deformed at 950^{o}C is similar, though steady state region is not observed under this deformation conditions. The critical and peak stress values increase linearly with logarithmic of Zener Hollomon (Z) parameter. It is also observed that both critical and peak stress values are smaller when specimen was hold for 300s at the deformation temperature in comparison to the specimens deformed after holding for 2s. These differences in critical and peak stress values, with holding time of 300s and 2s, are more pronounced for higher values of Z, whereas, for smaller Z values these differences are negligible. This indicates that Nb, as a particular alloying addition, has a significant role in controlling the recrystallisation mechanism.

REFERENCES

[1]. P. Zhao and J.D. Boyd, Materials Science and Technology, 20, 2004, p. 695.

[2]. V. Raghavan, "Physical Metallurgy", PHI Learning Private Limited, New Delhi, Second Edition, 2011, p. 137.

[3]. A. J. Bryhan and W. Troyer, Supplement to the welding journal, 1980, p. 37.

[4]. Kostryzhev, A. G., Alshahrani, A. Al., Zhu, C., Ringer, S. P. & Pereloma, E. V., Materials Science and Engineering A: Structural Materials: Properties, Microstructure and Processing, 581, 2013, p. 16.

[5]. H. Mohrbacher, "Principal effects of Mo in HSLA steels and cross effects with microalloying elements", International Seminar in Applications of Mo in Steels, Beijing, China, June 28, 2010.

[6]. B. Pereda, A. I. Fernandez, B. Lopez and J. M. Rodriguez-Ibabe, ISIJ International, 47, 2007, p. 860.

[7]. G. R. Ebrahimi, A. Momeni and H. Eskandari, Iranian Journal of Materials Forming, 2, 2015, p. 43.

[8]. A. J. Deardo, International Materials Reviews, 48, 2003, p. 371.

[9]. M. Opiela, W. Ozgowicz, Journal of Achievements in Material and Manufacturing Engineering, 55, 2012, p. 759.

[10]. W. B. Lee, S. G. Hong, C. G. Park, K. H. Kim and S. H. Park, Scr. Mater., 43, 2000, p. 319.

[11]. M. G. Akben, B. Bacroix and J. J. Jonas, Acta Metall., 31, 1983, p. 161.

[12]. M. Y. Seok, I. C. Choi, Y. Zhao, D. H. Lee, J. A. Lee, and J. Jang, Steel Research Int., 85, 2014, p. 1.

[13]. F. E. H. Bakkali, A. Chenaoui , R. Dkiouak , L. Elbakkali , A. Omar, Journal of Materials Processing Technology, 199, 2008, p. 140.

[14]. M. Gomez, L. Rancel , B. J. Fernandez, S. F. Medina, Materials Science and Engineering A, 501, 2009, p. 188.

[15]. S. F. Medina , A. Ouispe, ISIJ International, 36, 1996, p. 1295.

[16]. S. F. Medina , A. Ouispe , P. Valles , J. L. Banos, ISIJ International, 39, 1999, p. 913.

[17]. I. Tamura, C. Ouchi, T. Tanaka , H. Sekine, Thermomechanical Processing of High Strength Low Alloy Steels, Butterworths & Co. (publishers) Ltd, London, 1988, P. 34.

[18]. N. D. Ryan and H. J. McQueen, Canadian Metallurgical Quarterly, 29, 1990, p. 147.

[19]. G. R. Stewart, J. J. Jonas and F. Montheillet, ISIJ International, 44, 2004, p. 1581.

[20]. E. I. Poliak and J. J. Jonas, Acta Materialia, 44, 1996, p. 127.

[21]. E. I. Poliak and J. J. Jonas, ISIJ International, 43, 2003, p. 692.

[22]. E. I. Poliak and J. J. Jonas, ISIJ International, 43, 2003, p. 684.

[23]. A. Najafizadeh and J. J. Jonas, ISIJ International, 46, 2006, p. 1679.

[24]. Abdullah M. Alshahrani, “The effects of niobium and dynamic recrystallisation on microstructural homogeneity of microalloyed steels”, Doctor of Philosophy thesis, School of Mechanical, Materials and Mechatronic Engineering, University of Wollongong, 2013.